FLOW ANALYSIS OF AN EXISTING HAWKER AIRFRAME USING TRANAIR

Mohammad Reza Shahsavari

A Thesis
in
The Department
of
Mechanical and Industrial Engineering

Presented in Partial Fulfillment of the Requirements
for the Degree of Master of Applied Science in Mechanical Engineering at
Concordia University
Montreal, Quebec, Canada

August 2007

Your file Votre référence
ISBN: 978-0-494-34649-5
Our file Notre référence
ISBN: 978-0-494-34649-5

ABSTRACT

FLOW ANALYSIS OF AN EXISTING HAWKER AIRFRAME USING TRANAIR

Mohammad Reza Shahsavari

The objective of this work is to analyze an existing HAWKER airframe using a full potential CFD code, TRANAIR, developed by Boeing. The airframe geometry is obtained by scanning an existing HAWKER 800 and is analyzed by TRANAIR solver. Full potential solvers are advantageous in CFD analyses because of fast computations and low memory requirement. The current work evaluates TRANAIR, a full potential solver with finite elements discretization using a Cartesian unstructured gridding. In addition, specific airframe simulation features as well as limitations are evaluated. Viscous TRANAIR analysis is compared with the Navier-Stokes analysis obtained from another very common CFD package, Fluent. First, a comparison is performed for DLR-F4 wing/fuselage configuration. Experimental data is used for the comparison of total lift coefficient and pressure distribution on the wing surface. TRANAIR viscous analysis by coupling the boundary layer is described and the effects of boundary layer are analyzed through a test case. The simulation on the existing HAWKER airframe is performed to evaluate the capability of TRANAIR to solve the flow over a real and complex geometry. The full configuration aircraft at cruise condition and the effects of different nacelle parameters are detailed, concentrating on aft-mounted nacelles used vastly in the business jets. Good agreement is found between TRANAIR and Navier-Stokes results. The work also demonstrates the ability of CFD to solve the flow on existing aircrafts.

ACKNOWLEDGEMENTS

I would like to thank CAE Canada for funding and support this research work.

I wish to thank my supervisor, Professor Marius Paraschivoiu, for all his supports, patience, advises and managements throughout this research.

I also express my thanks to my wife, Anoosheh, who tolerated me and my absences during this work.

TABLE OF CONTENTS

LIST OF FIGURES

LIST OF TABLES

NOTATIONS

A	Surface Area
C_L	Lift coefficient
C_P	Pressure coefficient
C_τ	Shear stress coefficient
D	Drag force
E	Error indicator
H	Shape factor
H_k	Kinematic shape factor
J	Pressure integral over flow field
L	Lift force
$\dot{m}$	Mass flow rate
M	Mach number
M_c	Cut-off Mach number
M_e	Mach number at boundary layer edge
N	Number of freedom degrees
P	Pressure
q	Local velocity magnitude
r_P	Local to free-stream total pressure ratio
r_T	Local to free-stream total temperature ratio
R	Gas constant
Re	Reynolds number
$s(i)$	Blending function for density upwinding
S	Surface
T_s	Sutherland temperature
v	Local velocity
V	Velocity
V	Volume
y^+	Non-dimensional normal distance from the boundary surface

Greek Letters

α	Angle of attack
β	Free stream tube to fan-face area ratio
δ	Boundary layer thickness
δ^*	Displacement thickness
$\delta\Omega_i$	Surface element
ϕ	Perturbation potential
Φ	Potential function
Ψ	Extrapolated potential values of boundary boxes

γ	Specific heat ratio
η	Span-wise location percentage
λ	Step length
μ	Kinematic viscosity
μ	Doublet strength
μ_{ref}	Kinematic viscosity at reference temperature
θ	Momentum thickness
ρ	Density
$\tilde{\rho}$	Upwinded density
ξ	Green's function
ζ	Differential operator

Vectors and Matrices

F	Discrete operator
$\overline{F}_{X^n}$	Jacobian of matrix F linearized about X^n
G	Discrete Green's function
L	Finite element operator
$\vec{n}$	Unit normal vector
N	Preconditioner for reduced set of elements
Q	Source unknowns matrix
R	Residual matrix
T	Discrete far-field operator (Poisson)
T	Preconditioner for global grid points in reduced set
$\hat{V}$	Normalized velocity vector at the element centroid
$\vec{W}$	Total mass flux
X	Matrix of unknowns

Superscripts

(1)	Global grid points that are not in reduced set or stagnation regions
(2)	Global grid points in reduced set or in stagnation regions
o	degree

Subscripts

∞	Free stream
c	cut-off value
FF	Fan face
Hil	Hill face of nacelle

i	Direction (x , y, or z)
j	Direction (x , y, or z)
k	Direction (x , y, or z)
l	Lower
L	Lift
P	Pressure
ref	Reference condition
T	Temperature
u	upper

Abbreviations

AF	Approximate Factorization
AGPS	Aero-Grid Paneling System
AOA	Angle Of Attack
CAD	Computer-Aided Design
CFD	Computational Fluid Dynamics
GMRES	Generalized Minimum Residual
LBO	Local BOxes
MAC	Mean Aerodynamic Chord
MMO	Maximum Operating Mach number
PWBHV	Paneling Wing, Body, Horizontal, Vertical
RANS	Reynolds-Averaged Navier-Stokes
SLOR	Successive Line Over-Relaxation
TPS	Turbine Power engine Simulators
TSD	Transonic Small-Disturbance

Chapter 1

1 INTRODUCTION

1.1 Application of CFD for full model aircraft simulations

Today, aircraft aerodynamic simulations based on Computational Fluid Dynamics (CFD) are essential for designers and analyzers. The importance of simulation is mainly in the preliminary design process. The basic purpose of the conceptual design is predicting the aircraft lift, drag, main structural dimensions (e.g. wing span and fuselage length, etc.), wing type and configuration and nacelle thrust and configuration. This can be best estimated and adjusted by the aerodynamic simulations. Even in detail design, the results of simulations can be used and the limitation issues or boundary levels can be followed effectively. In addition, installation effects related to the components mounted on the wing and fuselage can be best taken into considerations with a full model aircraft simulation analysis.

Clearly, there is a tradeoff to perform analysis with either wind tunnel test or CFD simulation, as there are many parameters affecting the aircraft design. The market for aircraft manufacturers is very competitive and challenging. They should give a high value to the issues related to total cost and design, manufacture, test and delivery times. Although wind tunnel tests can give more reliable results due to covering all the flow behaviors (as well as those already unknown), CFD simulation analyses play a great role in aircraft design because of their lower costs, ease of implementation, consuming less

time, etc. Manufacturing and installation of the model, test stands, appropriate fans and instrumentations are very expensive and time consuming. For some of the cases, it is necessary to build a 1:1 scale model, which dramatically increases costs and time. On the other hand, wind tunnel walls and the model stands have negative effects in simulation. They also make analysts use many correction factors, which are all experiment-based.

Comparing to wind tunnel tests, CFD simulations can be performed easier. They need a primary investment for computer hardware and software, which is much less expensive comparing to wind tunnel equipment. Although there is still no exact solution for the turbulent flow, CFD codes have been developed extensively in recent years and considering a delta factor, they can be trusted well for turbulent flow cases. The rapid time of performing CFD analyses is remarkable today, especially in the preliminary design process, in which lower time costs can play a primary role as the whole project might be refused at the end. Full aircraft simulation can be performed at a relatively lower cost comparing to wind tunnel test. In addition, many effective and professional post processing software are available that can illustrate important features of the flow, which probably cannot be seen well in wind tunnels.

Among CFD codes, the full potential solvers are the fastest. In the following section, complete explanations of these codes, their history and the advantages using them are given. This thesis focuses on one of the most popular full potential codes, TRANAIR, that has been developed by NASA Ames and Boeing company. Note that the aerodynamic design of the Boeing 777 at cruise conditions was performed with the TRANAIR code [27].

1.2 Non-linear full potential methods

The use of non-linear full potential methods goes back to more than 35 years and still continues, especially in the aircraft industry. During this period the non-linear full potential solvers have been extensively developed, been optimized efficiently, and been commonly used in aerodynamic design of aircrafts or other external aerodynamic fields for cruise flight conditions. Reference [1] provides a historical review of different potential flow models and particular features.

The main reason that makes the non-linear full potential methods very usable and efficient is the speed of convergence. Basically, numerical iteration schemes for potential solvers (full/linear) converge in fewer iterations than iteration schemes for the Euler or Navier-Stokes equations and clearly each iteration is less expensive. The fast convergence of full potential solvers comes at the price of physical limitations of the model. In fact, the formulations of all potential solvers are based on isentropic, irrotational flows. It is the reason why full potential codes will have errors, for strong shock waves solution or when viscous effects, particularly flow separation, exist in the flow field.

Several issues need to be considered when solving transonic flows via the full potential method. First, transonic flows are very sensitive to even small perturbation in flow conditions or geometrical characteristics. Second, linearization of full potential equations for transonic flows will destroy the physics of the problem and consequently the shock wave prediction. Third, viscous effects are extremely important in transonic flows, therefore many important effects caused by viscosity e.g. shock/boundary layer interaction, the decambering effect created by the addition of displacement thickness,

trailing edge effects and near-wake effects should be taken into consideration. A historical survey of techniques for transonic flow CFD solutions can be found in reference [2].

Full potential formulations (like other methods) can be considered in conservative or non-conservative form, which lead to different solutions for transonic applications. For shock wave solutions, the non-conservative form of the full potential equations produces an error in the form of a mass source that causes an error in the shock position and strength, but use of the conservative form does not guarantee an accurate resolution of the shock wave. In fact, the error introduced by the non-conservative form involving only weak shocks is not large, and produces results (for inviscid computations) in better agreement with experiment than the conservative approach. It is due to an effective mass source introduced (with non-conservative form of equations) at shocks. It should be noted that if accurate viscous corrections are done via coupling a boundary layer code to the full potential code, the conservative form will produce the correct physical answer, at least within the limitations of the irrotational and isentropic assumptions, but non-conservative form will not. Recently, new developed potential flow codes are based on conservative formulations, and this trend is anticipated to continue.

Full potential formulations are also used for small disturbance flows. For these kinds of flow, many approximations are made based on their simple nature and therefore they are used for transonic flows in a more convenient way (TSD potential equation). Normally, in the TSD potential equation the characteristics directions are symmetric about the x-axis, in contrast to the full potential equation.

When using full potential solvers, it is necessary to stabilize the supersonic regions of the flow. This can either be done by the artificial density spatial discretization approach or by flux upwind schemes. Basically, artificial density schemes are simpler and more reliable for stabilization, but for several applications involving weak shock waves the flux upwind schemes are superior for capturing shocks.

Various iteration schemes are employed in full potential solvers. The vast majority of all full potential solvers utilize the SLOR (successive line over-relaxation) iteration scheme. Other iteration schemes, including AF (approximate factorization) and multi-grid schemes are used occasionally and have superior convergence characteristics, i.e. solutions are obtained with fewer iterations and less computer time. Time accurate scheme is one of the most prominent iteration schemes that are used for unsteady flow problems.

There are four major sub-areas related to transonic full potential methods for complex geometry applications. Those are as follows:

1) Chimera zonal grids (overset grids)

2) Patched zonal grids

3) Cartesian unstructured grids

4) Unstructured grids

One of the most important grid approaches that are used in full potential solvers extensively, especially in the solver analyzed in this thesis (TRANAIR), is the Cartesian unstructured grid approach. This approach utilizes a grid composed of squares in two dimensions or cubes in three dimensions. Each Cartesian grid cell can be discontinuously

subdivided into smaller cells in the regions of high flow gradients. Figure 1-1 shows how this gridding approach creates the mesh around a 2-D square. Unstructured approach is

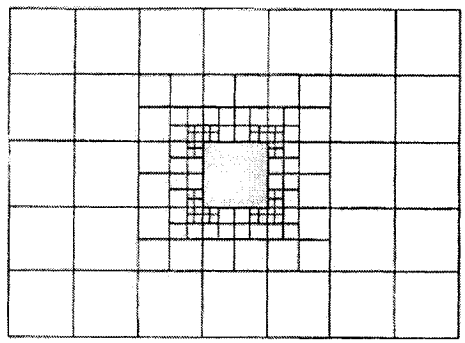

Figure 1-1: *Unstructured Cartesian grid approach around a square[1]*

generally more accommodating in the treatment of complex configurations, but is less computationally efficient.

1.3 TRANAIR solver

In this thesis, the TRANAIR full potential code, some of its features, the gridding strategies and many other issues related to this code along with the results for some case examples are presented. TRANAIR is a system consisting of many computer codes developed for analyzing the compressible viscous/inviscid flows around any complex configuration at subsonic, transonic or supersonic free stream Mach numbers. This system utilizes the nonlinear full potential equation to analyze or design different configurations and is able to be coupled with a boundary layer to consider viscous effects. The numerical method of TRANAIR uses different and independent discretizations for the configuration geometry and the volume flow field. In fact, the surface discretization of the configuration geometry is done in a mesh developing

software called "AGPS" [3] and the volume discretization is done by the TRANAIR code itself.

TRANAIR started to be developed in 1984, when NASA Ames made a contract for feasibility study on this full potential solver. In continuation of this contract and as the technology to analyze transonic flow with uniform orthogonal field was developed, another contract was made by NASA Ames in 1987 for the expansion of the technology with the development of grid refinement techniques. Some of the final and complementary parts of this contract were funded by the Boeing Company. Then, an equivalent version of TRANAIR (two-dimensional/axisymmetric) was developed in 1989-1990. From this time, TRANAIR continued to be developed with improvements in coupled boundary layer, adaptive grid refinement technology and design capability, all funded and sponsored by the Boeing Company. In addition to these improvements, several extensions of the TRANAIR code are developed to solve problems in electromagnetics, acoustics, unsteady flow and aeroelasticity.

There are different kinds of boundary conditions available in TRANAIR to allow for the simulation of different components e.g. inlets & exhausts of engines, wakes, porous walls for modeling the wind tunnel and impermeable surfaces for solid objects. TRANAIR is also able to produce different regions of different total pressures and temperatures in the flow field. This capability is used for special regions like engine exhausts for powered nacelles.

One of the most important advantages of TRANAIR comparing to other similar or non-similar codes is the ability of automated adaptive gridding. In TRANAIR, the flow field is divided automatically into some user-controlled locally refined rectangular grids.

These grids are created one after another and the refining/coarsening strategy on the next grid is based on the solution done using the Newton steps on the previous grid, and the local regions that are defined by the user for adaptive refining/coarsening. The automated adaptive gridding will be discussed comprehensively in section 2.4.

There are many special and operational features that make TRANAIR much more useful and practical. Complex configurations modeling, automated solution adaptive grid generation, wind tunnel wall influence calculations, design/optimization, restart and grid sequencing solution are some of the most interesting capabilities among those features. As TRANAIR is a solver based on full potential formulations and based on what is explained in section 1.2, it is not able to predict flows dominated by viscous effects (other than boundary layer) or by strong transonic flow effects.

TRANAIR is divided in three main programs, which are run sequentially. These programs are the input processor, the solver and the output processor. There is also a binary converter program to make the output graphics files. For each program, there are some files that should be entered as input, based on the necessities of the solution, and many other files are generated in the output. Figure 1-2 shows a schematic of the programs with input/output data communications.

In chapter 2, more details describing the TRANAIR code including the formulation, the numerical method, discretization, solution techniques, automated adaptive gridding, boundary layer coupling and different boundary conditions are explained.

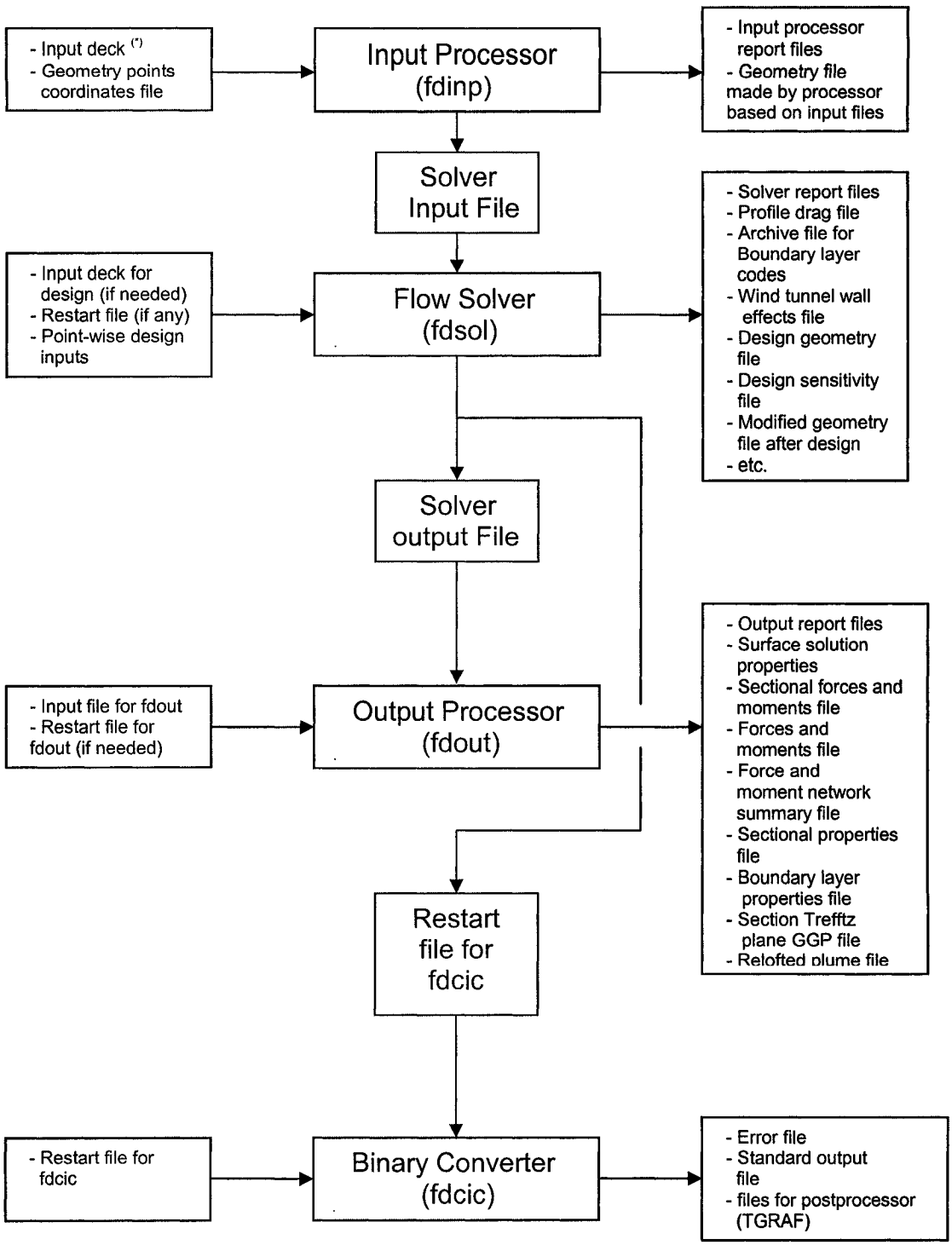

(*) Input deck is the input file for input processor containing information about global box, local refinement regions, flow characteristics, boundary layer, solution control, adaptive gridding control, reference dimensions, etc.

Figure 1-2: *TRANAIR flow chart*

1.4 Review of full potential codes and TRANAIR method/application

Several different codes based on the full potential approach along with their grid generation and discretization methods, iteration schemes, boundary conditions and their applicability are reviewed here-in. The first full potential solution method using conservative form was developed by Jameson [4] for solving transonic airfoils in 1975. This work continued by a series of three-dimensional full potential solvers called FLO27, FLO28 and FLO30 ([5], [6] and [7]), and all utilized the SLOR iteration scheme. There has also been a widespread effort for developing full potential codes at Boeing. These works started by development of the first generation of linear potential methods (Boeing-TA230 code), which used the Neumann boundary conditions combined with the source panel scheme of the Douglas Neumann program and variations of the vortex lattice technique, and continued with the linear methods second generation, Boeing-A502 (similar to PANAIR), which was a panel method program featured the use of curved panels and higher quadratic Sp-lines to discrete values located at specific points on the network. Finally, TRANAIR was developed as a comprehensive code to overcome the problems that previous codes had, mainly as prolonged convergence because of development of shocks in the flow field, not capturing accurately the weak and double shocks, boundary layer coupling contributed problems, etc. F. T. Johnson et al. [8] gives a detailed history of CFD development at Boeing. The paper describes mainly potential codes and their contribution in each of the Boeing's airframe designs and a brief comparison of TRANAIR with other Navier-Stokes and Euler/coupled boundary layer codes.

T. L. Holst [1] gives a history of different potential, and specifically full potential, approaches. He makes a complete comparison between conservative versus non-conservative forms of the potential equations in the aspect of shock capturing, uniqueness and accuracy. In this work, the use of flux upwinding or artificial density utilized by different potential codes for supersonic regions stabilization is explained.

In CFD, the design work is much more complex than the aerodynamic analysis, because of the large variety of approaches that are available in design. Tery L. Holst [1] introduces the design methods that are used to overcome and consider these complexities. There are different gridding and discretization methods (explained by Tery L. Holst) developed for complex geometry applications. Among those, the unstructured and the unstructured Cartesian grid methods are best for handling complex geometries. For Cartesian grids the ease of implementation and generality are results of the simple manner in which the intersection between an analytically defined Cartesian grid and arbitrary CAD-defined geometry can be computed. TRANAIR uses the unstructured Cartesian grid method in a finite-element flow solver.

Antony Jameson has been contributing significantly to different approaches for the full potential method. He developed a finite volume method calculating transonic potential flow by the use of the global mapping sequences [9]. He also gave some details and remarks about the calculation of this method to prove and show the results accuracy [10]. In this method, he proposed to circumvent the geometric difficulties by deriving a discrete approximation on a mesh constructed from small volume elements, which can be conveniently packed around the body.

Since 1984, when TRANAIR was first developed by NASA ames, continuous research has impressed various relevant areas such as gridding strategy, automated adaptive gridding, design and modification, unsteady flow sample cases and nacelle applications, etc. In TRANAIR, box finite elements (for 3D) are defined by a Cartesian unstructured grid that is not dependent on the boundary definition. The tri-linear approximation is used for box elements and for time/storage saving, special element stiffness matrices are introduced for boxes cut by any boundary surface. D. P. Young et al. [11] explain comprehensively how TRANAIR solves a specific problem by starting with global box definition and ending with discrete system solution using a preconditioned GMRES algorithm. Problems of practical interest have often many different length scales, therefore, Young and his colleagues use local grid refinement in TRANAIR.

To ensure robust convergence in TRANAIR, a solution procedure is developed [11] for the discrete equations. This method employs a combination of two preconditioners for a GMRES solver. One of these preconditioners is a sparse direct solver with a drop tolerance. The other is a Poisson solver on the uniform global grid, which insures that the far field boundary condition is satisfied. TRANAIR uses Green's function defined on a uniform global grid in conjunction with the fast Fourier transform to impose the boundary of the computational grid to be very close to the object. This generally reduces the number of finite elements needed to solve a given problem. R. H. Burkhart [12] explains the definition, existence and uniqueness of the free-space Green's function for the discrete 3-D Poisson equation on a general unstructured Cartesian grid based on the theory of multidimensional Fourier series. He also presents an integral method and a

Taylor series method for deriving the asymptotic expansion of the Green's function, including explicit computational formulas for several higher order terms.

TRANAIR uses an automatic adaptive method for flow field discretization. In this method, the grids are adapted to numerical solutions of the last run by refining/coarsening the local rectangular finite elements based on the values of error indicators computed for each element. M. B. Bieterman et al. [13] explain the details of adaptive gridding approach with several computational problems. They also explain the steps through which a new grid is constructed based on adaptive gridding.

TRANAIR is distinguished as a user-friendly tool for the high quality aerodynamics analysis. One needs not much CFD knowledge to be able to work with this code, and basically, the analysis knowledge is much more needed for the results coming out of this code. M. F. Smith [14] explains the common steps involved in generating CFD results out of TRANAIR. He explains that one of the most difficult steps in TRANAIR is the flow filed gridding for either new or occasional users. If inappropriate controls are specified in input, the regions of interest might not be properly refined, leading to incorrect results. Setting the appropriate controls requires good analytical skills (understanding the physics), but does not necessitate full CFD knowledge.

TRANAIR is applied to many different aircraft configurations. Basically, the analysis of objects mounted on the wing (e.g. external stores) is very complicated due to the mutual interference of the fuselage, wing, pylon and other mounted components. Therefore, the analysis of these components is very useful and TRANAIR helps researchers in this field. M. Madson et al. [15] did analyses with TRANAIR on a very high tapered wing accompanying with a finned-store and its pylon in high Mach numbers

(0.95 and 1.2) and compared the forces, moments information and pressure distribution with the experimental data to validate the TRANAIR results in very extreme cases with high interference. M. Madson [16] also did a TRANAIR analysis on the F-16A fighter full configuration with fuel tank mounted on wing and showed the importance of utilizing adaptive gridding of field for better estimates of flow close to surface boundaries with high curvatures or sharp tips, etc. He also illustrated the poorness of TRANAIR (at the time of those analyses) to predict the pressures well in the regions with channeling effect (wing lower surface inboard of the fuel tank). A. Cenko and M. Madson [17] analyzed the F/A-18E aircraft wing with the TRANAIR and PANAIR codes in different Mach numbers and compared the results against the experimental data. They concluded that while PANAIR gave better results for subsonic flows, TRANAIR provided better for transonic flows.

TRANAIR is also very useful in analysis of nacelle in different flow conditions and engine/airframe integration. In TRANAIR, the capability of introducing the regions with different total pressures and temperatures caters the possibility of powered nacelle analysis to get the thrust and nacelle drag data. A. W. Chen et al. [18] analyzed different turbofan engines (short and long by-pass) in powered situation, mounted on the wing or isolated. They illustrate explicitly how the difficulties of generating a surface fitted grid to a complex geometry (that exist in most Navier-Stokes, Euler and full potential codes) are avoided in TRANAIR by the use of a hierarchically (adaptive) refined rectangular grids. In addition, R.G. Melvin et al. [19] explain the effects of engine exhausts on the wings, struts and nacelles. They also explain the several formulations capable of modeling engine exhausts for the accurate simulations of engine installations on modern

commercial aircrafts. In their research work, the role and effect of total pressures and temperatures in exhaust plumes are explained. In addition, they detail and compare the exhaust wakes boundary conditions in TRANAIR and in Euler codes. Then the analysis of a turbofan engine nozzle for axisymmetric condition at two different Mach numbers, one at the cruise Mach and the other at a very low free stream Mach number, were performed by TRANAIR and an Euler code and the results were compared and validated against experimental data.

One of the very useful features of TRANAIR is the design capability. There have been developments in the design capability of TRANAIR during the period of 1995 to 1999. Introducing the multi-point design capability in TRANAIR reduces the cycle time and cost in the design of commercial aircrafts. R.G. Melvin et al. [20] and W. Jou et al. [21] present the developments of the aerodynamics design methods for the TRANAIR code.

1.5 TRANAIR analysis, objectives and outline

As mentioned in section 1.4, TRANAIR code can be used in different applications. But, this solver is mostly applied to the aircraft analysis and because of that, most works found in literature are for full aircraft geometries or aircraft single components in conjunction with/without the other components. Nevertheless, TRANAIR is not a good tool for drag prediction, and for this purpose, Navier-Stokes codes can offer better results. That is why results concentrate mainly on lift, pressure distribution, forces and moments and their comparison with experimental data or other CFD codes.

There are many constraints for TRANAIR to give good convergence or reasonable results. These constraints include the limitations in angle of attack due to separation, surface roughness and the quality of mesh for different components, the limits of high

Mach number applications for the Mach numbers close to MMO (maximum operating Mach number for the clean configuration), the limits of fuselage closure in the aft because of boundary layer high transpiration, the wing elevation, the gridding that can be created by AGPS mesh developer (Aero-Grid Paneling System) and specialized for TRANAIR, inlet mass flow rate for the nacelle, etc. In this thesis, all these constraints are addressed and detailed along with their effects on convergence and/or results for lift and wing pressure distributions.

TRANAIR utilizes a very user-oriented geometric modeling and mesh developer tool, called "AGPS". These codes (TRANAIR & AGPS) are strongly linked and it can be said that doing a good analysis in TRANAIR without AGPS is a very difficult job. There are many features existing in AGPS, the most critical items are graphics interactivity and general geometry programming that includes full programming functions such as mathematical operations and control constructs (e.g. Do-loops, etc.). AGPS can create the best input file for TRANAIR based on the flight condition introduced or the conditions of the wind tunnel simulation. It can create patched-gridding, which is very useful for gridding the complicated cases like full geometry aircraft with nacelle. In addition, it has some constraints that affect the aerodynamic analysis of TRANAIR. In this thesis, the interface between TRANAIR and its mesher, AGPS, is described and the constraints in TRANAIR caused by the mesh are pointed out.

TRANAIR, by itself, is an inviscid solver. For more accurate physical analysis and having close-to-reality results, a boundary layer code (mainly integral type) is coupled to the full potential solver. The boundary layer coupling has many advantages as well as moving the shock position to its right place and adjusting the strength of the shock. It also

gives a good and real meaning and usability to the Kutta condition that is applied to the inviscid TRANAIR. This (KUTTA condition) occasionally causes some errors at the wing trailing edge in the form of big jumps in a small area. To see the advantages of viscous effects, the pressure distribution on the wing for viscous and inviscid TRANAIR are compared for one aircraft case and the results of coupling the boundary layer in TRANAIR are given (in chapter 4).

In this thesis, for validation of the TRANAIR methodology, many analyses and comparisons are performed with TRANAIR for two different aircraft; a wind tunnel model (DLR-F4, wing and fuselage) and a full scale aircraft (HAWKER 800). The main focus is on the total lift coefficient and wing pressure distribution (Cp) at different wing airfoil cross sections and mostly the results from two CFD codes, TRANAIR and FLUENT (N.S) are compared. For the DLR-F4 case, experimental data are available and the results are compared with them as well.

Aircraft components, especially wings, are highly affected by the presence of nacelles. In the literature, the analyses of nacelle different parameters for the isolated nacelle or nacelle in conjunction with other aircraft components can be found. As an example, R. Rudnic et al. [22] analyzed the influence of increasing the engine size and vertical/horizontal engine position variation on the aircraft aerodynamics and generally on lift, for turbine power engine simulators (TPS), very high by-pass ratio and ultra high by-pass ratio engines. In general, all of the analysis addressing engines has been done for the wing-mounted nacelles.

The originality and contribution of this thesis is the use of existing aircraft surfaces via laser scanning and analyzing those surfaces by different solvers. In fact, the quality of the

surfaces coming out of laser scanning is not the same as the design quality. This can cause many difficulties and problems in the solver convergence or even the results, because of the improper quality of the consequence grids. But, the results are more realistic and can present a real flight situation, as least in the surface quality point of view. The other contribution of this thesis is that the aircraft configuration taken for this analysis (HAWKER 800) has a body-mounted or aft-mounted nacelle. Although both wing-mounted and aft-mounted nacelles have great impact on the wing aerodynamics, their influence is different. Basically, the negative effects of aft-mounted nacelles are relatively more, as they are close to the wing root, and as the effect of nacelle/body interference will also be added. In this thesis, different aspects of nacelle influence on wing aerodynamics (e.g. nacelle mass flow rate and the fan-face position, etc.) are pointed out and lift and pressure comparison in some wing cross sections are compared with results from a Navier-Stokes analysis.

Therefore, based on the above-mentioned explanations, the objectives of this thesis are enumerated as the follow:

1- To explore different features in TRANAIR full potential code, the proper discretization type for this code based on the necessities of finite-elements solution and different aspects regarding the interfaces between the solver and the mesh developer.

2- To identify limitations and requirements of the TRANAIR full potential code, both related to the disretization (e.g. abutment, mesh quality, etc.) and the full potential solution boundaries (e.g. separation, Mach number, etc.) as well as the aircraft components configuration.

3- To understand different advantages of viscous analysis by performing viscous vs. inviscid analysis with TRANAIR solver.

4- To analyze the effects of different aspects related to aircraft (e.g. wing elevation, surface quality, bumps and waves, etc.) on generated total lift or wing pressure distribution and the methods to increase the lift and to see the sensitivity of the TRANAIR solver to each of those.

5- To check the accuracy of TRANAIR code at different situations by performing TRANAIR/Navier-Stokes or TRANAIR/Navier-Stokes/experiment analyses.

6- To analyze the effects of aft-mounted nacelles on the flow around the wing and the generated total lift.

7- To analyze the effects of nacelle different parameters (e.g. nacelle area ratio, inlet mass flow rate, fan-face position, etc.) on the flow around the wing and generated total lift.

8- To demonstrate the feasibility to calculate lift coefficient of an existing airframe.

The outline of the thesis is as follows:

In chapter 2, the formulations and the theory behind the TRANAIR code along with some of its features are described. Chapter 3 explains the constraints and limits in TRANAIR for convergence and reasonable results as well as the limits in the TRANAIR-AGPS interface. In chapters 4 and 5, the analysis of the DLR-F4 and HAWKER 800 are described. The model implementation for both cases, run characteristics and flow characteristics are reported and finally the analysis results are illustrated and discussed. In chapter 6, the conclusions of the works and analyses done in this thesis along with the recommendations for future are presented.

Chapter 2

2 TRANAIR NUMERICAL METHOD

2.1 Governing equations and problem definition

As it is explained in section 1.2, in full potential models it is assumed that the flow is isentropic and irrotational. Therefore, based on these assumptions and taking the flow to be steady, the conservative full potential equation of aerodynamics (conservation of mass) can be written as equation (2.1) in the TRANAIR code and be solved using a numerical method :

$$F(\Phi) = \vec{\nabla}.\rho\vec{\nabla}\Phi = 0 \tag{2.1}$$

In equation (2.1), the scalar Φ (velocity potential) is the variable that should be solved instead of the three-dimensional velocity vector. The density ρ and pressure P can be found with the following equations:

$$\rho = \rho_\infty \left[1 + \frac{\gamma-1}{2} M_\infty^2 (1 - \frac{q^2}{q_\infty^2})\right]^{\frac{1}{\gamma-1}} \tag{2.2}$$

$$P = P_\infty \left[1 + \frac{\gamma-1}{2} M_\infty^2 (1 - \frac{q^2}{q_\infty^2})\right]^{\frac{\gamma}{\gamma-1}} \tag{2.3}$$

where q is the magnitude of the local velocity $q = \left\|\vec{\nabla}\Phi\right\|$, ρ_∞ and M_∞ are the freestream density and Mach number respectively, and γ is the ratio of specific heats.

There are some boundary conditions applied to equation (2.1). As x coordinate approaches $\pm\infty$, the perturbation potential $\phi = \Phi - \Phi_\infty$ is too small and can be approximated as zero. It is called the far field boundary condition. On the impermeable surfaces, e.g. solid objects' surfaces, the normal mass flux condition is zero:

$$\rho\left(\partial\Phi/\partial n\right) = 0 \tag{2.4}$$

On other surfaces, like nacelle inlet, the normal mass flux is a specified function, which relates directly to the area ratio of freestream to nacelle inlet face (refer to [11]):

$$\rho\left(\partial\Phi/\partial n\right) = \mathrm{g1} \tag{2.5}$$

If we consider the potential to be equal to a function ($\Phi = g$) on all surfaces, the tangential flow on the nacelle exhaust surfaces can be avoided by taking 'g' to be constant.

In all potential codes used for analysis of lifting objects as well as TRANAIR, wakes must exist and extend downstream from lifting components. These surfaces allow circulation not to be zero for the potential flow. Refer to [11], the boundary conditions on a wake are as follows:

$$\hat{n}.\Delta\left(\rho\nabla\Phi\right) = 0 \tag{2.6}$$

$$\Delta P = 0 \tag{2.7}$$

In equations (2.6) and (2.7) Δ represents the jump across the wake for that parameter and P can be found by equation (2.3). Equation (2.6) is mass conservation across the wake and equation (2.7) is the requirement for conservation of normal momentum. By linearization of equation (2.7) about the freestream pressure, the equivalent Dirichlet

boundary condition can be concluded, which forces $\Delta\Phi$ to be constant along the wake in the freestream direction.

Refer to [11], "the full potential equation is a consequence of the Bateman variational principle, namely that the integral of pressure over the flow field is stationary." This integral can be written as:

$$J = \int_{\Omega} pdV + \int_{\partial\Omega 1} g1\Phi dS - \int_{\partial\Omega 2}\left(\rho\frac{\partial\Phi}{\partial n}\right)(\Delta\Phi - \mu)dS + \int_{\partial\Omega 3}\rho\frac{\partial\Phi}{\partial n}(\Phi - g)dS \qquad (2.8)$$

in which g1 is the given mass flux data on $\partial\Omega 1$, $\Delta\Phi$ is the jump in potential across the wake surface $\partial\Omega 2$, μ is the unknown representing the jump in potential on $\partial\Omega 2$ determined by equation (2.7), α denotes the average of the upper and lower surface values and 'g ' is the given Dirichlet data on $\partial\Omega 3$. Detailed information about the "Bateman variational principle" can be found in [23] and [24]. The last integral of equation (2.8) is somewhat unstable. Therefore, it might be needed to modify the last integral to be more reliable numerically. In addition, the discontinuities in slope from one panel to another will impress the solution. That is why, it is necessary to add a surface integral to equation (2.8) for high curvature surfaces. Detailed information for these modifications can be found in [11].

For stable numerical formulation, the Dirichlet boundary conditions and wake surfaces are modified. Moreover, the Neumann boundary conditions for impermeable surfaces are modified to consider boundary curvatures. The modifications of the wakes are discussed in detail in [19].

TRANAIR is capable of analyzing regions with different total pressures and temperatures. This capability is useful for the analysis of nacelle exhaust plume. For these regions, the boundary conditions and definitions of pressure and density will be

changed. Refer to [11], equations (2.9) and (2.10) show the modified pressure and density in these regions:

$$p = p_\infty r_p \left[1 + \frac{\gamma - 1}{2} M_\infty^2 \left(1 - \frac{q^2}{q_\infty^2 r_T} \right) \right]^{\gamma/\gamma - 1} \tag{2.9}$$

$$\rho = \rho_\infty \frac{r_p}{r_T} \left[1 + \frac{\gamma - 1}{2} M_\infty^2 \left(1 - \frac{q^2}{q_\infty^2 r_T} \right) \right]^{1/\gamma - 1} \tag{2.10}$$

For the wakes separating the exhaust regions from other regions, there are two jump boundary conditions to be applied. First is the static pressure continuity, which is similar to equation (2.7), and second is a modification in equation (2.6) to make the answer less sensitive to the position and shape of the wake, especially when total pressure and temperature differences are large. Therefore, the second boundary condition is as the following equation (refer to [11]):

$$\hat{n}.\Delta W^* = 0 \tag{2.11}$$

In which:

$$W^* = \frac{\rho_\infty q_\infty}{\rho_0 q_0} \rho \nabla \Phi \tag{2.12}$$

In equation (2.12), q_0 is the velocity that makes $p = p_\infty$ in the specified region and ρ_0 is the density at this velocity. In this way, the Bateman principle shall also be modified for the wakes separating exhausts from the other regions. More explanation of exhaust plume wakes can be found in [19].

2.2 Discretization

The boundary of the specific problem (e.g. the surface of an aircraft) is defined in all over space via introducing the coordinate information of the unstructured Cartesian paneling

nodes. The computations in TRANAIR shall be restricted to a finite sub-region of the whole space to have reasonable storage and cost. TRANAIR does this restriction by looking for the regions where the sources (used for Prandtl Glauert equation) are significant and then by making the computational domain on those regions. When the computational domain is defined, a uniform *global grid* of rectangular boxes will be constructed in that domain. The global grid will be further refined hierarchically. For an optimized storage saving, an *octtree data structure* is used in TRANAIR, which gives a useful extraction of different kinds of information, e.g. the nodes location, element centers (centroids), the size of boxes, their level and their adjacency, node indices and identity of boundary boxes. In the following subsections, a description of how discretization is done in TRANAIR is provided:

2.2.1 Computational grid

The boundary surfaces of the simulating objects are introduced to TRANAIR by networks of panels. AGPS, the geometry software, can easily generate sufficiently flat paneling in such a way that the errors related to flat panel assumption can be neglected comparing to other errors. The volume grid is generated in TRANAIR automatically in a hierarchically manner. It means the global grid can be refined locally and every box can be divided to eight equal-sized smaller boxes. The process of repeating the local refinement is controlled by two important criteria:

1- The *length scale* of the surface panels utilized to introduce the boundary surface, which is used for the boxes close to boundary panels. These box elements are refined, if the weighted length scale related to the panel is smaller than the length scale related to these box elements.

2- *"Special regions of interest or disinterest [11]"* can be refined with selected minimum and maximum refinement level. Such refinement is useful where large gradients (e.g. shock waves, etc.) may exist away from the boundary surfaces.

As soon as all refinements are completed, the grid is checked not to possess boxes abutting on an edge (neighboring boxes) with more than one refinement level difference. This procedure is called *grid legalizing*. Once the grid is legalized, it becomes ready for the next steps.

Based on the grid that is already legalized, the boundary value problem is discretized via a finite element method. Then the *element trial function*, which is the standard trilinear function with eight unknowns (one at each corner point of the element), is introduced. To have minimum storage, certain second-order terms will be added to the trilinear trial function for uniform grid (operator for Poisson's equation).

2.2.2 Computational domain

For the sake of storage and CPU cost, the computational domain shall be restricted to a special finite region. This important feature is performed by introducing different finite element operators for far field and inside the computational domain.

If we take the function of unknowns to be Q, the differential operator as ζ, Green's function as ξ and the discrete operator as F, then the original differential full potential equation, equation (2.1), can be written as the following (refer to [11]):

$$Q + (F - \zeta)\xi * Q = 0 \tag{2.13}$$

Outside the finite region, $F = \zeta$ resulting Q = 0. Thus, the Q unknowns are limited to a bounded region, and therefore, computational grid can be limited to a region where the discrete operator F cannot be well approximated by the discrete far field operator T. The

far field operator T requires a discrete Green's function (G) that satisfies an appropriate discrete far field condition and T(G*Q)=Q for each Q.

The explanations given in previous paragraph proves why in TRANAIR the computational domain needs only to be applied to the regions containing nonlinear flow. For a wing at transonic flow conditions, the grid typically ends one or two chord length away from both sides. For the Wakes, although they produce sources and sinks that extend to infinity, their influence can be computed by using a downstream Green's function assuming that their sources and sinks are constant in the downstream direction. This enables the TRANAIR users to terminate the computational domain a few boxes downstream of the configuration.

In TRANAIR, the far field operator is considered to be similar to a Prandtl-Glauert operator as equation (2.14), which is the full potential equation linearized about freestream velocity (refer to [11]):

$$F\Phi = \left(1 - M_{\infty}^{2}\right)\Phi_{xx} + \Phi_{yy} + \Phi_{zz} \tag{2.14}$$

The computational domain must include one layer of unrefined global grid boxes on each face of that, in which the discrete operator is equal the far field discrete operator (F=T). The boxes in this layer should not coincide with any boundary surface (except wakes in downstream side) and must remain unrefined up to the end of refinement process. These unrefined boxes layer or *buffer zone* can be seen in Figure 2-1 with hatched lines.

Therefore, three kinds of boxes will be available in a grid. First, the far field boxes in which F=T (buffer zone). Second, near-field boxes that do not cut by any boundary and $F \neq T$. Third, boundary boxes, which are the boxes cut by a boundary surface. Each of

these boxes may contain several flow regions each with their own unique element trial function and own element stiffness matrix.

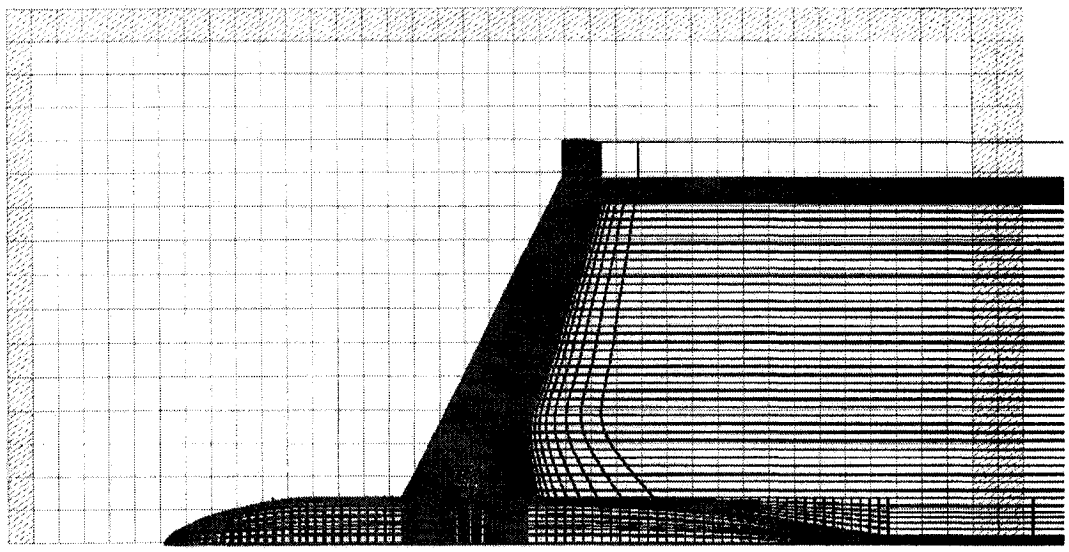

Figure 2-1: *Buffer zone around the configuration in global grid*

2.2.3 Finite element operators

Once the global grid and computational domain are identified and grid boxes inside the domain are made (both refined and un-refined), *element stiffness matrices* are then defined by taking variations of the functional J (equation (2.8)) with respect to each of the eight corner unknowns of the element. The variations function is as following (refer to [11]):

$$\delta J = -\int_{\Omega} \rho \nabla \Phi . \nabla \delta \Phi dV = -\sum_{i} \int_{\Omega_i} \rho \nabla \Phi . \nabla \delta \Phi dV \cong -\sum_{i} \rho_i \int_{\Omega_i} \nabla \Phi . \nabla \delta \Phi dV \qquad (2.15)$$

Where ρ_i is the value of ρ at the center of the elemental region Ω_i. Thus, same element stiffness matrix is used for element boxes not facing a boundary surface differing by a

constant factor that depends only on the refinement level of the element and ρ_i. This concludes much less storage of memory.

In every iteration process, density which is a function of the velocity is estimated at the center of each element. Therefore, it is necessary to get discrete equations for velocity at the center of elements in terms of the unknowns at the corners. It is good to note that only one velocity equation needs to be stored for all far and near field box elements, as they are similar. It results additional savings in storage.

Boundary conditions on the impermeable object surface can introduce discontinuities in Φ or $\nabla\Phi$. That is why one element trial function is necessary for the boundary boxes that connected to the surface boundary. In TRANAIR, such subset of boundary boxes is called D-region. In D-regions, it will be possible to have more than one element trial function in a special box and more than one unknown at the grid point, if the D-region cuts a wake as well. This represents a slight complication, since each element trial function is still parameterized by eight unique unknowns. In Figure 2-2, different D-regions are illustrated around an arbitrary boundary surface.

Each D-region has its own element stiffness matrix, which must be stored, but these elements represent typically only a small part of the elements (less than 20%) needed to give an accurate solution. Hence, the required storage is acceptable.

After defining the element matrices for the boundary boxes in D-regions, TRANAIR will identify D-regions and their boundary surfaces in a given boundary box.

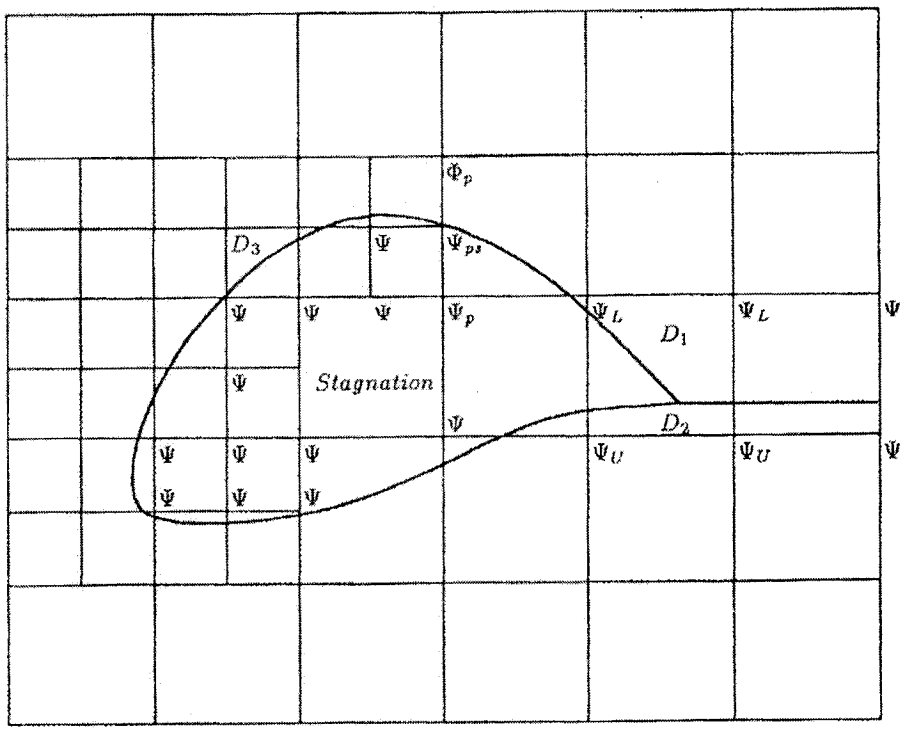

Figure 2-2: *Placement of unknowns in D regions [11]*

2.2.4 Dissipation

Basically, for supersonic regions of the flow standard first-order density upwinding is used in full potential codes to produce the required artificial viscosity. It is necessary to eliminate non-physical expansion shocks in supersonic flow regions and it can be done by density upwinding via density biasing or flux biasing. Such an upwinding is considered by replacing ρ in the full potential equation with the following (refer to [11]):

$$\tilde{\rho} = \rho - \mu \hat{V}.\nabla - \rho \tag{2.16}$$

Where $\hat{V}$ is the normalized local velocity, $\nabla - \rho$ is an upwind undivided difference and μ is a switching function given by:

$$\mu = \max\left(0,1 - M_C^2/M^2\right) \tag{2.17}$$

In which M is the local Mach number and M_C is the cutoff Mach number (a Mach number very close to 1).

There are six faces in every element. In TRANAIR, for each box face a density is selected for upwinding in the operator generation phase. For a uniform grid with no boundaries, each box has a single box adjacent to it in all its six faces. If there is grid refinement, two other cases can happen. In case, the adjacent box is refined, the density used for upwinding is calculated by averaging the densities for the four adjacent refined elements. If the adjacent box is coarser, then three densities are averaged to give the density (used for upwinding) of the forth similar box. In TRANAIR, the form of upwinding equation will become as following (refer to [11]):

$$\tilde{\rho} = \rho + \mu \sum_{i=1}^{6} \max(-\hat{V}.n_i, 0) s(i) \sum_j C_{i,j}\left(\rho_{i,j} - \rho\right) \tag{2.18}$$

Where i rotates over the six faces of the box, j over the averaged densities and C_{ij} is the coefficient for each of the four densities contributing to density upwinding, $\hat{V}$ is the normalized velocity at the centroid of the element $s(i)$ is a blending function to make the upwinding differentiable.

The upwinding mentioned above is first-order, introducing an error. For D-regions, special operators must be made based on local information about box adjacency (available in octtree data) to get the accurate value of upwinded density.

2.3 Solution

2.3.1 Linear solution algorithm

The discretization explained in section 2.2 gives a large and non-linear system of equations that are poorly conditioned. To overcome this problem, TRANAIR uses a Newton's method to solve this system by the preconditioned GMRES. Equation (2.1) is the main equation that shall be solved.

Element stiffness matrices are generated using exact moment integrals and multiplication by stored density values (equation (2.15)). Primarily, the finite element operator 'L' is evaluated by multiplying each element stiffness matrix by the current vector of unknown values. T is the constant coefficient discrete Poisson operator on the global grid, which is explained in 2.2.2. To apply the far field condition, source unknowns (Q) are introduced on the global grid and are defined by $T\Phi = Q$. Except near the wakes, L is taken to be equal to the operator on the boundary and exterior of the computational domain (L=T). Therefore, non-zero Q sources are restricted to inside of the global grid. To define Φ (and therefore L) it is needed to calculate $T^{-1}Q$, when Q is given. T^{-1} is evaluated by convolution with Green's function (G). Detail information of how T^{-1} is evaluated can be found in [12]. Now, the linear system of equations can be written as the following:

$$L\begin{pmatrix} T^{-1}Q \\ \Phi \\ \Psi \\ \mu \end{pmatrix} = f \tag{2.19}$$

In which Ψ is the extrapolated values of boundary boxes, Φ is other variables on the refined grid and μ is the doublet parameters on wakes.

Equation (2.19) has to be solved iteratively and since the system is non-definite, the GMRES method of SAAD and SCHULTZ [25] is chosen as the basic iterative solver. For some of the special boxes near the internal boundaries, TRANAIR uses a left preconditioner. Therefore, a *reduced set* of unknowns is generated consisting of all unknowns at corners of boundary boxes, refined boxes or boxes with total temperature and pressure different from freestream values. Therefore, another preconditioner (N) has taken to be the global stiffness matrix limited to the reduced set. For reduced set, it is probable to do a direct sparse factorization of N preconditioner. This is good because of two important reasons:

1- The reduced set is extensively smaller than the total degrees of freedom in the problem.

2- A *drop tolerance* can be defined and used for sparse elimination process allowing small elements in the decomposition to be dropped as they are created. *"In the full potential case, the drop tolerance is the most effective strategy" (refer to [11]).*

To differentiate the Q unknowns of global grid preconditioned by T^{-1} and Q unknowns of reduced set preconditioned by N^{-1} that overlap each other (close to surface boundary), it is necessary to use an additional preconditioner T for the Q source unknowns at global grid points in the reduced set. Therefore, the preconditioned equation at reduced set unknowns can be written as the following (refer to [11]):

$$TN^{-1}\left(f - LT^{-1}X\right) = 0 \tag{2.20}$$

Where X is the matrix of unknowns set as:

$$X = \begin{pmatrix} Q^{(1)} \\ Q^{(2)} \\ \Phi \\ \Psi \\ \mu \end{pmatrix} \tag{2.21}$$

In this equation $Q^{(1)}$ is source unknowns at global grid points that are not in the reduced set and not in stagnation regions (inside the boundary), $Q^{(2)}$ is the source unknowns at global grid points in the reduced set or in stagnation regions, Φ is the values of the velocity potential at points on locally refined grids, Ψ is the values of velocity potential in the boundary basis functions and μ is the doublet strengths at leading edges of wake networks.

Finally, all the residuals R for different X matrix unknowns will be defined. More details of how preconditioned residuals are evaluated, can be found in reference [11].

In this method, the convergence depends deeply on the *drop tolerance* used in sparse solver. "Introducing a drop tolerance sufficient to reduce fill and work by one order of magnitude typically causes the number of iterations required for convergence to at most double" (refer to [11]). In TRANAIR, the drop tolerance and number of iterations can be adjusted in input file preprocessor and solver. For some of the complicated cases, e.g. aircraft full configuration with nacelle, because of high refinement levels, it is necessary to reduce the drop tolerance and increase the number of iterations almost at the same rate. In these cases, because of using more iterations, the time of convergence is considerably higher.

As was mentioned earlier, a sparse factorization of preconditioner N is used for the reduced set of boxes. Sparse solver has a general input capability contributing matrix elements to be entered in any order. This capability is particularly convenient with finite

elements. A drop tolerance is utilized to skip and drop small elements in the lower and upper factors as they are generated. Each element in the decomposition is compared to the magnitude of the diagonal entry of the current row by making a ratio and skipped when this ratio is smaller than the tolerance.

The contributions to the global stiffness matrix (e.g. sparse solver, etc.) have to be sorted and coalesced to produce the final global stiffness matrix. "Most elements of global stiffness matrix have contributions from 8 element stiffness matrices in subsonic regions and about 64 in supersonic regions", (refer to [11]).

To end this section we shall note that one key to maintain sparsity is a good transformation ordering for the rows and columns of the matrix. In TRANAIR, to order the unknowns, *nested dissection* is an optimum method to be used for sparse matrices coming from discretizations of elliptic partial differential equations on uniform rectangular grids. The details of how sorting and nested dissection are done in TRANAIR can be found in [11].

2.3.2 Non-linear solution algorithm

In non-linear cases (mostly transonic), existing a strong shock is probable. If the grid is fine enough, it can even capture the re-expansion phenomenon at the foot of the shock, which causes velocity to increase after the shock. In non-linear problems, TRANAIR uses a damped Newton's method. In each iteration, the solution of a linear problem, which is discussed in 2.3.1, is necessary. This is done by using a preconditioned GMRES algorithm, because interesting practical problems are usually huge and not well conditioned. Refer to [11], for solving the problem F(x)=0 with Newton's method, some initial approximate solutions are given to set:

$$X^{n+1} = X^n + \lambda\left(\delta X^{n+1}\right) \tag{2.22}$$

$$\overline{F}_{X^n}\left(\delta X^{n+1}\right) = -F(X^n) \tag{2.23}$$

In the above equations δX^{n+1} is the solution of the linear system, λ is appropriate step length and $\overline{F}_{X^n}$ is the Jacobian for F linearized about X^n. Equation (2.23) can be solved using GMRES algorithm, without ever explicitly generating the Jacobian for the full non-linear problem. For the full potential equation, the preconditioning is similar to that used for linear systems given in equation (2.20). For non-linear algorithm the definition of the reduced set, which is discussed in 2.3.1, should be modified to include all elements where upwinding is used.

Newton's method is not usually convergent. In the full potential case, the initial field solution is taken to be $\phi = 0$, which usually is not a good approximation to the solution. For this reason, the Newton's method does not usually work well for large problems or for those with shocks. Therefore, for not getting divergence or even very slow convergence in the problem, *damping* of Newton's method should be considered for large transonic problems. Several different damping strategies can be used. One of the damping strategies that is useful in some of the cases is to limit λ (step length) in such a way that the solution X^{n+1} does not have local Mach numbers greater than a predefined value, namely as cutoff Mach number. This prevents incorrect large velocities from stopping the convergence. In TRANAIR, it is possible to use this damping strategy, and typically, the amount of cutoff Mach number is taken to be $\sqrt{5}$.

In large and complicated transonic cases, convergence of Newton's method can be stopped due to a strong shock formation in the wrong location. When this error happens

in the problem, a local damping method can not usually move the shock more than one node in each iteration, resulting in very slow convergence. For these cases, the solver needs something more than local damping. To improve convergence, a "*problem-dependent dissipation parameter*" (refer to [11]) is introduced. This parameter is used in a continuation process called *viscosity damping*. In viscosity damping process, the switching function for density upwinding, calculated with equation (2.17), is corrected by multiplying by a constant number (1.5 to 3), and reducing the cutoff Mach number. In this situation, the amount of artificial viscosity increases and it applies to a larger region of the flow. Then after some Newton steps, the multiplying factor will be reduced and the cutoff Mach number will be increased up to the situation in which the desired level of dissipation is achieved. With using viscosity damping, convergence is fast after the initial viscous problems are partially solved.

The disadvantage of the continuation approach (viscous damping) is the high CPU time (cost) of even partially solving the viscous problems. One of the best features to make up the cost mentioned above is *grid sequencing*, which reduces the need for damping Newton's method. Grid sequencing causes the problem to be solved first on a coarser grid, then the solution of that to be interpolated to a finer grid, and to be used the interpolation as an initial guess to solve the finer grid.

Normally, in transonic cases for a wing or the combination of wing and other parts, it can be predicted that two shocks exist on the wing. One of them is a mild or strong normal supersonic to subsonic shock and the other one is an oblique supersonic to supersonic shock. In TRANAIR or other full potential codes, dense grids have to be used to accurately capture the oblique shock. Basically, for the cases with two probable

shocks, viscosity damping is necessary and is considered for approx. 2/3 of the TRANAIR iteration steps.

2.3.3 Cost of the method

For most of the non-linear cases, the norm of residual is reduced by five orders of magnitude in the solution. For linear problems, eight orders of magnitude in residual are obtained. In the TRANAIR input files, there is a feature to adjust the order of magnitude needed for the residual convergence. It should be noted that TRANAIR has several user-specified parameters that impress cost. For instance, the drop tolerance used in the sparse matrix solver, the number of viscosity damping continuation steps, and the number of Jacobians computed can be referred as some of those parameters.

The total CPU cost of the TRANAIR method has a direct relationship with the number of degrees of freedom N (number of unknowns). The memory storage also increases approximately linear with number of degrees of freedom. Of course, both the CPU cost and memory storage are directly sensitive to the value of drop tolerance used in Jacobian matrix decomposition.

As mentioned earlier, grid sequencing also reduces CPU time and memory external storage significantly and causes a more reliable and better convergence, but a more effective gridding method (in the aspect of cost and storage) that is used in TRANAIR repeatedly is the automatic adaptive gridding strategy which will be discussed in section 2.4.

Finally, the advantage of a Cartesian grid finite element method is evident, since the storage required for the element stiffness matrix grows rapidly as the order of element is

increased. When almost all of the elements have the same element stiffness matrix, very large savings in storage can be achieved.

2.4 Adaptive grid method

In TRANAIR, the grids can be built in two different ways:

1- *Grid sequencing mode*, in which the final grid is specified by the user in the input file and the code automatically de-refines this grid to make the coarser grids in the sequence.

2- *Solution adaptive mode*, in which the successive finer grids are made internally by the code via performing grid refining/coarsening based on the estimates of the local error computed for the elements.

Grid sequencing requires user knowledge of solution characteristics to input parameters that control refinement. In other words, the user should know where exactly to do the refinement for each problem. It is a difficult job, especially for novice users. An automatic solution adaptive refinement capability would solve this problem and would greatly increase the reliability of the method and reduce its cost. That is why studies related to adaptive gridding for CFD problems has been very interesting for researchers for many years.

In adaptive gridding, the elements in a grid with relatively large *error indicator* values are bisected in each coordinate direction. If the previously refined similar elements have relatively small error indicator values, a pack of them containing eight neighboring elements will coalesce together to make a coarser element. The error indicators are calculated from local solution values, after a converged solution is achieved.

Successive initial grids are assumed to differ by at most one refinement level at any point in space and consequently it is always advantageous for cost reasons to utilize some geometry-based local refinement in the initial grid. This refinement is carried out automatically by adaptive gridding according to user specified tolerances. Adaptive method is conservative in such a way that some efficiency and automation are sacrificed for *reliability* and *flexibility* (e.g. more CPU time in adaptive gridding for more reliable results). For flexibility, employing same adaptive grid method and user controls for linear and non-linear problems, subsonic and supersonic free stream inviscid flow analyses, boundary layer coupling analyses, geometry design runs, time harmonic unsteady aerodynamics analyses, all in both 2D and 3D versions of the code, can be referred.

There are five steps in adaptive gridding, which are as follow:

1- Computing local error indicators

2- Computing local error predictors

3- Applying specified grid refinement controls

4- Applying gridding strategy

5- Constructing a grid

To calculate the error indicators, local differences of velocity components can be used. Refer to [13], the indicator for an element outside of all surfaces can be defined as equation (2.24):

$$E_\infty \equiv \max_j \left[\left(\Delta v_1^j\right)^2 + \left(\Delta v_2^j\right)^2 + \left(\Delta v_3^j\right)^2 \right]^{1/2} \tag{2.24}$$

Where, Δv_i^j is the difference across the element's j^{th} edge (face) of the element centroid values of the i^{th} velocity component. The maximum in equation (2.24) is taken over all faces connected to smaller elements. Faces connected to larger elements are not

considered in calculating error indicator. For elements near or crossing a surface boundary, the error indicator E_∞ is defined similarly, but when element faces are lying completely inside of a configuration, these faces are excluded in computing the maximum in equation (2.24). Figure 2-3 illustrates, in the case of a two-dimensional airfoil, the directions in which velocity components are differenced to compute error indicators for five elements A to E.

In equation (2.24), one can also use momentum (ρv) instead of velocity (v), exact element face jumps instead of element centroid differences, sums instead of maxima over element faces, face normal components of v in place of the sum, etc. For the analyses performed in this thesis, velocity components of each element are considered to calculate error indicators.

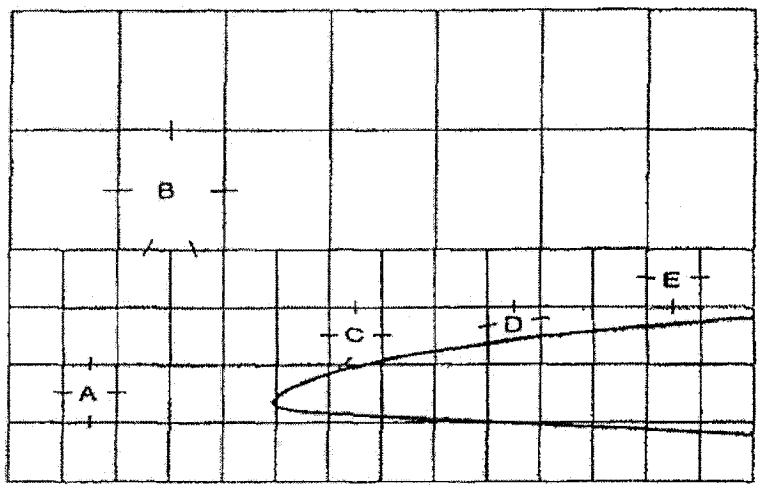

Figure 2-3: *Directions for velocity components differencing to compute error indicators, [13]*

Local error predictors are generated from the error indicators. To do so, TRANAIR uses an algorithm consisting of one or two sweeps of local averaging (smoothing) algorithm. Every sweep consists of nodal values of neighboring element error indicators

and then trilinearly interpolating the nodal values back to element centers to form the predictors. More details of error predictors can be found in [13].

It is important that regions of greatest interest are introduced to the code. The mechanism for that in TRANAIR is the use of specific zones (step 3 of adaptive gridding). A weighting factor for the error predictors is specified for each zone along with minimum and maximum permitted local grid sizes associated with each of the zone's eight corners. The boundaries of these zones and their related controls are introduced via TRANAIR input files. These zones are called LBO regions.

Then, gridding strategy is applied (step 4). It consists of marking some of the elements with the *largest scaled error predictors* to be refined, and marking some groups of eight previously refined similar neighboring elements with the smallest scaled error predictors to be coarsened. There are two essential aspects of the adaptive gridding strategies. They are as following:

1- Because, the problems simulated by CFD are usually steady, local grid refinement is more important than coarsening.

2- A refinement level limiting procedure is used that prevents refinement of the smallest elements in some of the later grids in order to refine more larger elements

There are some intermediate grids, which do not increase the number of elements. Their responsibility is to rearrange the elements of previous grid in order to better equilibrate their error indicators. Such grids are referred as *error equilibration grids [13]*.

Finally, an oct-tree data structure describing the new grid is generated from the previous oct-tree using the list of marked elements and grid information (step 5). Refer to

[13], three different principles are used to determine the choices of error indicator and gridding strategy employed in practical TRANAIR runs. They are as the followings:

1- "*Near-surface flow characteristics are more important than those for off-body flow.*"

2- "*Design engineers typically desire the same accuracy per local chord length scale on many wing-like surface sections.*"

3- "*Minimize the chances that latent (hidden) solution features will go undetected.*"

Repeated local grid refinement associated with some solution characteristics becomes a problem when the characteristics drive the gridding process to the situation that other important solution features cannot be detected due to grid shortage. Such undetected characteristics are referred as *latent features*. A typical example of latent characteristic that is very probable and can occur in 3D steady aerodynamics problems is a very weak oblique shock in subsonic free stream flow on top of the wing or other surfaces. If grid refinement is not forced to occur in the associated regions, latent features can not be detected in an adaptive grid run. Reliable detection of all significant solution features is one of the most important practical tasks of any adaptive grid method for CFD problems. To reduce the chances that latent features will go undetected, the TRANAIR code can be used in a mode, in which a *sequence of grid refinement level limitations* is applied. But, using limited level of refinement has this disadvantage that some areas with high curvature (e.g. leading edge) can not be captured well and then can not resolve well the airfoil stagnation point and leading edge solution details. To overcome this problem, TRANAIR has this capability (by using LBO regions) that as grids get finer and the final

grid is approached, the refinement levels permitted at any point in space get gradually less restrictive until reaching a specified final permitted level for that point.

To finalize this part, it should be noted that estimation of the shock location on a wing can be misled independent of how much additional grid are employed, if one is to severely limit grid refinement in any of the following locations: the wing leading edge, the wing trailing edge, where enforcement of an accurate KUTTA condition is required, or near the wing. But, such harmful effects have not been experienced with the present adaptive grid method, because such grid refinement restrictions are not explicitly specified and do not occur with typical code usage.

More details about adaptive gridding method can be found in [13] and [26].

2.5 Boundary layer coupling

Viscous effects in transonic flow can be taken into considerations through coupling the boundary layer. At high subsonic Mach numbers, boundary layer effects substantially change shock strength and position (normally reduce the strength). Therefore, coupling the boundary layer to the code will have the advantage of correct shock estimation (in addition to other advantages).

The boundary layer solution provides a set of transpiration boundary conditions for the inviscid solver. In TRANAIR, the viscous solution can be attained by coupling one of the boundary layer codes, *A411* or *ISES*. A411 code is described as a loosely coupled code and can work well for fully attached flows, but ISES is a closely coupled one. In ISES boundary layer, the viscous flow and the coupling equations are combined and solved together. This improves the convergence and allows for converging mildly separated

flows as well. That is why, for all of the analyses in this thesis, ISES boundary layer code is used.

In TRANAIR, the influence of a boundary layer on an external inviscid flow can be approximated by a transpiration boundary condition model. By injecting or extracting mass through the boundary layer, this model can efficiently simulate the viscous/inviscid interaction. Several transpiration models can be used in TRANAIR. They are as the following:

1- 1-term transpiration model

2- 2-term transpiration model

3- Mixed transpiration model

The 2-term model has better accuracy (than 1-term) and can more accurately represent general changes, e.g. camber or thickness changes, but is not robust for large movements. Therefore, to utilize the advantages of two models they are combined to form the mixed transpiration model. A schematic of this model can be seen in Figure 2-4. More details about transpiration boundary conditions and the deriving equations for each model can be found in [27].

The way in which a boundary layer is to be calculated on a surface is specified through user-defined *ribs*. A rib consists of an ordered set of one or more rib segments, each containing ordered points of a network. The TRANAIR input processor will automatically try to find *wake filaments* for ribs associated with the lifting surfaces (e.g. wing ribs). Profile drag can be calculated using the boundary layer quantities computed at the end of the lifting wakes (wakes that are connected to lifting surfaces).

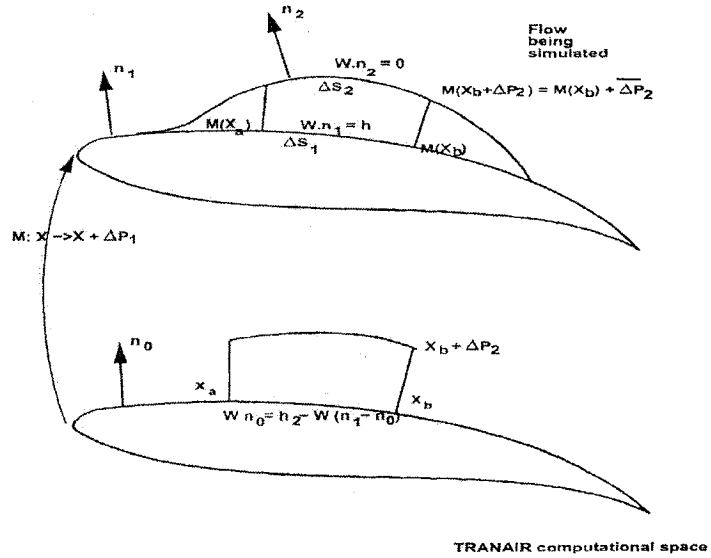

Figure 2-4: *Mixed transpiration model [27]*

For both A411 and ISES codes, wing-like objects (swept/tapered) and axisymmetric objects (body, nacelle, etc.) are simulated with different boundary layer types. For the axisymmetric option, an appropriate axis of symmetry is specified by giving two points on the axis. Therefore, if the object is not even parallel to X direction, these two points can generate the axis and the simulation can be continued. For the wing-like objects, the sweep angle of leading edge and trailing edge relevant to each rib shall be given to the solver.

One of the important parameters in modeling the boundary layer is the *trip location* for transition to turbulent boundary layer. When ISES boundary condition is used, almost for all of the wing-like objects (except horizontal tail, which is too backward) a laminar attached line solution is used. But, if the momentum thickness is taken to be θ, as soon as Re_θ>100, the solution will transition to turbulent. The ISES boundary layer has the capability of *free transition*. This automatic transitioning capability yields a very non-

linear set of interaction equations and can cause more difficulty in solution convergence than a fixed transition location.

In addition to Re_θ, the other parameter that affects the transition start is *kinematic shape parameter*, H_k. In TRANAIR, some of the important boundary layer parameters and thicknesses, namely as shear stress coefficient (C_τ), momentum thickness (θ) and displacement thickness (δ^*) are used just to initiate the boundary layer solution. The value of these parameters should be selected to ensure reasonable values of kinematic shape factor (H_k) and local Reynolds number based on θ (Re_θ).H_k is determined from the shape parameter (H) by equation (2.25):

$$H_k = (H - 0.7175(\gamma - 1)M_e^2)/(1 + 0.2825(\gamma - 1)M_e^2) \tag{2.25}$$

In equation (2.25), the shape factor can be found from the following equation:

$$H = \delta^*/\theta \tag{2.26}$$

In addition, M_e is the local Mach number at the edge of the boundary later.

In laminar flow, if H_k=3 or greater, then the transition starts. Therefore, in TRANAIR, for laminar flow C_τ is chosen to be 1.e-7, θ and δ^* are chosen in such a way that $H_k \approx 2.5$. And in turbulent flow C_τ is taken as 0.03, $H_k \approx 1.5$ and Re_θ>200.

Axisymmetric objects are taken to have turbulent boundary layer over the entire surface. More details about TRANAIR boundary layer can be found in [27].

2.6 Summary of TRANAIR numerical method

TRANAIR solves the full potential equations based on a finite element discretization on an arbitrary configuration. There are many boundary conditions available in TRANAIR to introduce a variety of boundaries to the problem. In TRANAIR, to perform the

discretization, a computational domain is defined and a uniform rectangular global grid is constructed on that domain. Then, the necessary refinements are done in the initial grid. To save the storage and CPU time, the computational domain can be restricted to the regions in which the discrete operator cannot be well approximated by the discrete far field operator. Finite element operators, namely as element stiffness matrices, can be defined by variations of the Bateman equation. Except the boundary boxes or boxes very close to the surface boundary (D-regions), the element stiffness matrices for the similar elements (for example all elements inside the computational domain) are the same and it causes much more saving in storage and CPU time. To have more stability in supersonic regions of flow, a first or second order upwinding is performed via density or flux biasing.

For more linear problems, the linear solution algorithm is used and the element stiffness matrices are generated to be applied to linear system of equations. For reduced set of unknowns or all unknowns at corners of boundary or refined boxes and boxes with different total temperature and pressure, an extra left preconditioner is constructed. For the element stiffness matrix of the reduced set a drop tolerance can be defined to skip relatively small values in each row comparing to the diagonal entry based on the tolerance value and get more sparse operator (sparse factorization). To keep the sparsity, a proper transformation ordering for rows and columns is performed in TRANAIR by nested dissection of matrices. After all these procedures, a linear system of equations is solved iteratively by the GMRES method. For non-linear cases, probably with a strong shock wave, TRANAIR solves the linear system of equations via a damped Newton's

method. In large and complicated transonic cases, in addition to local damping, a problem-dependent dissipation parameter is necessary to converge the solution.

In TRANAIR, grid sequencing and adaptive gridding method reduce the CPU time and storage remarkably. Adaptive gridding is performed based on the local error indicators calculated for each element, the local error predictors, the LBO regions taken around important components and the gridding strategy. Refinening/coarsening strategy is in such a way that latent solution features will not go undetected.

In TRANAIR, integral boundary layer codes (ISES or A411) can be coupled to the inviscid code to account for the viscous effects. The boundary layer used in these codes is a mixed transpiration model. In TRANAIR, it is possible to define a completely laminar or turbulent boundary layer to a component. It is also possible to consider a free automatic transition from laminar to turbulent via the boundary layer parameters introduced to the solver.

Chapter 3

3 TRANAIR REQUIREMENTS AND CONSTRAINTS

Although TRANAIR is a user-friendly software that needs little CFD knowledge to work with, there are many issues and limits that should be taken into considerations. These issues and limits are mostly analytical and the user needs to have a good analytical understanding of the physics. In addition, many of the constraints come from the nature of the full potential equations and the way TRANAIR solves the problem. That is why, it is also necessary to have a good understanding of the full potential model.

In TRANAIR, if the requirements do not meet and/or the constraints are trespassed, many error files will be generated depending on the kinds of error that TRANAIR has faced. These errors can be related to input processor, solver or output.

The requirements and constraints in TRANAIR can be categorized as the following items. It should be noted that the information given about these items is based on the experience with two aircraft models, DLR-F4 and HAWKER 800 full configuration analyses. The detail information of the model implementation and the results for these models are given in chapters 4 and 5.

3.1 Gridding and discretization

As was explained in section 2.2.1, the surface gridding that is generated by the mesh developing software (AGPS) is introduced to TRANAIR by networks of panels. TRANAIR builds its own orthogonal solution adaptive grid. Therefore, the only inputs

that TRANAIR requires are a representation of the surface, flow conditions and the controls for the grid adaptation process.

3.1.1 Abutment

In TRANAIR, two surface networks that share an edge do not have to have their entire points match but at least the first and last points on one network edge must match points on another network edge. It is called *abutment*. Meeting the abutment requirements is one of the most time-consuming tasks that have to be done in AGPS. If abutment is not satisfied completely, there will be leakage from the configuration and TRANAIR is not able to identify the interior and exterior of the surfaces on those areas. The abutment tolerance can be adjusted in TRANAIR. But, using this parameter is a little tricky, because if it is large, then the abutment is not safe, and if it is too small, it causes double or multiple abutments in an edge, which leads to panel collapse when TRANAIR processor attempts to abut near edges. Therefore, an appropriate value for abutment tolerance has to be taken.

Abutment tolerance also depends on the number of digits after the decimal for the geometry points' dimensions given to the solver. Because of that, the *truncation* problem may happen in geometry points, which causes an interior/exterior mismatch. One of the most probable areas for truncation is the boundary of wing and wing tip. Some of the edge panels of wing cannot abut to wing tip related edge panels. To overcome this problem, the best way is to give the geometry points coordinates with more digits to the solver and decreasing the abutment tolerance.

3.1.2 Local Boxes

As was mentioned in section 2.4, a number of rectangular boxes containing each or important parts of the configuration should be introduced to TRANAIR. These boxes are called *LBO* (Local BOxes). Once the LBO regions are specified, the grid adaptation process can be prescribed by user-defined controls. In this step, TRANAIR adds grid into the solution slowly so that gradients can develop and attract grid as the solution matures. Controlling the grid adaptation process is a bit of an art. On one hand, the number of the boxes identified in the first grid, intermediate grids and the target number of boxes in final grid is predefined and limited. On the other hand, one of the things that affect the running time and storage is the number of defined boxes, especially for the last grid that shall be defined carefully. The reason is that with a high number of boxes in grids, a huge amount of memory will be needed without giving extra benefit. The user shall have a good sense of how many boxes have to be used in each grid and in final grid for each case in such a way that both the running time and storage/memory are minimized and the results are accurate enough. In addition, choosing the LBO regions, their dimensions, their diversity and location and the controls for grid adaptation will become very crucial because of the element number limit. One of the strategies that can be taken is to use different LBO regions in TRANAIR. For example, it might be needed to use additional LBO's for the regions with very sharp curvatures (e.g. wing leading edge) or regions with high probable gradients (e.g. shock wave locations). For one of the analyzed cases (DLR-F4) the solution without the special LBO's for the wing leading edge results in a very inaccurate total C_L and it proves the importance of these regions. In Figure 3-1, the wing LBO and some different additional LBO regions on leading edge of

the HAWKER wing in different span-wise locations are illustrated. These additional leading edge LBO's help to have very high refinement levels at a small region close to the leading edge without any necessity to such high refinement levels in other regions even inside the wing LBO and without magnetizing the grids extensively in such a way that other important regions are able to reach the desired level of refinement.

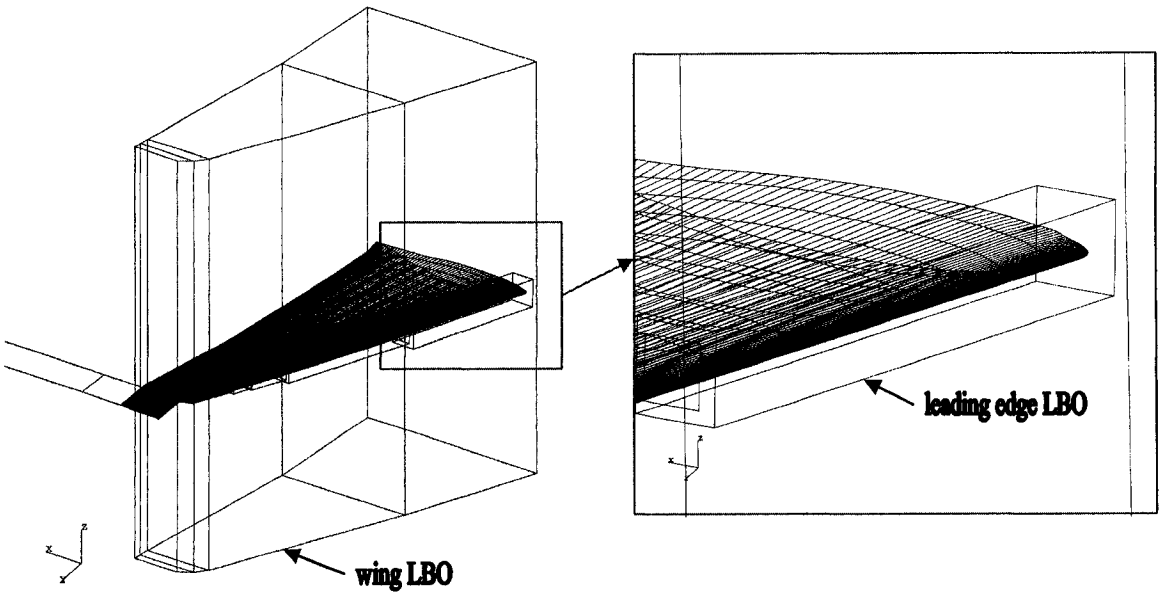

Figure 3-1: *Different wing LBO regions*

It is experience that for wing-like objects the LBO box is better to start almost a quarter of chord ahead of the wing and ends a quarter of chord behind the wing. The very tip of the wing or the base of the fuselage are not desired to be included in LBO as *they have very high gradients and attract the entire grid.* For aircraft configurations, vertical or horizontal tail LBO regions are not recommended to use in general, since they magnetize the grid from the wing and body. It is better to omit them; unless they are critical, that for those cases the maximum box number should be increased further. It is also true for the fuselage, when fuselage pulls off the grid excessively. The wing LBO

includes areas on the fuselage near the wing root, which is the primary fuselage area requiring adaptation. Therefore, in some cases the fuselage LBO can be skipped or shrunk to a small area of the fuselage around the wing.

3.1.3 Grids

Grids have different requirements for different objects. There are two points to consider when evaluating grids on a wing-like object. First, the geometry should be adequately represented. For an airfoil, the freestream panel-panel angularity change should be kept below 5° to look relatively smooth. Second, there should be enough grids to capture aerodynamic effects including span-wise variations and shocks. If significant aerodynamic gradients across a single panel or a few panels are found, adding grid density is probably a good idea. In addition, TRANAIR does not have any problem with the skewed grid, provided it exists in relatively flat regions. In some regions of the fuselage or vertical tail, the skewed grid can be used.

One of the ways to make consistent gridding with right abutment for the intersection of some parts (e.g. horizontal and vertical, nacelle and strut, etc.) is the use of *patched grids* at intersections. In the analyses of this thesis, many patched grids are used because of the complexity in meshing the whole geometry configuration and for keeping the mesh compatible to use in TRANAIR. Patched mesh limits the extend of projecting one network (like horizontal) into another network (like vertical) without making any problem in abutment. In Figure 3-2, the patched gridding interface between horizontal and vertical tails of HAWKER 800 is illustrated.

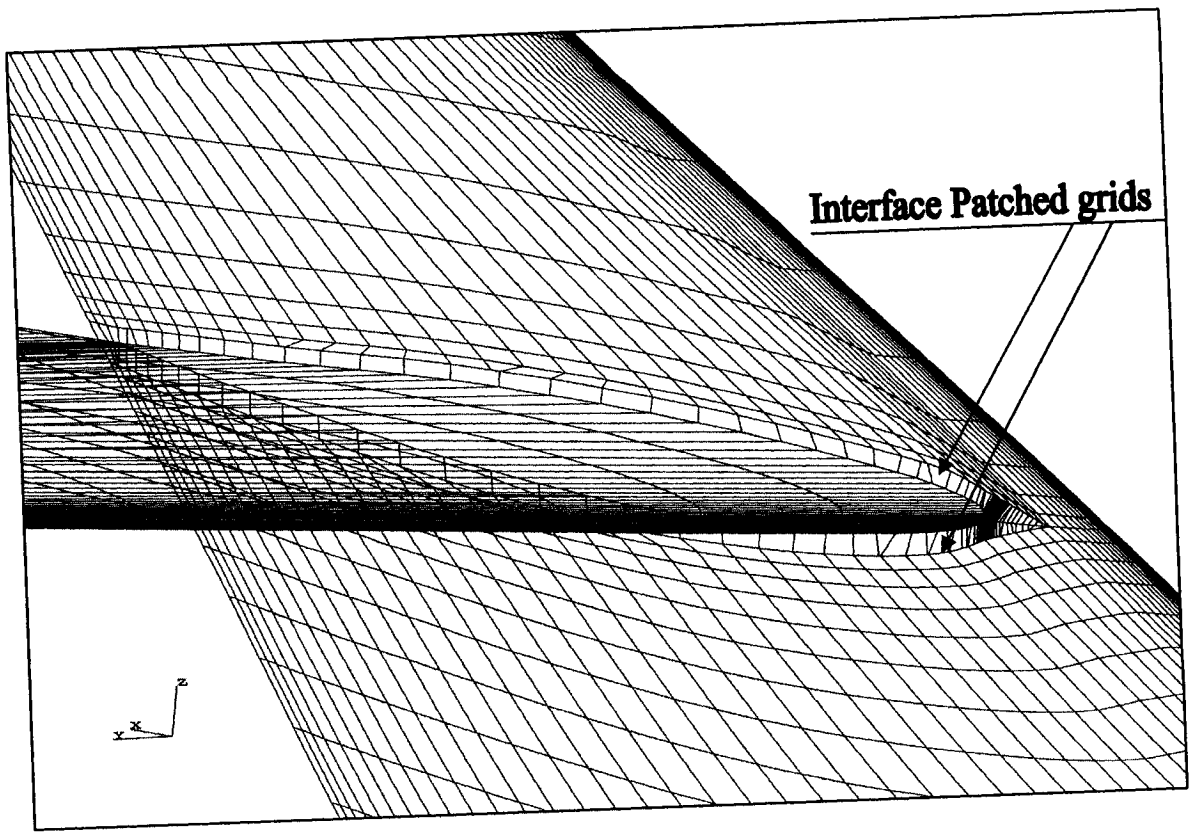

Figure 3-2: *Interface patched grids between horizontal and vertical tails*

When aft-mounted nacelle exists in the configuration, the method to do gridding is to split the fuselage with additional upper/lower segments. The wing/pylon/vertical abutments shall be dealt by splitting the body up into multiple upper/lower sections. For the Hawker 800 case, five body sections (overall) are used in the wing/pylon/vertical configurations, each going from nose to tail and progressively wrapping up around the fuselage (five sections are upper/lower for wing, upper/lower for pylon, lower for vertical). Abutments are handled by a patched grid boundary to de-couple the grids.

Finally, it should be noted that the *quality of gridding* is very crucial for convergence. In one of the new gridding packages of AGPS (BizJet package developed by Boeing in 2007) improvements are made for creating grids with higher quality fore and aft on the body. It is done by making a bunch of cuts in constant X and gridding up the resulting

curves. It improves the mesh robustness. Moreover, great improvement is made in gridding the wing/body leading edge region. This causes the HAWKER case with nacelle converges easier at a Mach number of 0.75 (M0.75) and even more up to M0.77, but with lower quality grids convergence even in M0.72 is made with many difficulties.

3.2 Wakes

As was explained earlier, in full potential solvers the use of wakes is mandatory. There are different types of wakes used in TRANAIR, which are mainly as follows:

1- *Viscous wakes* (KT14) that permits simulation of thickness through transpiration and is an essential feature for viscous calculation of the object attached to it. The viscous wake shall continue at least a chord downstream from a lifting surface and then connects to a KT18 wake.

2- *Standard wakes* (KT18) or non-viscous wakes are attached to the configuration or a downstream edge of viscous wakes.

3- *Carry-over wakes* (KT16 viscous or KT20 non-viscous) that are used to define wakes with collapsed upstream edge or wakes with constant doublet strength.

4- *Design wakes* (KT9) that are commonly used to represent powered plumes of nacelles.

For all types of wakes except the design wake, the boundary conditions applied is as follows:

$$\vec{W}_u.\hat{n} - \vec{W}_l.\hat{n} = \beta \tag{3.1}$$

$$\phi_u - \phi_l - \mu = 0 \tag{3.2}$$

where $\vec{W}_u$ and $\vec{W}_l$ are the upper and lower mass flux of the wake, μ is the equivalent doublet strength, ϕ_u and ϕ_l are the upper and lower perturbation potentials. For all the non-viscous wakes, the parameter 'β' is taken as zero.

To account for induced drag due to the wing tip, the wing tip wake has to be added as well, which in nature is similar to standard (KT18) wakes. Wing tip wakes should be at least as wide as one of the coarsest boxes in the global grid. These wakes should also not be included in any of the wing LBOs, as they pull the grids off toward themselves and the grid distribution in more important areas, such as the wing root, will become insufficient. In Figure 3-1, the location of the wing tip wake and its width can be seen.

Carry-over wake should be a point-wise connection between the body and a linear line on the standard KT18 wake. In fact, it can be said that for all the lifting objects there should be KT14 and KT18 wakes one after another. Both of these wakes shall be connected to body by carry-over wakes. The first requirement for a carry-over wake is that it matches the body along a network edge. In most cases, it should also be normal to the solid surface. Carry-over wakes must perfectly abut the wing wakes (KT14 & KT18) grid edge.

It is not necessary to extend the wake more than typically 50 chord lengths. Too long wakes only make the storage larger without extra benefit. For some cases in which truncation problem exists, it is needed to input the points coordinates with more digits. For these cases, it is sometimes beneficial to limit the wakes length more in such a way that their points coordinates become one digit less and prepare enough space for one more digit after the decimal. In Figure 3-3, different kinds of wakes are illustrated.

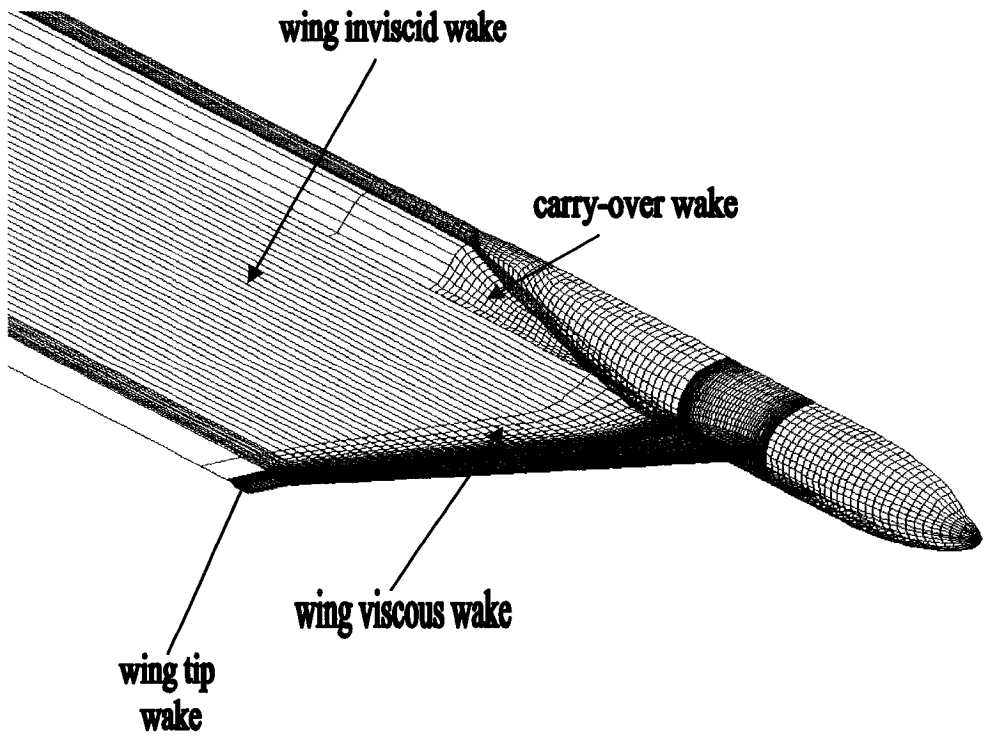

Figure 3-3: *Different wakes for DLR-F4 aircraft configuration*

Finally, it should be noted that the fuselage is closed at the end with a base surface with special boundary conditions. Viscous and standard wakes should also attach to the fuselage at the fuselage base to account for fuselage calculations.

3.3 Surface smoothness and grid quality

For the HAWKER 800 case, the geometry input files generated by the laser scanning produced a geometry with some unsmooth surfaces. These problems caused the quality of the out-coming mesh to be less than what TRANAIR expected. The roughness, especially when is the case for the wing, causes many convergence problems in the TRANAIR solver. As an example, for the HAWKER 800 case, which has a rough wing surface, the convergence at M0.75 is too difficult. Basically, if the Reynolds number becomes larger

and passes a limit (varying by case), the solver fails due to surface smoothness. For the HAWKER 800 case, the limit of Reynolds number is approximately 17 million at M0.75, when flying at T=228.72 K and P=30091.5 pa.

One way to overcome the surface and mesh roughness problem is using a mesh *smoothening technique*. It can be done in AGPS by the smoothening commands. The problem of these smoothening commands is that they change the geometry. The decision to smooth a surface mesh with these commands will depend on the priorities of the problem that is analyzed, because it alters the geometry. It is possible to freeze some of the important points (e.g. leading and trailing edges) and do the smoothening locally in some special regions. In this way, the geometry change will be minimized. For the HAWKER 800 case, the mesh smoothening with freezing important points is used. It not only helps for converging the case at larger Mach numbers, but also improves the lift and pressure distribution on the surface.

Another way to remove the roughness issue is to use filtering software that is developed for this purpose to skip all the existing wiggles and recesses. This approach is only recommended for non-lifting surfaces (e.g. fuselage) only when the lift analysis is done (not drag), because it alters the geometry extensively.

Smoothing is best accomplished by *re-lofting* the objects, especially lifting objects. Re-lofting slices the object into cuts with tight control. Then the cuts are discretized and combined to form a baseline grid and the surface is fitted to form a smoother baseline loft. Wing re-lofting is a very good and efficient way to remove surface roughness, but should be done very precisely to avoid modification of the geometry, especially for regions with very high curvature and surface gradients (e.g. leading edge) with tight

control of the cuts. Re-lofting causes, the wing cut curves (that are to be used for griding) to be much more *planar*. If the cuts are not planar, they cause problems in convergence near separation (or for the areas with mild separation). For the HAWKER 800 case, smoothening the wing only was not enough for convergence at M0.75, and wing re-lofting had to be used as well. For this case, the body re-lofting helps in avoiding many problems due to roughness, to lack of a clean airfoil-like wing/body intersection, and to difficulties having the wing in its original vertical position, etc.

In the new meshing AGPS package developed by Boeing in 2007 (BizJet package), professional grid smoothing feature (elliptic smoothening) has been added to improve the mesh robustness.

Finally, about the smoothening of the wakes it should be noted that the wakes are generated manually from the end of the lifting objects. Basically, for the wakes the Y and Z coordinates of all points are constant and X varies. Therefore, the wakes are usually very smooth. The only wake that may suffer from roughness is the carry-over wake (KT20). By the way, the smoothness of carry-over wakes is not very important for the solver and does not have any impact on the results, as KT20 wakes only need to map vorticity.

3.4 Input data

If the solution is normal and is not a restart or design type, the following input files are necessary for the TRANAIR solver:

1- *Files generating control file ($case.files)*, that indicate to the solver which kind of output information should be created during and after the run. As an example, the information regarding boundary layer, different kinds of drag, surface properties,

moments and forces, etc. may be added or neglected by the controls used in this file.

2- *Input deck ($case.i.inp)*, that has all the controls necessary for solution, boundary layer, LBO regions, mesh adaptation, property inputs (e.g. Mach number, angle of attack, etc.), surface properties controls, reference dimensions and many other useful controls and inputs for the solver. In the input deck many controls can be applied, for example prescribe the C_L and have it find angle of attack (AOA) or prescribe a series of AOA's and have it run the results for all of them at one time. One can specify the elevator and have it run through a series of deflections, or can specify design deflections and have it change the geometry to match a drag, etc. *The options in input deck are endless.*

3- *Geometry coordinates file ($case.poi)*, that contains the coordinates of all the mesh nodes representing the surfaces and wakes. It also contains the values of the 'β' parameters for all the wakes explained in section 3.2.

4- *A run control bash file ($case.job),* that specifies the locations in which all the generated files are going to be saved, the name of the case and the mode in which TRANAIR should run.

There are some important issues regarding the input deck (file 2) of TRANAIR:

For TRANAIR the Reynolds number is needed only when the viscous analysis is done and the boundary layer model is assessed. This input is in the form of Reynolds per unit mean aerodynamic chord (M.A.C.).

In TRANAIR, most of the input parameters are dimensionless. Because of that, there is no need to set some of the parameters. For example, temperature and pressure in

TRANAIR code are non-dimensionalized by free-stream values and hence do not need to be set manually. The specification of Mach number, Reynolds number and viscosity is sufficient to determine all other free-stream flow parameters for external aerodynamics. Mach and Reynolds numbers are input, and the viscosity is hard-coded via the viscous model. It is actually dangerous to specify extra variables for the flow condition, since they may not be specified consistently, which leads to ambiguity for the solver.

3.5 Boundary layer effects

As was mentioned earlier, the boundary layer code is coupled to the TRANAIR inviscid code to account for viscous effects. One of the limits related to boundary layer is *too large transpiration* problem. It happens, when a part of the boundary layer pierces the inviscid part of the flow more than what is expected, based on the calculations done for the boundary layer thicknesses. This problem can exist when there is a rapid change in the geometry in regions where it is not expected to be such large changes and gradients. The transpiration problem, in fact, seems to be similar to the separation of the boundary layer at the sections with rapid closure. For business jets, the transpiration problem in TRANAIR can be seen further, because of their limits in fuselage geometry, especially its length. For the HAWKER 800 case, a boundary layer 'too large transpiration' problem exists but is limits to the aft end of the fuselage on both upper & lower body grids (body upper and lower the wing). It happens due to the rapid closure of the aft body grid at the last row, where the diameter pinches down to quarter the size in one point. The issue arises because of the extreme closure of the HAKER 800 body and it is incompatible with the default aft body cut in the TRANAIR grid automation.

When the transpiration problem happens, the TRANAIR code does not converge. There are two ways to overcome this issue:

1- If it happens at the aft end of the body, re-gridding the body base at one or some sections forward can be useful. In this way, the areas with a large transpiration problem will be out of the calculations with only a small change in geometry and consequently in lift and drag forces. The limit of applying this method is the vertical tail. For some configurations, the position of the vertical tail does not allow for enough movement of the body base forward.

2- Freezing the boundary layer ribs in the sections where transpiration happen. If the boundary layer calculations are skipped in these regions, the boundary layer parameters will be frozen with the values for those in last point's calculations. In fact, freezing does not disable the viscous effects in the problematic areas. It only uses the boundary parameters of the other similar points.

In the HAWKER 800 case, both of these two methods are used.

Whenever the transpiration problem is not limited to a small region and is distributed in whole geometry (e.g. body), the reason may be not transpiration itself. In most of these cases, the reason for such a problem is *scale dependency*. It is also called a truncation related abutment issue. This problem is related to the scaling dependency and not the result of an issue with the boundary layer. However, the solver senses a boundary layer separation at many points and fails. This problem can be solved by scaling up the dimensions by 1k or 1000k, whichever applies better.

In TRANAIR, a fully turbulent/laminar boundary layer or a mixed one with predefined trip location can be specified for each viscous object. Normally for 1:1 scale cases with

high Reynolds numbers, it is recommended using a fully turbulent with trip specification, as the laminar specification is probably physically impossible to achieve physics at these conditions. But, in most wind tunnel model analyses in TRANAIR, the wings and body are laminar with trip specification to avoid the inconsistency of a short laminar run. It's important to set the Reynolds number to the desired values and remember that wind tunnel simulation typically includes a trip strip that transitions and modifies the flow (typically 10% chord), while flight simulation is typically fully turbulent [27].

In viscous analyses with shock waves, the shock-boundary layer interaction shall be taken into consideration. When shock waves appear, the pressure at the surface will be smeared out a little due to two effects. First, subsonic flow in the boundary layer smears out the pressure distribution of the shock wave above the boundary layer (physical effect). Second, limits on cell size and numerical dissipation will smear out the shock (numerical effect). It shows itself like a bunch of Mach contours very close to each other in a small region. They create a thick line instead of clear contours at those areas and smears out the shock clearly. Other methods to recognize the shock waves in TRANAIR or other solvers using integral boundary layers include looking at boundary layer characteristics (δ^*, δ) and skin friction which both jump at shock locations.

Inviscid versus viscous flow analysis can be challenging since Euler and full potential solutions have limited amount of dissipation to stabilize the shock location. Anthony Jameson [28] illustrates this well and demonstrates that two shock locations are possible for the wing, unless dissipation is added. For this purpose, most inviscid solutions include some amount of dissipation to stabilize convergence. Several Euler codes add enough dissipation to move the shock to approximately the right location. *TRANAIR's*

dissipation is minimal, so it can be said that the inviscid TRANAIR solution is more inviscid than most CFD solutions. Theoretically, increasing the Reynolds number to infinity (or very large) should yield inviscid results. Practically, CFD viscosity models and numerical schemes are not designed for very high or very low Reynolds numbers. The best thing to do, when analyzing shock location, is to compare pressure distributions at constant C_L as well as constant α (angle of attack). For attached flow, constant C_L comparisons are typically better since they reflect how an aircraft actually flies. For separated flow, constant α comparisons are better. In the analyses of this thesis, only constant α comparisons are done between TRANAIR and Navier-Stokes. The reason is that it is not possible to prescribe a C_L and change α appropriately to give such C_L in Fluent. For the DLR-F4 case, an inviscid/viscous analysis is reported in chapter 4.

To finalize this part, it should be noted that TRANAIR and almost all of the full potential codes could not converge when strong boundary layer separation exists. That is why these solvers are used mostly for the aircraft analysis at cruise with angle of attack close to zero, in which the separation probability is minimal. But, in higher positive or negative angles the TRANAIR code can not be used (because of strong separation) and basically the Navier-Stokes codes can be used much better for these circumstances. It should be noted that increasing the Reynolds number leads to more attached flow. But, in TRANAIR, Reynolds number is an input parameter and can not be changed within the run.

3.6 Mach number and angle of attack

In TRANAIR, there is a Mach number limit for convergence depending on the flow conditions (Reynolds number, etc.) and the configuration geometry. As an example, for

the HAWKER 800 case, M0.75 is a challenge in TRANAIR. For this configuration, the extracted cruise Mach is about 0.70 and the maximum operating Mach is approximately 0.77, considering the cruise altitude to be between 30 to 35 Kft, which is typical for this kind of aircraft [29]. This proves that M0.75 is close to MMO for this case, which is typically hard for TRANAIR to reach due to the probable separations that may happen. Because of the above-mentioned issues, convergence at M0.75 cannot occur for the HAWKER 800 case, unless the necessary modifications in surface roughness, boundary layer large transpiration areas, etc. are applied. For other geometries, users should have enough experience to overcome the convergence issues, when working at Mach numbers close to MMO.

For the cases of very high Mach (close to MMO) one of the ways to get full convergence, if partial convergence exists, is to decrease the drop tolerance for the matrix decomposition (half or even less) via the necessary adjustments in the input file. It will improve convergence, but the time cost will be larger, as the number of iterations has to be increased almost with the same ratio.

In TRANAIR, increasing or decreasing the angle of attack (AOA) from zero can avoid convergence due to separation. As an example for the HAWKER 800 case, separation is likely on the horizontal tail at -2^{o} angle of attack. The reason is that the horizontal tail has to produce negative lift and to satisfy this it takes an angle of approximately -1.6^{o} with the aircraft horizontal axis, when flying parallel to free stream flow AOA=0^{o} (as shown in Figure 3-4). Therefore, the tail angle of attack will be roughly -3.6^{o}, when AOA=-2^{o}. Transonic flow separation at high Mach numbers and -3.6^{o} angle of attack is not surprising. TRANAIR will generally fail to converge for fully and strongly separated

flows. For the HAWKER 800 case, AOA= -2° condition is close to the limit in TRANAIR.

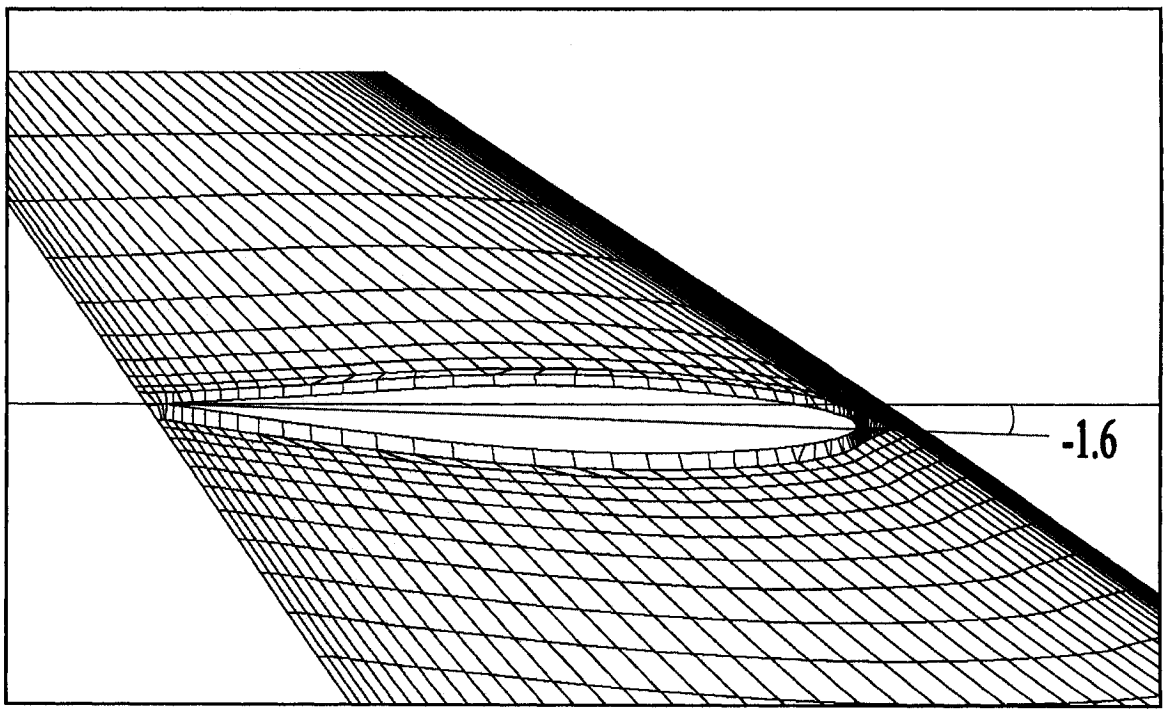

Figure 3-4: *HAWKER tail negative angle with respect to free stream direction*

For some cases with nacelle, it is possible to improve convergence by increasing the angle of attack, especially on the aft body due to the flow off the pylon, which lifts down at $\alpha = 0^{\circ}$. On a large transport aircraft that Boeing has analyzed once, convergence was best at $\alpha = 1^{\circ}$ not at $\alpha = 0^{\circ}$, since the wing had lower surface shocks and separation at $\alpha = 0^{\circ}$ flow. For the HAWKER 800 case (with nacelle), the same phenomenon is experienced. For this case the best convergence is also reached at $\alpha = 1^{\circ}$, and in contrary to that, convergence at $\alpha = 0^{\circ}$ is difficult due to wing outboard separations happening in lower surface. Because of this fact and considering that aircraft has to increase its height gradually from the beginning of cruise to the end (due to weight issues), the cruise angle

of attack is considered to be between 0^{o} and 1^{o} for some aircraft cases, when the aerodynamic analysis is being doing.

3.7 Configuration components

Body

As was mentioned in section 3.5, rapid closing of the body in the aft end causes the large transpiration problem and separation of the boundary layer. In section 3.5, the methods to overcome the transpiration problem are explained, but the best way is to consider all these issues in the design time. Design should avoid rapid closing of the body in the aft end, but it is not the first priority in design and lift to drag ratio is more important.

Vertical tail

One of the configuration problems related to the vertical tail is the leading and trailing edge sweep angles. Sweep angle should not exceed 90^{o}; otherwise, the relevant boundary layer rib calculation will have errors. For some kind of business jet configurations, such problem exists in the blunt vertical root, where the light is mounted. The sweep angle for these parts can be set to zero, since only a small area of the vertical has high sweep angles.

As the number of the grids is very crucial, it is not needed to have detail vertical tail tip gridding, since it is a non-lifting surface. It avoids pulling off the field grids close to this part. In addition, the inviscid vertical on the aft body might actually make the run worse at higher Mach numbers (for some cases when failure of convergence occurs on the body), since the boundary layer tends to reduce shock strength. The run cases with viscous vertical are more robust. Therefore, considering that it is possible to take

boundary layers for some of the components and take the others as invisicd, it is recommended to use a viscous vertical for all the analyses.

Horizontal tail

When the lift analysis is major part of the aerodynamics, the horizontal tail has a less priority comparing to wing and body. It only makes a negative lift, which is much less than the positive lift generated by the wing. The horizontal tail sensitivity is critical, if the purpose is to determine the drag for a trimmed aircraft and not just a fixed tail angle. In this case, special LBO regions are needed for horizontal tail.

Wing

One of the limits that have been experienced in most of the business jets is the wing position issue. The lower part of the wing/body intersection does not include a clean 'airfoil-like' curve in most business jets, because the surfaces overlap or are close to overlapping. Basically, wing is usually kept in the lowest possible elevation in business jet designs, because the wing and nacelle shall have minimum effects one to another and also lift shall be maximum. There is such a problem for the HAWKER 800 case and in some of the analyses the position of the wing has to be moved up to 15 cm. The new version of the BizJet package in AGPS for meshing wing/body/nacelle, which was released at the beginning of March 2007, contains several new features including the ability to model very low wings. It looks for an exact wing/fuselage intersection and if it cannot find one, it will project the inboard edge (locally) to the nearest point on the body. Alternatively, the wing can also be moved up slightly to get a geometric intersection and it will work fine as well, because its effect on lift is small. For the HAWKER 800 case, it

is found that moving up the initial wing position for 20 units (20mm in full scale) is sufficient to grid the configuration.

3.8 Nacelle analysis

In TRANAIR, there are three ways to model the nacelle for external aerodynamic analysis. They are all shown in Figure 3-5:

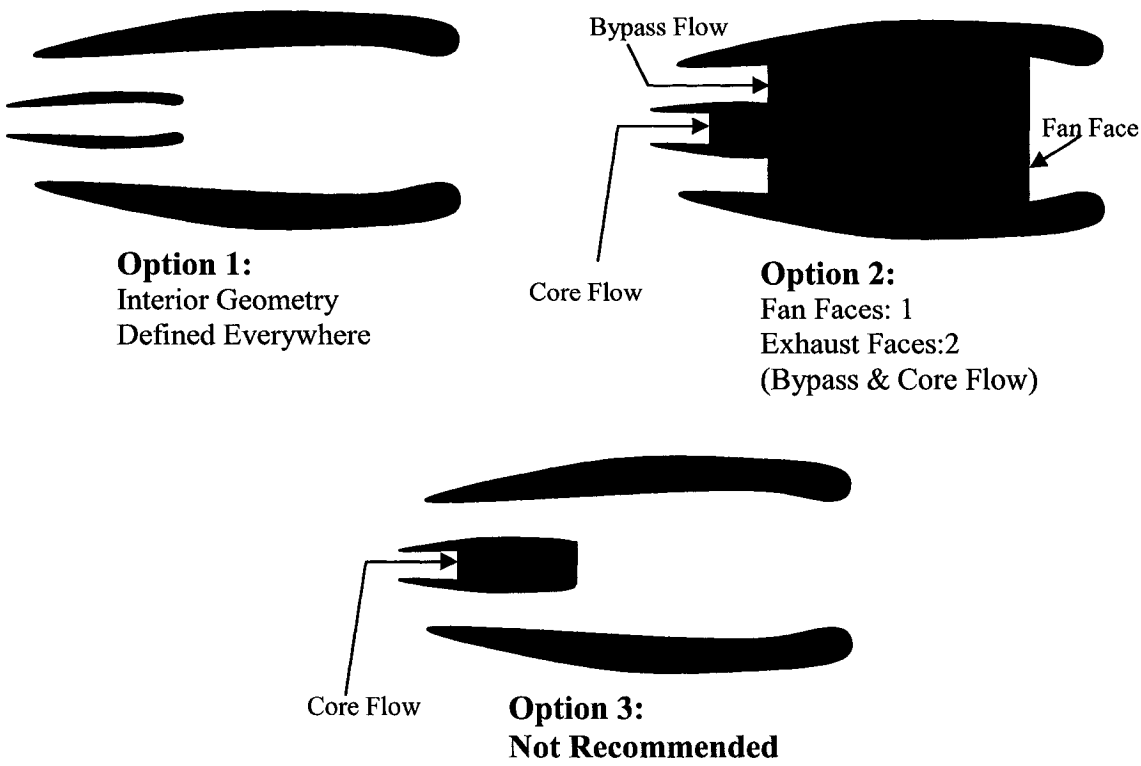

Figure 3-5: *Nacelle modeling options*

Flow-Through modeling can be achieved with either option 1 or 2. If the interior geometry is not fully available (which is the case for the HAWKER 800 nacelle), option 2 is the best. Option 2 is actually the safest nacelle modeling, because in the inlet fan-face, the mass flow rate can be adjusted and in the outlet exhausts the amounts of total pressure and total temperature ratios can be set. But, for this option, it is necessary to have an understanding of the values of these parameters, or to get them from the engine

manufacturer or from similar analyses registered in different papers. The fan-face and exhaust conditions may be set to simulate *flow-through* conditions or *powered* when using option 2.

It is also possible to use option 1, but it is vital to have the exact geometric information of the surfaces inside the nacelle, including nacelle and core inlet surfaces. Option 3 is not recommended, when there is not enough information of the nacelle inside geometry and engine exact information. The reason is that for this option there is only control on total characteristics of core flow and not on the mass flow rate in inlet. In these situations, the position of the core exhaust face shall be very exact and cannot be approximated; otherwise, the flow might be choked very easily in the nacelle duct.

One other option that arises in nacelle modeling is as shown in Figure 3-6. In this modeling type, all the faces (fan, by-pass and core faces) exist, but the core face moves aft to the end of the core cone. The reason of considering this option is that the geometry information of core cowl inlet surface is not available for many nacelle cases. TRANAIR does not recommend users to use this option; because it needs that the exit of fan and primary ducts should be smaller area than the base network (like converging nozzle).This helps stabilize the analysis and is representative of the flow. Therefore, using this model can cause sever problems in convergence. It is also possible to treat the core cowl as a solid object with no exhaust face, but this would probably send too much flow through the bypass that would choke the nozzle.

For powered nacelle analysis, material property specifications for different exhaust regions should be defined, as shown in Figure 3-7. These materials and their corresponding regions shall be defined in the input deck of TRANAIR. Material

properties here mean the total temperature and pressure ratio of that region to those of the free stream. For flow-through analysis, there is no need to specify regions with other material specifications.

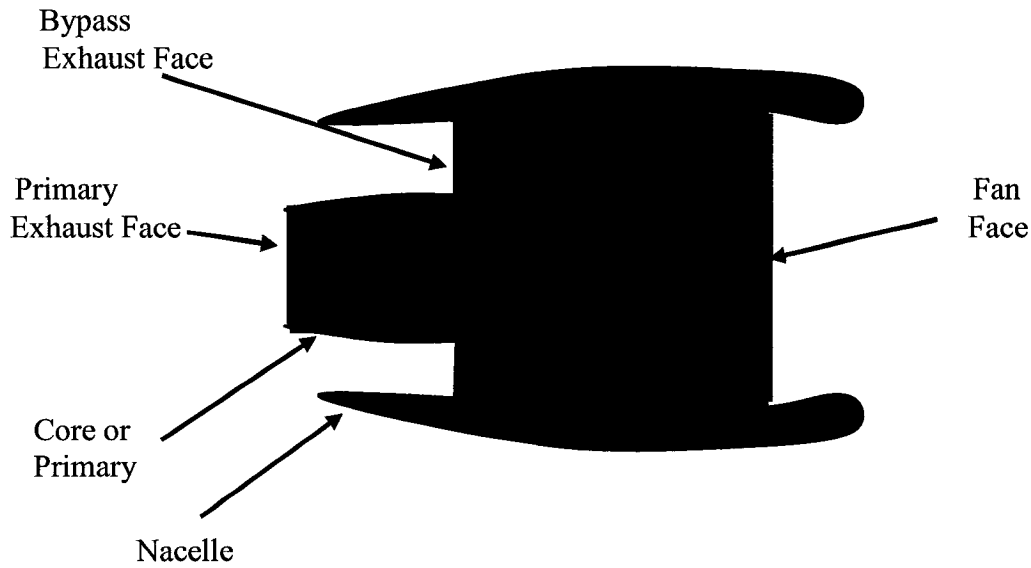

Figure 3-6: *Incorrect nacelle modeling in TRANAIR*

The critical point in nacelle modeling is '*not to make things complex*'. The primary nacelle effect will be how it affects the flow over the wing. The critical physics to capture are ingesting/sucking the proper airflow without choking the internal flow and

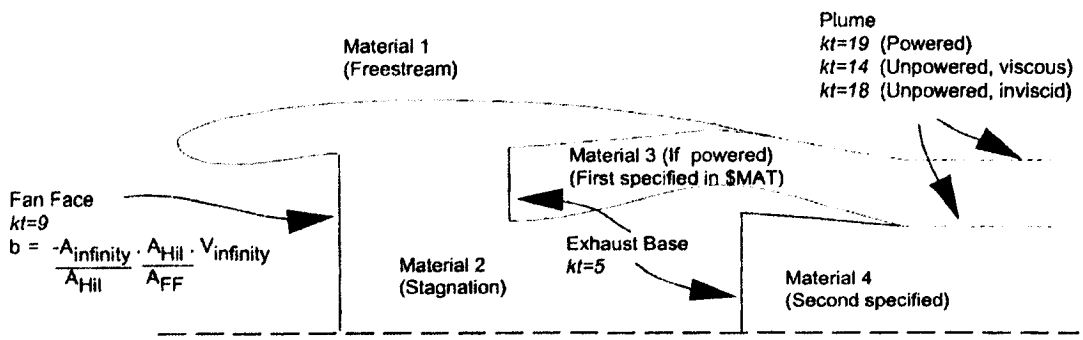

Figure 3-7*: Material definitions for nacelle in TRANAIR [27]*

providing the correct external lines with minimum drag. Therefore, only the elements shall be used that satisfy the above conditions without too much complexity. In most industrial analyses, a single exhaust face is used to simulate flow through conditions (instead of two exhausts) as a short-cut to dealing with the primary flow. *Actually, for flow-through modeling the details are not critical, unless precise drag values or choke/spill the internal flow is of interest.*

For powered nacelle cases, the inflow mass flow rate will change; therefore, fan-face with perturbation mass flow specified (KT4) shall be used for them. But, for flow-through cases different type of fan-face with total mass flow specified (KT9) is used. For the nacelle analysis in TRANAIR (both powered and flow-through), it is better to omit the fan hub. The critical point is ensuring that the inputs (e.g. area ratio) are consistent with the geometry. The area ratio ($A_\infty / A_{fan-face}$) is altered slightly with the inclusion of the fan hub and this must be taken into account. This is even more important at the core exhaust. If the core plug is included, exhaust settings will change significantly. If the correct amounts of fan and exhaust surface areas are not considered, the results will be off. Therefore, introducing incorrect surface areas can be one of the dominant sources of error in the C_P results, when option 2 is chosen for nacelle modeling. In chapter 5, nacelle modeled similar to option 2 will be analyzed by TRANAIR and results will be compared with Navier-Stokes to see these effects.

For the nacelle, the exhaust face positions should not be too far forward, because it can potentially cause adverse effects. The biggest effect of that is choking of the exhaust flow. The toughest part in adjusting the horizontal position of exhaust faces is maintaining consistency so that the mass flow is consistent between inlet and exhaust

faces while specifying pressure & temperature flow conditions. For the number of exhaust faces, it can be noted that single exhaust face for core (primary exhaust) is well as an approximation, as long as the exit face boundary conditions are consistent with the larger area (in equations (2.9) and (2.10), q should be the velocity of larger area) and the bypass to primary flow ratio is not important for the configuration. It is the case for the HAWKER 800 nacelle analysis for a flow through situation. In addition, a single by-pass exhaust face is standard in industry, as the nacelle bypass flow for a body mounted (aft-mounted) engine does not interact strongly with the wing/body or empennage.

For the exhaust wakes, it should be referred that core cowl exhaust wake can be considered as inviscid (following industry practice), therefore a KT18 wake (an inviscid wake) is sufficient. By the way, a KT14/KT18 wake system (a viscous wake followed by an inviscid) will work fine as well. Contrary to core cowl wakes, the by-pass exhaust shall contain both viscous and inviscid wakes. The configuration of the wakes has a great impact on the drag computed for the nacelle.

3.9 Summary

In this chapter, many issues regarding the limits, boundaries and the requirements related to working with TRANAIR and getting an exact solution out of this solver are described. As a summary, the explained items can be numerated as the followings:

1- The best surface representation in TRANAIR is a set of panels that are dense enough to account for the high gradients and that are abutted completely in the boundary of two networks.

2- Due to limits in the number of elements in each grid for minimum storage/CPU time issues, it is necessary to use different local box regions (LBO) with different

adaptation controls around the various aircraft components. For not magnetizing the grids toward an unimportant part of the field, choosing the LBO regions, their dimensions and diversity and the related adaptation controls are of vital tasks of the user in TRANAIR.

3- In the interface of some of the components, it is occasionally needed to use patched grids. Making such kind of grids in AGPS needs skills.

4- The quality of grids depends directly on how grids are made in AGPS. Using the best ways of gridding with right commands in AGPS helps the user do an efficient analysis with more exact results in TRANAIR.

5- In all potential solvers using the wakes are mandatory. In TRANAIR, there are different kinds of wakes that used for different purposes. They are mostly used for drag calculations of different components and circulation/lift calculations of the lifting objects.

6- Smoothness of the surfaces analyzed in TRANAIR has a great impact on convergence and the results, especially at higher Mach numbers. To improve the quality of the mesh, different smoothening methods are taken; among those, surface re-lofting can be referred as the best. The most important point in smoothening is not to change the original geometry largely, especially for the lifting objects.

7- In TRANAIR, different input files are necessary to introduce the surface mesh representation, flow characteristics, solution controls, reference dimensions, etc. As most of the input parameters are dimensionless, many other parameters can be calculated by them, and there is no need to input the other parameters.

8- For viscous TRANAIR analysis, the boundary layer separation or large transpiration of viscous to inviscid parts of the flow causes solver failure. Separation can have many reasons that only expert users can distinguish the right sources. In TRANAIR, similar to other solvers, viscous versus inviscid analyses are very useful to see the advantages of boundary layer coupling, shock/boundary layer interaction and many other important issues related to viscous effects.

9- In TRANAIR, based on the applicability and the scale of the case, fully laminar, fully turbulent or fully laminar/turbulent boundary layer with specifying the trip location can be used. Choosing the appropriate boundary layer and the location of the trips needs enough experience and skill.

10- There are limits in free stream Mach number and angle of attack, when analyzing the aircraft in TRANAIR. Performing a correct solution with Mach numbers close to maximum operating Mach number of the aircraft can be very challenging. In addition, high positive or negative angles of attack cause separation of the flow on the wing or horizontal tail that in turn concludes the solver failure. TRANAIR is one of the best solvers for analyzing the aircraft at cruise condition (cruise Mach number and angle of attack close to zero).

11- In TRANAIR, there are limits related to the geometry of different aircraft components configurations, adjustments, etc. When working with TRANAIR, the user shall have enough flexibility and knowledge to sacrifice the unimportant features of the problem for the important items.

12- Nacelle can be simulated with different methods in TRANAIR. When the exact geometrical information of the nacelle inlet duct is not available, the best way to

simulate the nacelle is to take a fan-face and two exhaust faces. In this method, the X position of fan and exhaust faces is important to get correct modeling and avoid choking conditions. In addition, introducing the correct area for fan and exhaust faces can lead to reasonable results.

Chapter 4

4 SIMULATION OF DLR-F4 AIRCRAFT MODEL

4.1 Introduction

In this chapter, aerodynamic analyses of DLR-F4, a small aircraft model used for wind tunnel simulations is performed. Basically, for each analysis described in this and the next chapter the work starts from meshing the configuration surface in AGPS, then exporting the node coordinates file to TRANAIR. As it was mentioned before, TRANAIR also needs an input deck to know the flow characteristics, run controls, LBO regions and their controls, box numbers in each grid and the necessary adjustments, boundary layer parameters, etc. After running the case, the TRANAIR job is finalized and the analysis starts. For an analyst the input characteristics and CPU cost are as important as the results, because for doing a good job, possessing widespread information for every aspect of the analysis is vital. Therefore, some extra information regarding the number of the boxes in first and last grids, CPU run time, boundary layer parameters, etc. is given.

It should be noted that for performing all the DLR-F4 case solutions, the automatic adaptive gridding strategy is used, which makes the best mesh distribution on the field, based on the number of available boxes, and the position of high gradient phenomena (e.g. shock waves, etc.) in the problem. About the convergence, it is good to note that all

the cases converge completely in less than or equal to 900 linear GMRES iterations and the convergence tolerance (final residual) has reached the predefined value of 10^{-5}.

For the DLR-F4 case, C_P versus X/C curves are given at different span-wise locations of the wing, then the trend of pressure change in each location and the effect of different parameters on the trend are discussed. To validate the TRANAIR solution, the same case is solved with a different method (Navier-Stokes solver- RANS model) and the C_P results for both methods are compared with the available experimental data. The Navier-Stokes runs were performed with Fluent by Mr. Xiaobao Jia. For a better validation, the analysis is done in different angles of attack and a C_L-α curve is also constructed to compare the trend of total lift change with angle of attack for TRANAIR and the experiment. In addition, total lift coefficient of different solvers for each case at the same Mach number and angle of attack is compared.

4.2 Model implementation

DLR-F4 is a simple aircraft configuration that contains a wing and a fuselage. It is a validation case, as many wind tunnel test models of this configuration have been made and tested experimentally and many CFD analyses have been performed. The geometry used for this analysis is prepared from the data published in the AGARD 303 report [30] and AIAA CFD Drag Prediction Workshop data [31]. The geometry data consists of points defining the body at constant fuselage stations and the wing at constant wing stations. In the AGARD 303 report all the data necessary for this model containing the reference information, wind tunnel dimensions, instrumentation, model and fixture stand dimensions, flow characteristics and the results for three different experimental cases (NLR-HST, ONERA-S2MA and DRA-8ftx8ft) are provided.

The geometry points are input to AGPS and used to construct the surface lofts. Then, the surface gridding is done by PWBHV (Paneling Wing, Body, Horizontal, and Vertical) meshing package in AGPS and the wakes' networks are generated. The number of mesh nodes for surface and wake networks is 12308. The mesh nodes coordinate file and the input deck is introduced into TRANAIR. The Cartesian unstructured surface mesh for the DLR-F4 fuselage and wing is shown in Figure 4-1.

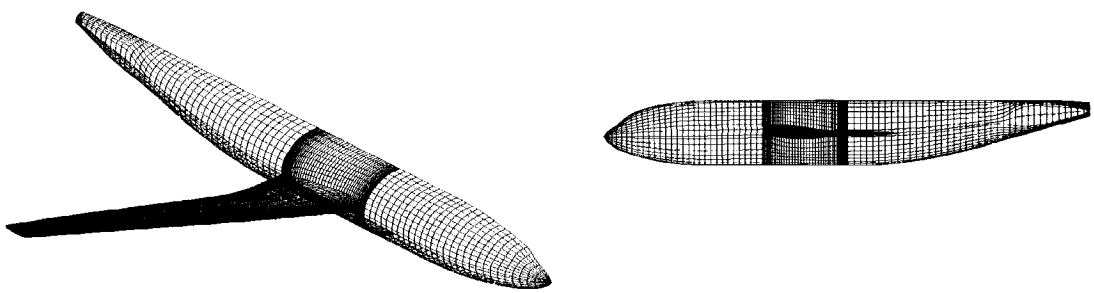

Figure 4-1: *Cartesian unstructured mesh for DLR-F4 model generated by AGPS*

In the input deck, for viscous analysis, the appropriate Reynolds number has to be used. In fact, TRANAIR has to simulate a wind tunnel and not a real flight test, as the results are to compare with the wind tunnel experiments. For this case, the amount of Reynolds per unit chord is adjusted to be 21276, which corresponds to Re=3e+6 that is used in transonic wind tunnel tests, considering that mean aerodynamic chord for DLR-F4 wind tunnel model is 0.1412 m [30]. Other boundary layer parameters, e.g. momentum thickness and displacement thickness are different, when doing a wind tunnel or a real flight analysis. For this case, the initial trip location from laminar to turbulent is considered on the wing at 10% of chord for both top and lower surfaces. Nevertheless, as soon as Re_θ(Reynolds of momentum thickness) becomes greater than 100, the solution

will transition to turbulent. For body, a fully turbulent boundary layer is considered with trip location of -1%. In addition, the initial conditions for maximum shear stress coefficient (C_τ), momentum thickness (θ) and displacement thickness (δ^*) for body are taken as 0.03, 0.1504 and 0.2642 sequentially to represent a turbulent boundary layer.

The target number of field boxes in the last grid is adjusted from 550 k to 950 k to get more accurate results and the initial grid box number is set to 20930 (161*10*13). The total CPU time for this case is approximately 1.5 Hrs on a 64-bit single CPU-3GHz P4 using a Linux system. The convergence level in TRANAIR is 10^{-5}.

In the next section a comparison of the results based on TRANAIR viscous solver, Fluent (Navier-Stokes) and the experimental data of NLR-HST are presented for the DLR-F4 configuration, at Re=3e+6, $M_\infty = 0.75$, and AOA=0°. In section 4.4, a TRANAIR viscous/inviscid analysis comparison is done for this model.

It should be noted that for the Navier-Stokes analysis the simple RANS model of S-A (Spalart-Allmaras) with single equation is chosen. The amount of y^+ for the boundary layer mesh close to the surface is taken approximately between 20 and 30. The number of mesh cells used in this model for the DLR-F4 case is approximately 2.23e+6. Finally, the convergence level in FLUENT (N.S) for this case is approximately 10^{-4}.

4.3 TRANAIR/Navier-Stokes/experimental data analyses

Total C_L computed by different codes and obtained experimentally is found in Table 4-1:

Table 4-1: *Total lift coefficient comparison of TRANAIR, Fluent (N.S) and other codes against experiment for DLR-F4 at M0.75 & AOA0*

	TRANAIR (viscous)	**Fluent (Navier-Stokes)**	**Experiment (NLR-HST)**	**Bombardier local Euler code with B.L. coupling (MGAERO), [34]**	**CFD++ Code (N.S), LES [34]**
Total C_L	0.6137	0.5935	0.5	0.63	0.55

TRANAIR and Fluent (N.S) total C_L are very close, although they use completely different methods. Offsets in TRANAIR C_L of about 0.1 relative to wind tunnel experimental data are somewhat typical and predictable [32]. CFD-to-experimental comparisons are generally complicated by several factors including the *mounting system*, *trip strips*, *model aeroelastics* and *wind tunnel wall effects*. Those differences, along with physical approximations in TRANAIR CFD model avoid precise matching of aerodynamic coefficients at a given α. Industry practice is to run a polar (α sweep) and shift the CFD data to overlap the experiment at one point in order to compare the shape of curves of interest. M. Hemsch and J. Morrison [32] explain the variability of CFD-DLR comparisons and confirm CFD-experimental differences. Therefore, more important task is the comparison of the lift curve slope $dC_L/d\alpha$ and if additional α computations show almost similar offsets, the solution is likely sound. Lift slope ($dC_L/d\alpha$) comparison is reported in Figure 4-4. In addition, it is good to compare the pressure distribution on the wing surface in different cross sections to consolidate such lift difference. In Figure 4-3, C_P at four span-wise locations for the same flow conditions is compared. The position of the span-wise locations in which the C_P curve is analyzed is shown in Figure 4-2.

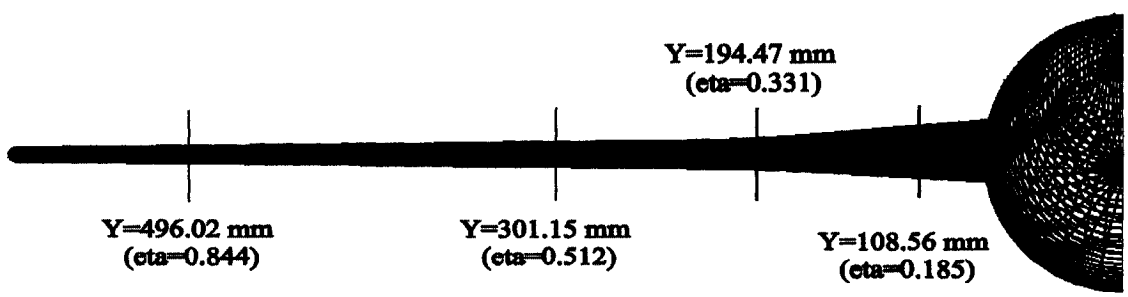

***Figure 4-2**: Position of analyzed wing sections for DLR-F4 configuration*

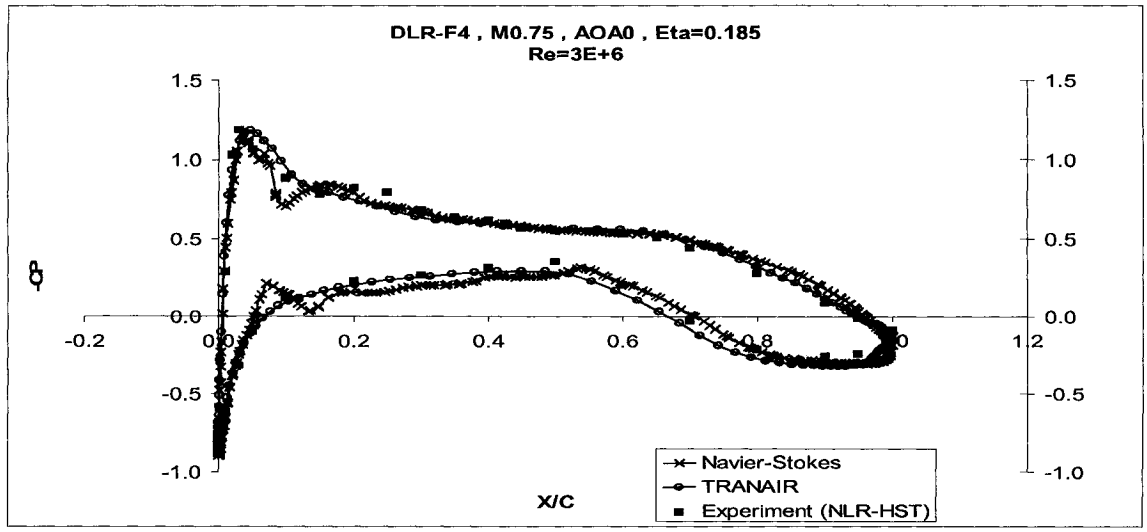

(a)

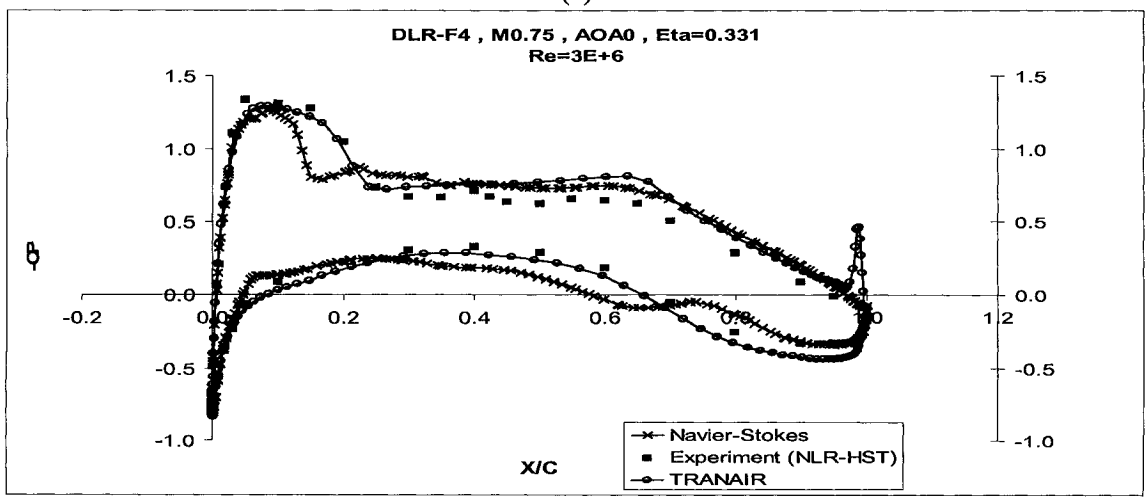

(b)

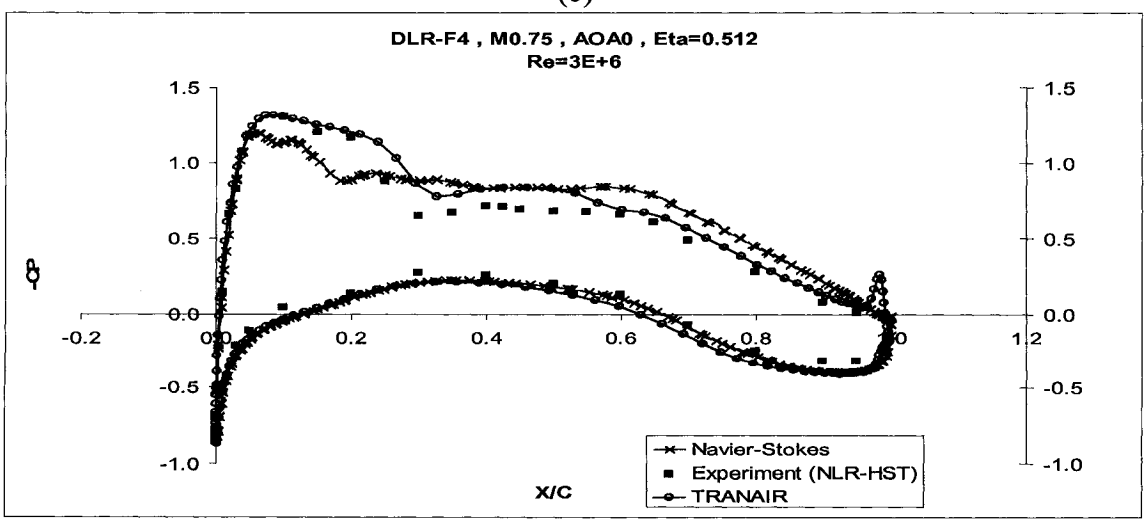

(c)

***Figure 4-3**: Pressure coefficient comparison of TRANAIR, Navier-Stokes and experiment for DLR-F4 at M0.75 & AOA0, (a) η =0.185, (b) η =0.331, (c) η =0.512, (d) η =0.844*

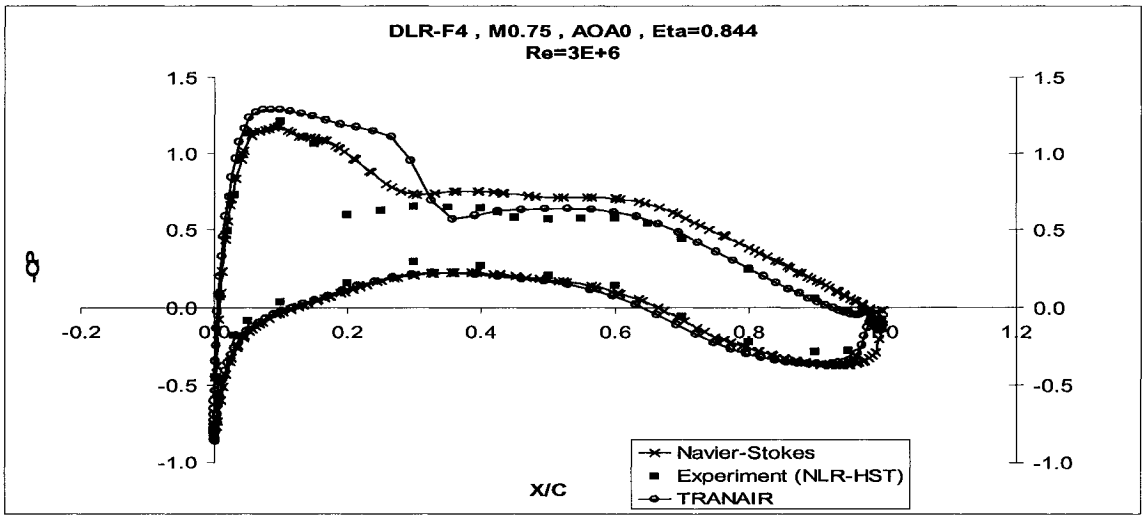

(d)

Figure 4-3- Continued

In Figure 4-2 and Figure 4-3, the parameter Eta (η) is the ratio of the Y coordinate of that cross section to maximum Y coordinate of the wing. One can see that there is a good agreement between all the CFD and experimental results for sections inboard. The match in C_P of inboard sections causes the total lift coefficients to be close. For inboard sections, TRANAIR distinguishes the shock location and strength very well. At $\eta = 0.331$ the shock sensed by Fluent (N.S) is a bit forward, which demonstrates accurate analysis of TRANAIR at cruise condition, if the boundary layer coupling is used. Comparing the convergence levels of both solvers (that mentioned in section 4.2) proves why TRANAIR results are more precise in this case. The only phenomenon that TRANAIR cannot catch here is a small expansion after the shock (in shock stem) on the top surface. Nevertheless, the effect of this expansion on the total lift is very low. The expansion in shock stem on the top surface close to leading edge (at about 15% of chord) is very clear in Figure 4-3(a).

As we move toward the out-board sections, Fluent (N.S) catches the location of shock wave considerably forward to what the experiment shows, but TRANAIR,s shock is a little backward. The difference in shock location is more for Fluent (N.S), and TRANAIR shows better agreement even in more out-board sections (Figure 4-3(c)). The reason of different shock locations is the different amount of dissipation added to the solvers for TRANAIR and Fluent (N.S) and the problem of both solvers to adjust the dissipation well in different steps of solution to move the shock to its right position. However, the dissipation in TRANAIR is better adjusted, as it shows much closer results.

For the most out-board sections, both CFD methods catch the location of shock wave forward comparing the experiment. The reason of this effect is the wing tip vortices and their effect on the wing pressure distribution. In TRANAIR, these vortices and the drag induced is simulated by taking a vortex sheet (wake) beside the wing at the wing tip. This approach shows some of the limitations in TRANAIR. Figure 4-3 (d) illustrates the shock location difference clearly.

The discontinuity in pressure at the trailing edge obtained by TRANAIR is due to applying the Kutta condition at the edge. This discontinuity can be seen in results of many full potential solvers [34].

As was mentioned earlier to validate the TRANAIR solution, it is better to compare the trend of the change in lift at different angles of attack ($dC_L/d\alpha$). Figure 4-4 illustrates the C_L-α curve for both TRANAIR and experiment (NLR-HST). This figure shows that off C_L value of approximately 0.1 is almost obtained for all angles of attack and for the whole range of TRANAIR applicability. Therefore, $dC_L/d\alpha$ for both TRANAIR and experiment is almost the same.

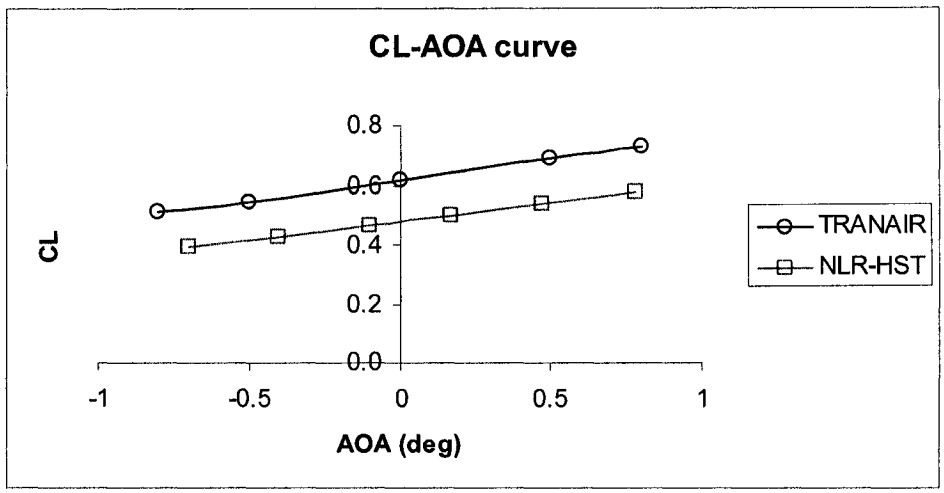

Figure 4-4: *CL- α curve for TRANAIR results on DLR-F4 model at M0.75 and experiment*

It should be noted that in getting the best solution from TRANAIR (that is shown in Figure 4-3), the following modifications are applied:

1- When the target number of boxes in adaptive gridding is increased from 550 K to 950 K, the total C_L changed from 0.62 to approx. 0.613, which shows the effect of using more elements in the final grid on exactness of the results. Of course, this effect is small, but can be needed for detail analysis. Note that by increasing the target number of boxes the time cost and storage also increase, in such a way that for the computer specifications mentioned in section 4.2 the memory limit does not permit the box number to be more than 950k. But, the solution for 900 k box number shows almost the same results and confirms the sufficiency of the boxes taken.

2- The solution without the special LBO's for the wing leading edge results to a total C_L of about 0.19, which is vastly different and this illustrates the importance of these regions. It is mostly beneficial to use three or more different LBO regions

even for one wing leading edge at different span limits. For this case, seven LBO regions for the wing at different span locations are used.

4.4 Inviscid versus viscous analysis

A comparison of wing pressure distribution at 4 cross sections of the DLR-F4 wing for TRANAIR inviscid code and TRANAIR inviscid coupled with boundary layer code (TRANAIR viscous) at M0.75 and AOA0° is shown in Figure 4-5.

As it was explained in Chapter 1 and in section 3.5, TRANAIR or better saying all of the inviscid solvers give strong shock waves on the wing. When viscous effects are added to the TRANAIR code, the shock-boundary layer interaction causes a shock strength reduction and more smoothening of shock area. This viscous modification can be seen in all parts of Figure 4-5 as weaker shock waves.

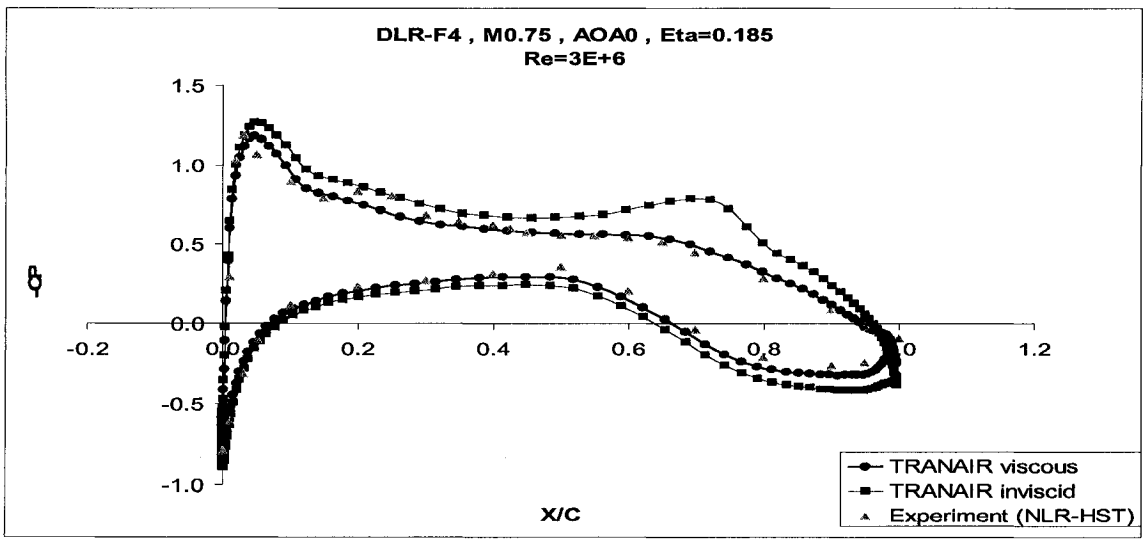

(a)

***Figure 4-5**: Pressure coefficient comparison of TRANAIR viscous and inviscid codes for DLR-F4 at M0.75 & AOA0 at 4 span-wise locations (a) η =0.185, (b) η =0.331, (c) η =0.512, (d) η =0.844*

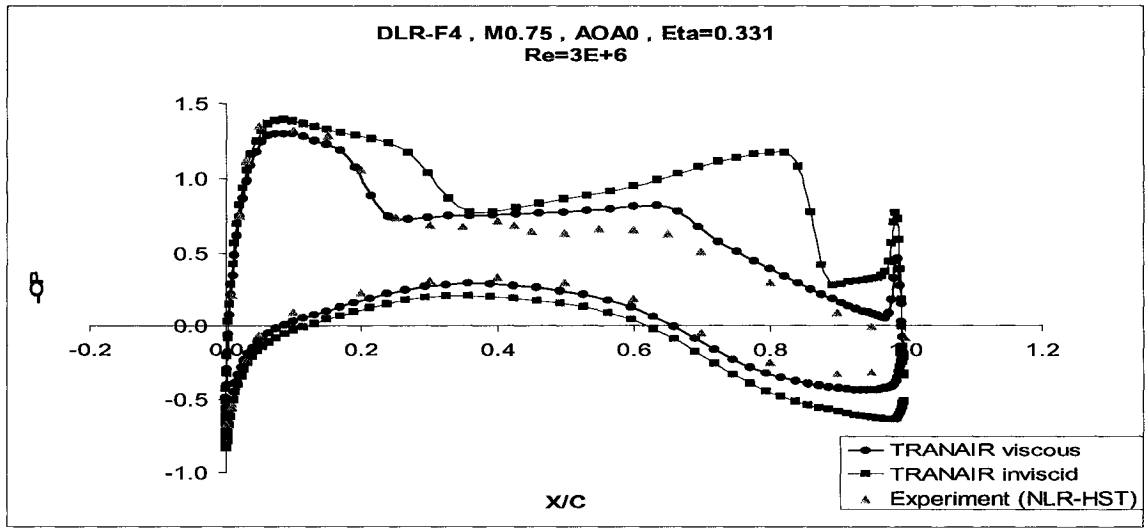

(b)

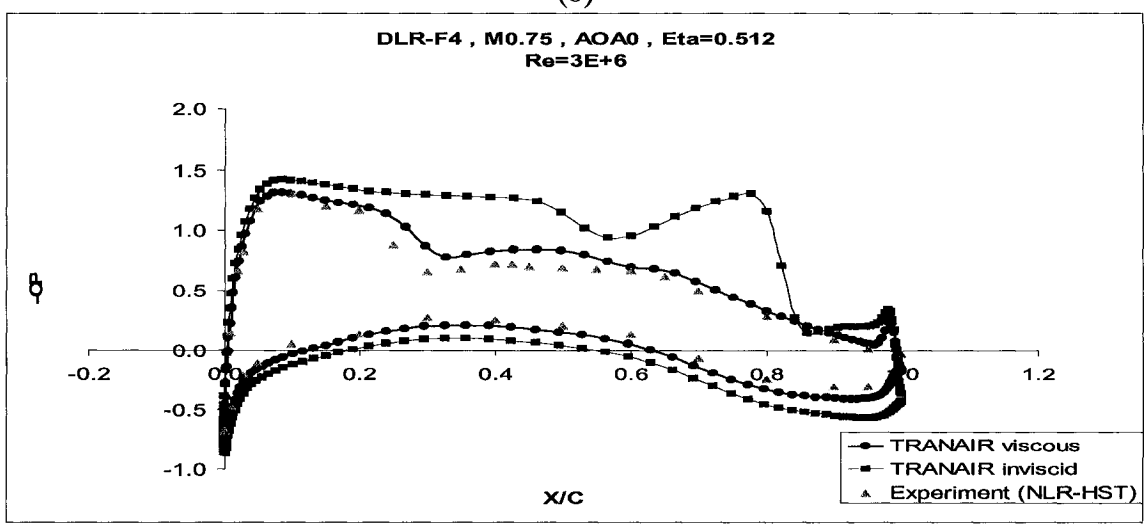

(c)

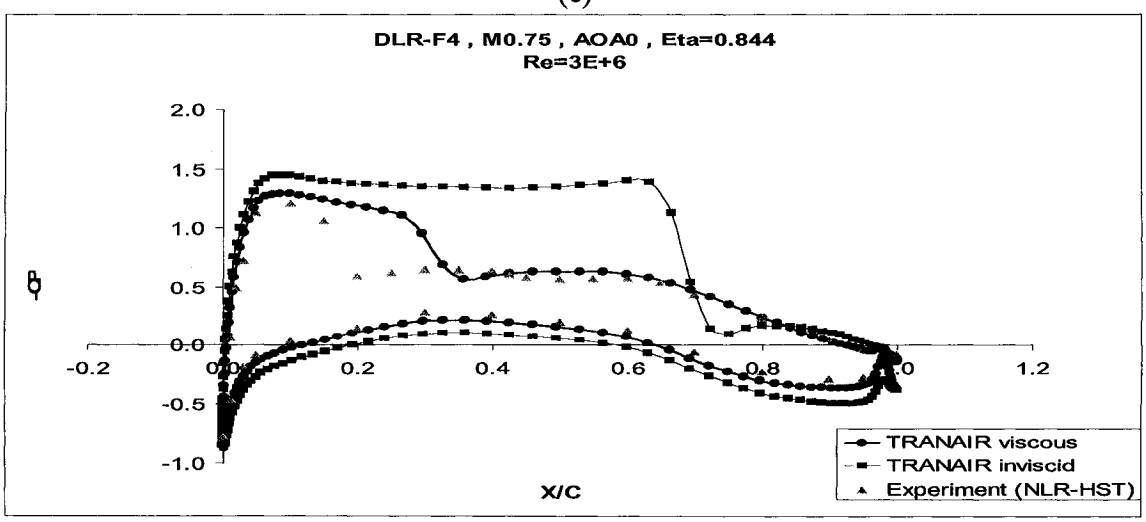

(d)

***Figure 4-5-** Continued*

Figure 4-5 shows that the inviscid shock location is much more forward than the viscous one. In references [23] and [33], the difference of viscous and inviscid shock locations is explained distinctively. Because of this reason, the resulted viscous values of the C_L are much less than inviscid C_L.

Figure 4-5 also shows that the inviscid solution results in two shock waves on the wing top surface at most wing sections except the out-board. At the wing out-board sections, the two shock waves coalesce to form a single strong shock. That is why, only one shock on the wing out-board in Figure 4-5 (d) can be seen, which is relatively stronger. In fact, *dissipation* in supersonic regions causes two shock waves to unify and transfer to the correct position. But, as was described earlier, the TRANAIR code effects due to dissipation are less than the other inviscid codes [11] and as a result two clear shocks can be seen in TRANAIR solution on the wing top surface. Coupling the boundary layer code adds enough dissipation to move both shock waves to their correct position and to unify.

The field Mach number contours for the TRANAIR viscous solution on the in-board of DLR-F4 wing (η=0.636) can be seen in Figure 4-6. This figure also shows the adaptive field gridding and several refinements in the special regions like wing leading edge and shock wave position.

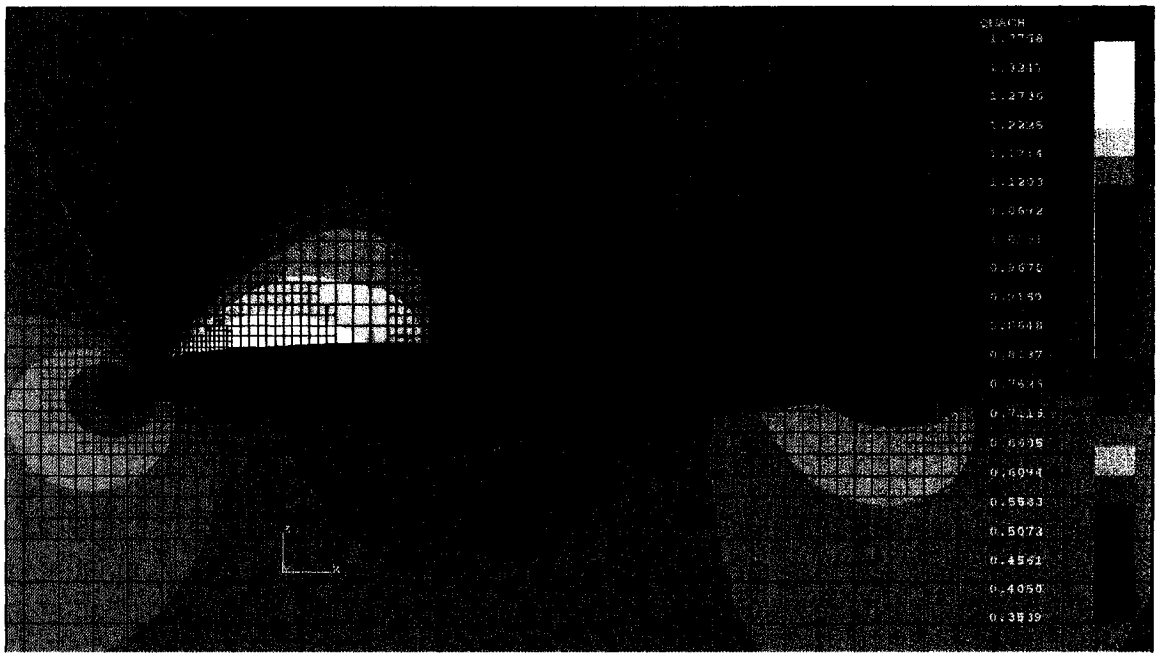

***Figure 4-6**: Field Mach contours for wing out-board of DLR-F4 (η =0.636) at M0.75 & AOA0 in viscous TRANAIR*

4.5 Summary

In this chapter a simple aircraft used for wind tunnel tests, DLR-F4, is analyzed by using the TRANAIR solver and the results for pressure distribution at different wing spans are compared with those obtained by FLUENT's Navier-Stokes solver and the experimental data. As the analyzed case is a wind tunnel based aircraft, the inputs for boundary layer characteristics in TRANAIR, mainly as Reynolds number, displacement and momentum thicknesses, trip locations, etc. shall be different with those for a real aircraft.

When performing CFD versus wind tunnel test comparison, the differences in the results are acceptable, provided they are in a limited margin. In fact, the effects of the mounting system, aeroelastics, wind tunnel walls, etc. are the main sources of these differences and it is better to compare the trend of changing the C_L with the angle of attack in an acceptable margin of angles.

The analysis done for this case at M0.75 and AOA0° shows good agreement of the results for both TRANAIR and Navier-Stokes solvers with the experimental data, although both solvers can not catch the shock location well at wing outboard sections due to wing tip vortices. In the TRANIAIR analysis, the effect of introducing sufficient number of boxes at the final grid and appropriate LBO regions for adaptive field refinement on the results can be seen very clearly.

In this chapter, a viscous versus inviscid analysis is performed by TRANAIR for DLR-F4 case. As expected, the viscous effects improve the position of the shock. Inviscid solution estimates two shocks at inboard and half-board sections. The dissipation added by viscous effects causes these two shocks to unify and adjusts the strength of the unified shock.

Chapter 5

5 SIMULATION OF AN EXISTING FULL AIRCRAFT CONFIGURATION

5.1 Introduction

CFD simulation is often used to design the shape of an aircraft or to analyze an already-designed aircraft based on the design geometry information. There are many defects related to manufacturing or installation that change the aerodynamic design. Some of these defects are taken into considerations during the detail design and the necessary corrections are applied. But, many other can not be predicted well due to the limits that might exist during manufacturing and installation of the components. Therefore, it is always a good idea to do a CFD analysis after the aircraft components installation to see the conditions of a real aircraft flight. Flight tests can contribute well in this matter, but as it is explained in section 1.1, there are many limits to use them.

This chapter deals with the aerodynamic analysis of a real existing aircraft, HAWKER 800. The geometry surfaces are input via the laser scanning of the real aircraft. In this way, all the irregularities, waves and recesses that reluctantly exist in the components surface due to manufacturing and installation issues are taken into account in the aerodynamic analysis. This work is new and original and can contribute to apply the necessary corrections in the new versions of the existing aircraft or other similar aircrafts.

Similar to the DLR-F4 analyses, the automatic adaptive gridding strategy is used for all the cases of HAWKER 800 that are analyzed in this chapter. About the convergence in

TRANAIR, it should be noted that all the cases converge completely, but the number of iterations are different for each case and they will be mentioned separately. The convergence tolerance (final residual) is set at a predefined value of 10^{-5}.

To validate the TRANAIR solution, the same cases are solved with a different method (Navier-Stokes solver- RANS model) and the C_P results for both methods are compared. All the Navier-Stokes solutions are calculated on FLUENT by Mr. Xiabao Jia. Total lift coefficient from the different solvers for each case at the same Mach number and angle of attack is also compared.

5.2 HAWKER 800 configuration analysis

5.2.1 Model implementation

HAWKER 800 is a mid-size twin-engine business jet, originally designed and manufactured by British Aerospace as the BAE 125 and came to market in 1993. The current version is identified as the Hawker 850XP and was certified for operation in 2006. The new version contains winglets (in contrary to HAWKER 800), which has extended the operating range of this aircraft.

Figure *5-1* shows HAWKER 800 aircraft and its laser scanning process.

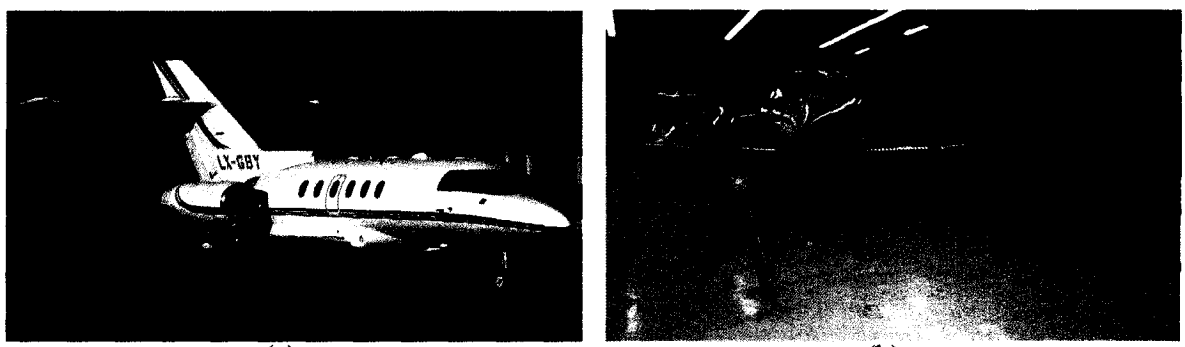

(a) (b)

Figure 5-1: *HAWKER 800, (a) Full configuration (figure from AIRLINERS.net), (b) laser scanning the existing HAWKER*

Basically, the aerodynamic design and test data for the real aircraft are a part of the design documentation and are not available for public use. Because of this reason, the analyses done in this section for the HAWKER 800 are not compared with any experimental data. Nevertheless, considering that two different CFD solvers are used in these analyses, the comparison of the results can be very interesting.

Different aerodynamic analyses are done for this aircraft to find out the effects of many important parameters. In the following sections, the effects of wing smoothness in the results and the convergence, wing elevation and wing bump are analyzed on the HAWKER full model without nacelle. Because of the importance of nacelle effects on the total lift and pressure distribution on the wing, the HAWKER 800 analysis with nacelle is done in another section.

The surface lofts are gridded by the PWBHV meshing package, but as the HAWKER 800 possesses T-tail and this package is not able to grid this kind of tails, meshing the horizontal tail is done separately and it is abutted to vertical by making a patched interface grid, as shown in Figure 3-2. In the TRANAIR analysis, the number of mesh nodes for surface and wake networks is 19472, which contains 17168 nodes for surface networks and 2304 nodes for the wakes. The target number of field boxes in the last grid is set to 950 k (similar to the DLR-F4 case) and the initial grid box number is 20400 (51*16*25). In TRANAIR, the total CPU time for this case is approximately 1 Hr. for M0.65 and 3.5 Hrs for M0.75 on a 64-bit single CPU-3GHz P4 using a Linux system. The number of iterations is set to 900.

For the viscous analysis, Reynolds number related to each Mach number (0.65 and 0.75) is calculated by taking the ambient temperature to be 228.72 K, which is typical for

30 to 35 Kft flight elevation. The pressure in this elevation is approximately 30091.5 Pa and density can be found by the equation of state:

$$P = \rho RT \rightarrow \rho = \frac{P}{RT} \rightarrow \rho = \frac{30.0915kPa}{0.287 * 228.72K} \cong 0.4584 \, {}^{kg}/_{m^3}$$

The kinematic viscosity can be computed via Sutherland's law,

$$\mu = \mu_{ref} \left(\frac{T}{T_{ref}} \right)^{3/2} \frac{T_{ref} + T_S}{T + T_S} \tag{5.1}$$

in which T_{ref} is a reference temperature (e.g. 273.15°K), μ_{ref} is the viscosity at T_{ref} and T_S is the Sutherland temperature. Therefore, considering that T_{ref}=273.15 K, $\mu_{ref} \approx$ 1.716e-5 ${}^{kg}/_{m.s}$, T=228.72 K and T_S=110.6 K, from equation (5.1) we will have:

$$\mu = 1.487e-5 \, {}^{kg}/_{m.s}$$

Then considering $V_\infty = M_\infty \sqrt{\gamma RT}$, the free stream velocity is found at each Mach number. Finally, the Reynolds number can be calculated by the following equation:

$$\mathrm{Re} = \frac{\rho * V_\infty * M.a.c.}{\mu} \tag{5.2}$$

In equation (5.2) M.a.c. is the mean aerodynamic chord that is equal to about 2.213 m for the HAWKER 800 model. Therefore, the calculated Reynolds number for Mach numbers 0.65 and 0.75 become 13.44e+6 and 15.5e+6, respectively.

5.2.2 TRANAIR/Navier-Stokes analysis

As it is explained in section 3.7, the HAWKER 800 has a very low wing, in that the wing/body intersection does not produce a closed airfoil-like clean curve. In AGPS, meshing this kind of wings was initially impossible without the BizJet package. Because

of that reason, the wing position is moved up for 15 cm to be able to do either the meshing in AGPS or a good wing elevation analysis. In this section, C_P and C_L comparison for TRANAIR and Navier-Stokes in Fluent (RANS model) are done for the HAWKER 800 case without nacelle with wing 15cm up relative to its original place at M0.65 and the worst case of M0.75. For Navier-Stokes analysis the simple RANS model of S-A (Spalart-Allmaras) with single equation is chosen. The amount of y^+ for the boundary layer mesh close to surface is taken approximately between 30 and 50 and the number of mesh nodes used in this model for the HAWKER 800 case is about 3.8e+6. Finally, the convergence level in Fluent (N.S) for this case is approximately 10^{-4}. In Table 5-1, total lift coefficients computed by TRANAIR and Fluent (N.S) in these Mach numbers are compared.

Table 5-1: *Total lift coefficient comparison of TRANAIR and Navier-Stokes for HAWKER case without nacelle with wing position 15 cm upper than original place*

C_L	**TRANAIR (Viscous)**	**Fluent (Navier-Stokes)**
M0.75, AOA0°	0.1556	0.1452
M0.65, AOA0°	0.1292	0.1160
M0.65, AOA0° (wing non-smoothed)	0.1667 (not completely converged)	0.1160

About the HAWKER analysis in TRANAIR, it should be noted that the wing is smoothed by re-lofting the wing surface and by using the smoothing commands in limited areas in the AGPS (as explained in section 3.3). If the smoothening is not done, a perfect and complete convergence cannot be obtained. To illustrate this, the amount of lift coefficient at M0.65, AOA0° computed by TRANAIR with non-smoothed wing is shown in the last row of Table 5-1. The final residual for this case is 2.496e-2 with 900 iterations. The results of smoothing in TRANAIR at both Mach numbers are in good

agreement with the results of a non-smoothened wing solved by Fluent (N.S), and it shows the higher sensitivity of TRANAIR to the surface roughness comparing to other solvers.

The wing had originally a bump underneath the in-board sections near the fuselage. This bump was due to an error happening during the generation of the IGES file from the laser scanning results. As described in the rest of this section, CFD is able to pick up such features so to correct any errors that may arise during the construction of the geometry. As this bump can cause many aerodynamic problems, two airfoil sections, one exactly in the middle and one in bump in-board are considered for C_P comparisons. In Figure 5-2, the position of these sections are illustrated. Figure 5-3 compares the pressure distribution on the wing surface by TRANAIR and Fluent (N.S) at these two sections.

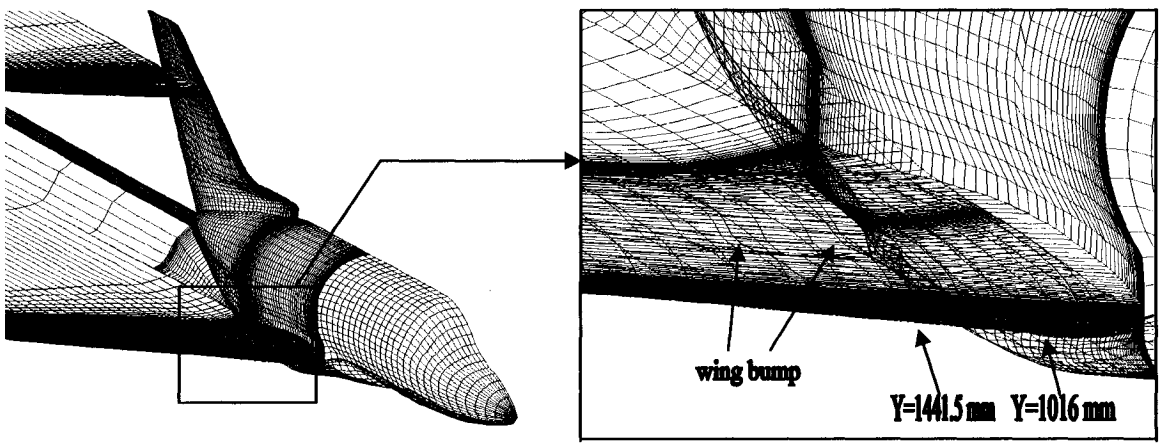

Figure 5-2: *HAWKER configuration, position of analyzed wing sections on the bump*

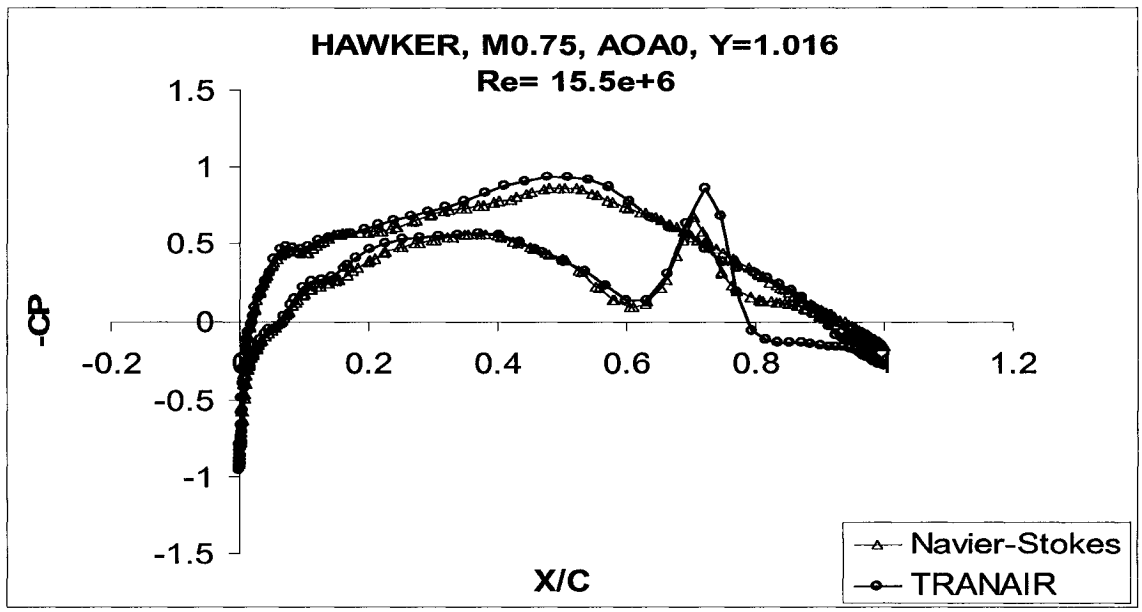

(a)

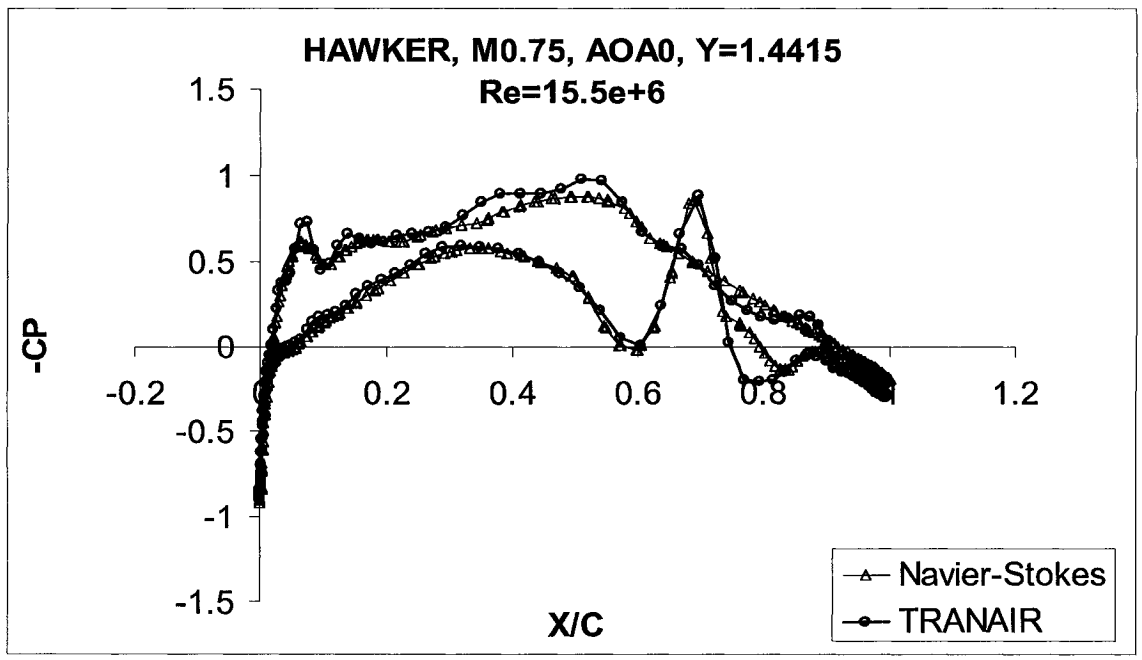

(b)

***Figure 5-3**: Pressure coefficient comparison of TRANAIR and Navier-Stokes for HAWKER without nacelle at medium and high Mach & AOA=0 on two wing bump sections (a) M0.75, Y=1.016 m, (b) M0.75, Y=1.4415 m,(c) M0.65, Y=1.016 m, (d) M0.65, Y=1.4415 m*

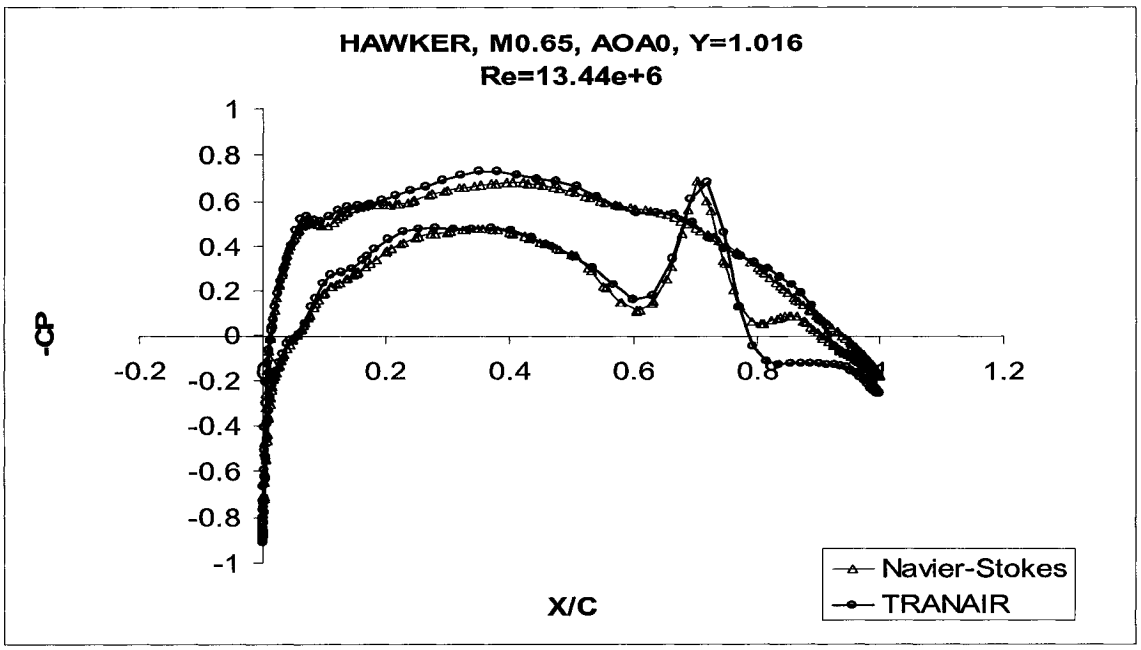

(c)

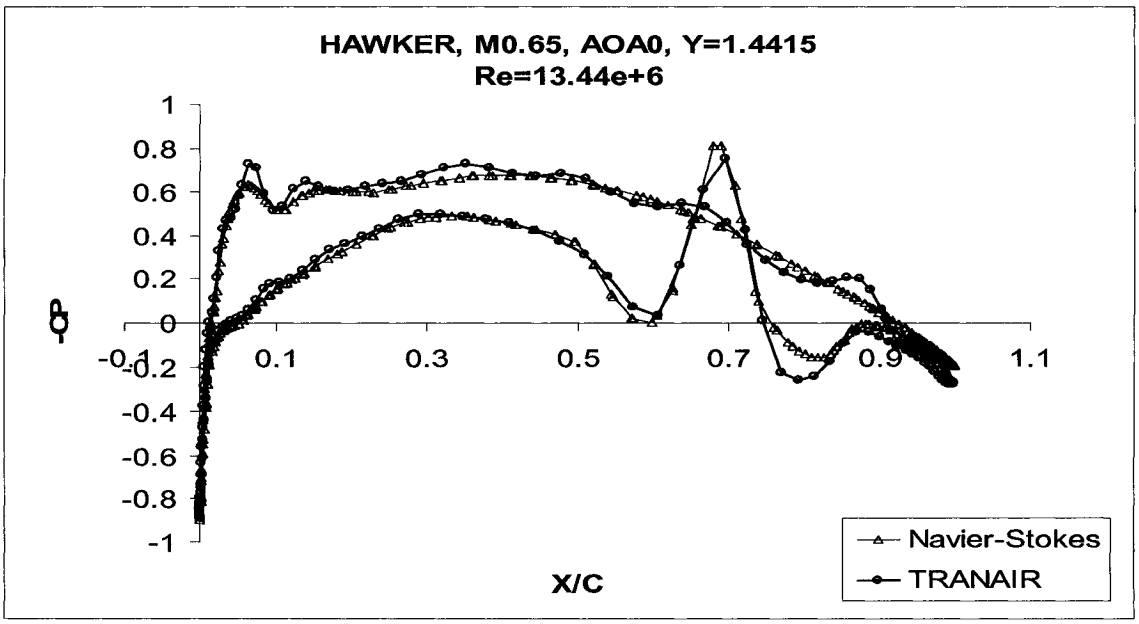

(d)

Figure 5-3- Continued

As can be seen from Figure 5-3, there is a very good agreement between the TRANAIR and Fluent (N.S) results almost at all locations and at both Mach numbers, although the geometry is complex and the solvers base are totally different. One of the

regions in which there is less agreement is on the wing lower surface after the bump near trailing edge. The reason can be a mild flow separation happening because of the bump and incorrect boundary layer calculations of TRANAIR in such regions. Both solvers anticipate the bump pressure distribution similarly.

The other difference is that TRANAIR solves a smoothened wing, but Fluent solves the original wing. This causes the TRANAIR calculated velocity close to surface to be a bit higher (pressure to be less) and due to this reason the TRANAIR pressure distribution line on both upper and lower surfaces is a little higher (i.e. lower pressures on both surfaces) than that for Fluent (N.S).

For M0.75, the differences are larger due to a higher Mach number, especially close to MMO. In fact, when the flow velocity and temperature makes the Mach number to be close to its maximum, many separations can be expected at different locations depending on the geometry smoothness and other parameters. Although TRANAIR can catch weak to mild separations, the exactness of TRANAIR solutions in these separated areas is not satisfactory.

One of the interesting aspects of both solvers results is the low predicted lift coefficient. For example, considering the aircraft weight to be approximately 12500 kg at the beginning of the cruise [29] and the wing area to be about 34.37 m^2 and aircraft flying at M0.75 cruise condition (AOA=0^o), the amount of C_L is calculated as approximately 0.3. But the values of lift coefficients resulted by both TRANAIR and Fluent (Table 5-1) are almost half of this amount. The reason of such big difference is wing leading edge and its vicinity on the top surface. Normally, the design of the wing leading edge shall be in such a way that the pressure drops dramatically in the first 20% of the chord on the top

surface (except the supercritical wings). In chapter 4, this condition can be seen well for the DLR-F4 wing in Figure 4-3. This pressure drop is strong enough that in some circumstances, Mach number exceeds the sonic line leading to supersonic flow regimes and the consequent shocks are expected too. But, for the HAWKER wing such high pressure drop in the first 20% chord of the wing top surface can not be seen. This can be due to the quality of the laser scan to make the geometry file and that the laser scan could not give a nice surface representation of the real wing in the leading edge region. Normally, except the supercritical wings, most of the lift should be generated in the first 20% to 30% of the wing chord, but it is not the case for the HAWKER wing that is analyzed.

5.2.3 Effect of wing bump

To analyze the effect of the bump on the wing lower surface, the bump is removed and a new geometry file for the HAWKER wing is generated. In addition, as there are too many irregularities and waves on the fuselage, especially in the vicinity of the wing, the fuselage surface is re-lofted by making parallel cuts on it and discretizing the cuts. Smoothing the irregularities on the fuselage, especially near the wing lower surface, helps to converge the case and to lower the wing (wing with bump) close to its original position.

In this section, the effect of bump located under the wing (due to wing construction error) is analyzed. To do so, the re-lofted fuselage in conjunction with the new wing (without bump) located at 15 cm up corresponding to its original position is analyzed by TRANAIR and the results are compared with those of the same aircraft condition but with the bump. As the bump position is very critical and it is very close to wing/fuselage

interface, two airfoil sections analyzed in section 5.2.2 (Figure 5-2) are considered here again. Figure 5-4 compares the pressure distribution on the wing surface at sections Y=1016 mm and Y=1441.5 mm at M0.75 and AOA=0°.

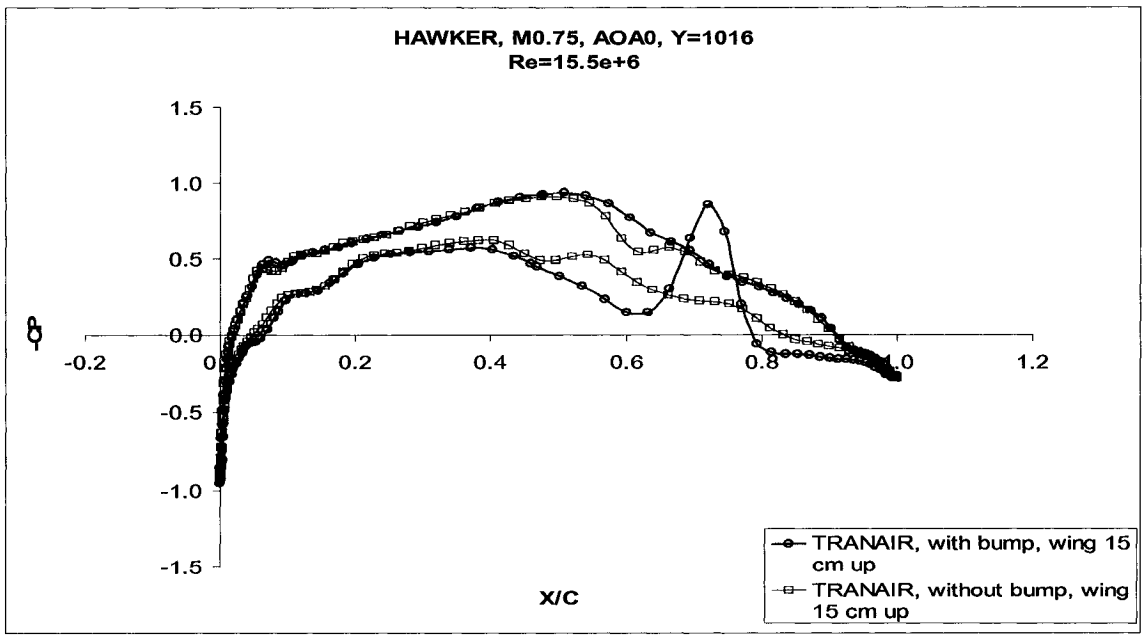

(a)

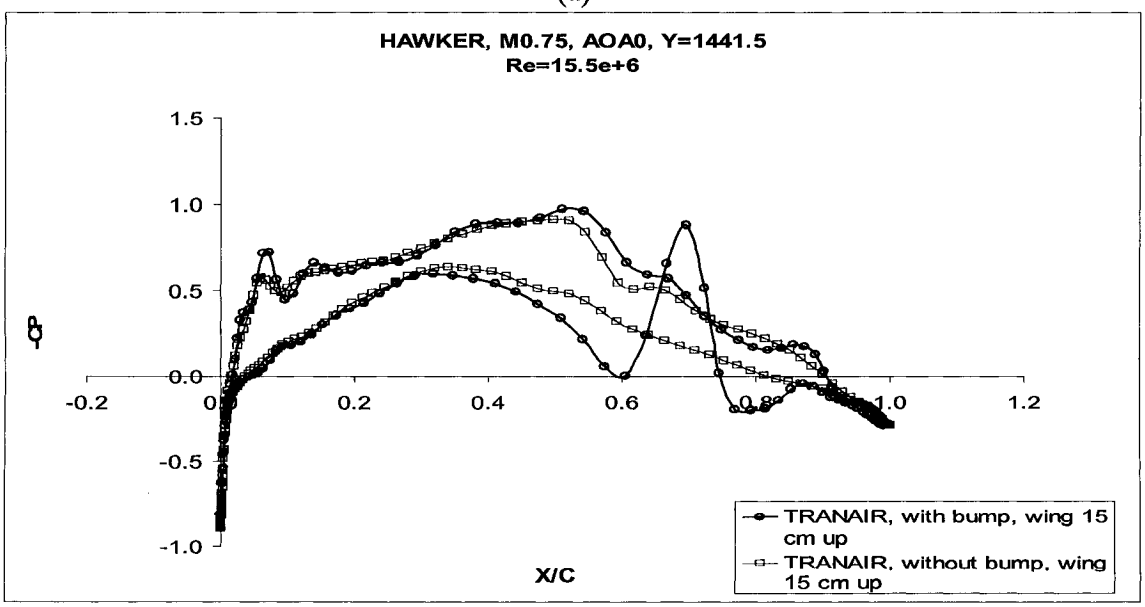

(b)

***Figure 5-4**: Pressure coefficient comparison for HAWKER with and without wing bump at 2 in-board cross sections on the wing bump position, (a)Y=1016 mm, (b)Y=1441.5 mm*

Total C_L for the case with bump is 0.1556 (refer to Table 5-1), but when the bump is removed, C_L is reduced to 0.1226. This result is either interesting or unexpected. In fact, the primary idea about the bump changes after this analysis. Unlike what is thought about the lift reducing effect of such irregularities, some of them can contribute to increase the total lift depending on their position, shape, etc. Figure 5-4 shows a large difference of pressures in two regions, first on top surface after mid chord, second on lower surface far before and after the bump location. The first one, which is not too remarking, is probably because of a little geometry change in top surface during the process of bump skipping. The reason is that the two modified curves representing the wing in the location of the bump are a little different, even on the top surface, from those having bump. From Figure 5-4, it is clear that this geometry change is toward the lift reduction, because the pressure increase on the wing top surface after the mid chord is a little forward compared to the case with bump. However, the second difference is much considerable and is directly due to wing bump. Bump causes very good velocity reduction far before and even after itself, which makes the lift higher. This can be seen much clearly in Figure 5-4(b), exactly in the middle of the wing bump. One can also see that the lift reduction due to geometry change on top surface is much less than that in lower surface due to bump removal. Therefore, it can be concluded that most of the lift reduction is due to the bump removal. Figure 5-5 shows the effect of wing bump with the Mach contours in the wing field at Y=1016 mm.

To finalize, it should be noted that CFD can contribute to detect such geometrical errors by analyzing the pressure distributions on different aircraft components.

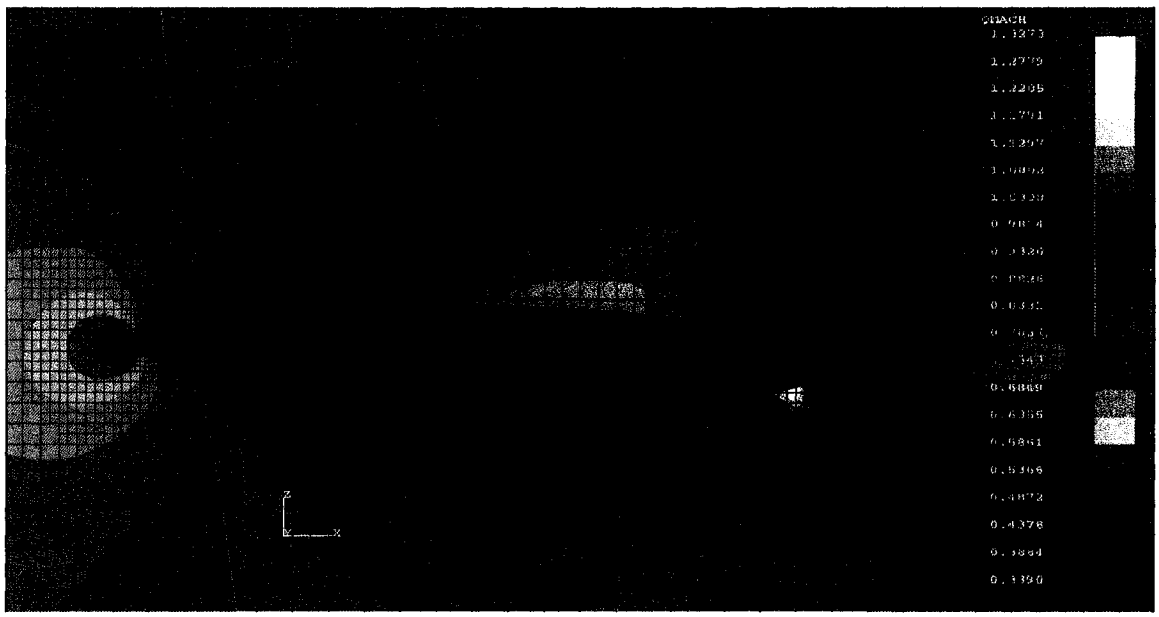

Figure 5-5: *Effect of wing bump- Field Mach contours for HAWKER wing at Y=1016 mm at M0.75 & AOA0*

5.3 Nacelle analysis

5.3.1 Model implementation

In this section, the effects of the nacelle on the HAWKER 800 configuration is analyzed for convergence, total lift and the pressure distribution at different span-wise locations. The nacelle analysis requires the BizJet meshing package of Boeing. With this package, not only different configurations of nacelle and pylon can be included in the analysis, but also the problem of meshing the very low positioned wing configurations is solved. Therefore, three modifications are made in this analysis:

1- The fuselage surface is filtered and smoothened by re-lofting and extra recesses and irregularities are removed (similar to 5.2.3).

2- The bump in wing lower surface is removed.

3- Due to bump removal and using the BizJet package, the wing moves back close to its original place (2cm up instead of 15 cm).

As explained in section 3.1.3 for the body-mounted (aft-mounted) nacelles, the body gridding becomes complicated due to the inclusion of one extra wing-like object, which is the pylon. In the package mentioned above, the fuselage can be divided into five longitudinal sub-surfaces; each gridded compatible to wing, pylon and vertical tail gridding requirements (patched meshing). In Figure 5-6, gridding these five sections in fuselage and gridding the nacelle and its required components are illustrated.

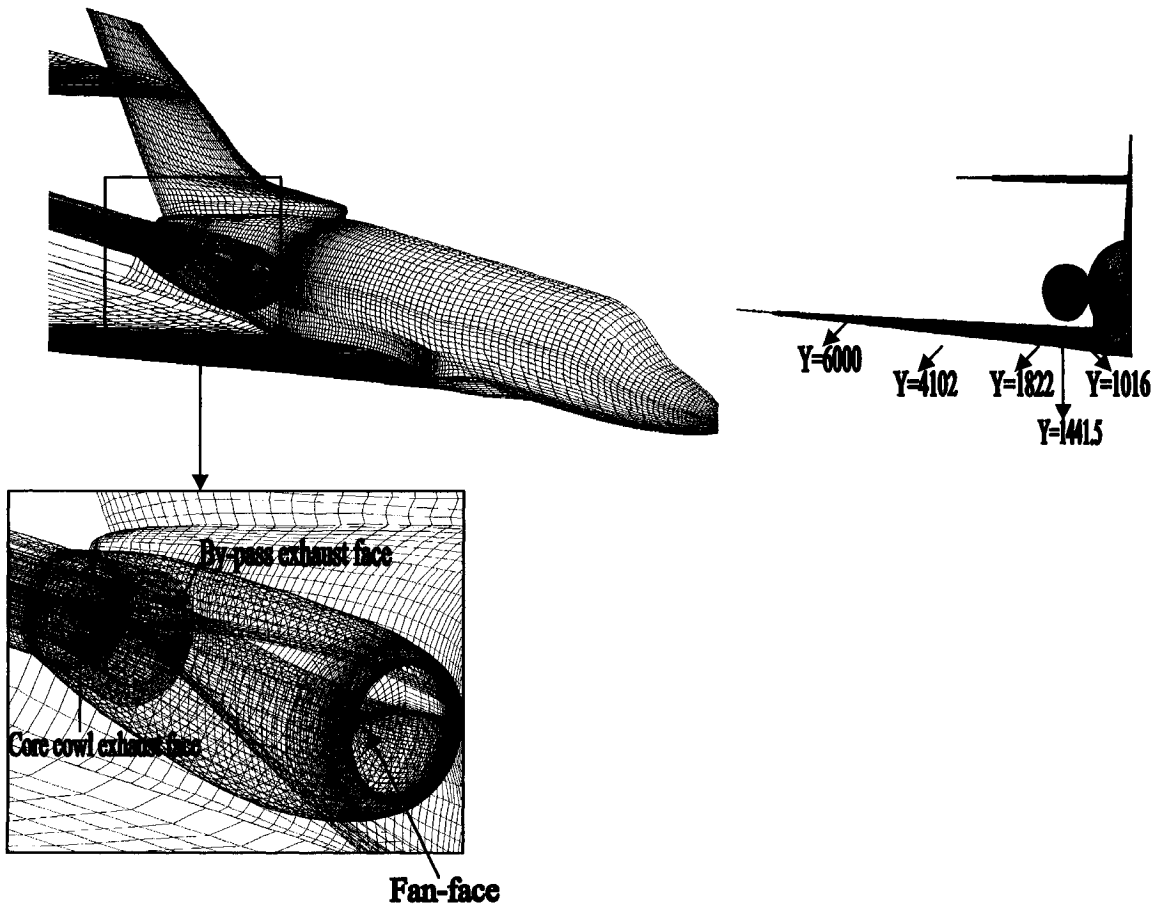

Figure 5-6: *HAWKER configuration with nacelle, surface gridding of all components*

The strategy taken and illustrated in Figure 5-6 for the nacelle components is similar to option 2 of nacelle simulation in Figure 3-5. For this kind of simulation, it is not required to have exact information of nacelle inlet duct. But, having the exact geometry for both nacelle inlet before fan-face (ram duct), and by-pass and core cowl ducts as well as the X

position of fan-face, and exhaust faces are very critical. Normally, these kinds of information are provided by the engine manufacturer, but as mentioned earlier, the aircraft and engine manufacturers do not give the design data of their products for public use. Therefore, for these geometries a linear change surface approximation is made and an approximation for fan and exhaust faces X position is taken, which seems not to be very exact comparing to the real design. It can be said that these approximations can be a few of the sources resulting difference between the numerical and the real aircraft.

The surface gridding of the HAWKER 800 full configuration in AGPS leads to 39619 mesh nodes for surface and wake networks, which contains 30535 nodes for surface networks, 2622 nodes for base networks and 6462 nodes for the wakes. In TRANAIR, the target number of field boxes in the last grid is adjusted to 576 k and the initial grid box number is set to 4464 (31*9*16). The total CPU time for this case is about 1 Hr. for M0.75, AOA=0° and approximately 0.5 Hr. for M0.75, AOA= +1° on a 64-bit single CPU-3GHz P4 using a Linux system. The maximum number of iterations is set to1500 instead of 900 (that used before), as 900 iterations for the full configuration with nacelle are not enough to get full convergence. For this case the drop tolerance has to be reduced almost with the same rate. Similar to other cases the convergence level at the last iteration is 10^{-5}.

In the following section, a TRANAIR/Fluent (N.S) analysis for this configuration is done at M=0.75 and two angles of attack (0° & +1°). Note that, for the previous cases, the gridding for solutions of Fluent (N.S) had no mesh adaptation, but due to importance of mesh adaptation for the simulation of the full configuration aircraft with nacelle, adaptation is used for meshing this case. It should also be mentioned that similar to

previous cases, for Navier-Stokes analysis the simple RANS model of S-A (Spalart-Allmaras) with single equation is chosen for this case. The amount of y^+ for the boundary layer mesh close to surface is taken approximately between 10 and 20. Finally, the number of mesh cells used for this model is approximately 10e+6.

5.3.2 TRANAIR/Navier-Stokes analysis, the angle of attack effect

For the model explained in 5.3.1, TRANAIR analysis is done for M0.75 and AOA= 0° and $+1^\circ$ with the following assumptions:

1- As there is no information about the nacelle inlet geometry, the fan-face position is estimated to be approximately X_{fan}=9800 mm.

2- Fan hub and exhaust plug are neglected from the TRANAIR analysis.

3- The area increase from nacelle inlet (Hill) up to the fan-face is considered linear.

4- The nacelle is taken to be in a *flow through* situation.

5- The fan-face mass flow rate is approximated by 38.6 kg/sec.

In TRANAIR, the nacelle inlet mass flow rate is introduced by giving the area ratio of $\beta = A_\infty / A_{fan-face}$, in which A_∞ is the nacelle inlet stream tube area and $A_{fan-face}$ is the fan-face area. Mass flow rate is calculated by equation (5.3):

$$\dot{m} = \rho_\infty * V_\infty * A_\infty \tag{5.3}$$

Taking $M_\infty = 0.75$ and T_∞=228.72 K, and $A_{fan-face} \approx 0.541325$ m^2 for the HAWKER nacelle, the parameter β is calculated as approximately 0.68. Total lift coefficients obtained in these calculations are tabulated in Table 5-2.

Table 5-2: *Total lift coefficient comparison of TRANAIR and Navier-Stokes for HAWKER case with nacelle with wing position 2 cm upper than original place*

C_L	**TRANAIR (Viscous)**	**Fluent (Navier-Stokes)**
M0.75, AOA+1°	0.1548	0.1593
M0.75, AOA0°	0.0156	0.0324
M0.75, AOA0° (finer mesh on leading edge)	0.0158	-

Table 5-2 shows that total C_L computed by TRANAIR at AOA=+1° is very close to the Fluent (N.S) results. The difference is within an acceptable margin. Note that for the HAWKER model with nacelle, TRANAIR's convergence is perfect at AOA= +1°. The time of convergence in this angle of attack (comparing to AOA=0°) that mentioned in previous section confirms this behavior as well, considering that the number of iterations for both cases are the same (1500). For the case AOA=0°, there is a remarkable difference in the obtained C_L of TRANAIR and Fluent (N.S). This can be best analyzed by checking the pressure distribution at some wing cross sections. Although the convergence levels of TRANAIR and Fluent are different (10^{-5} and 10^{-4} respectively), the same convergence levels are used for both AOA=0° and AOA= +1° for each solver, and it proves that the lift difference for the solvers at AOA=0° is not due to different convergence levels. The data in Table 5-2 also shows that the number of mesh nodes primarily chosen for the wing sections, especially in the leading edge area, has been fairly satisfying and refining the leading edge area discretization has not affected the total lift.

Figure 5-7 and Figure 5-8 compare the pressure distribution on the wing surface computed by TRANAIR and Fluent (N.S) at M0.75, AOA= +1° and AOA= 0°, both at inlet nacelle mass flow rate equivalent to $\beta = 0.68$. The comparison is done at three span-wise cross-sections, one inboard (Y=1441.5 mm), one half (4102 mm) and one outboard (6000mm). These positions are shown in Figure 5-6.

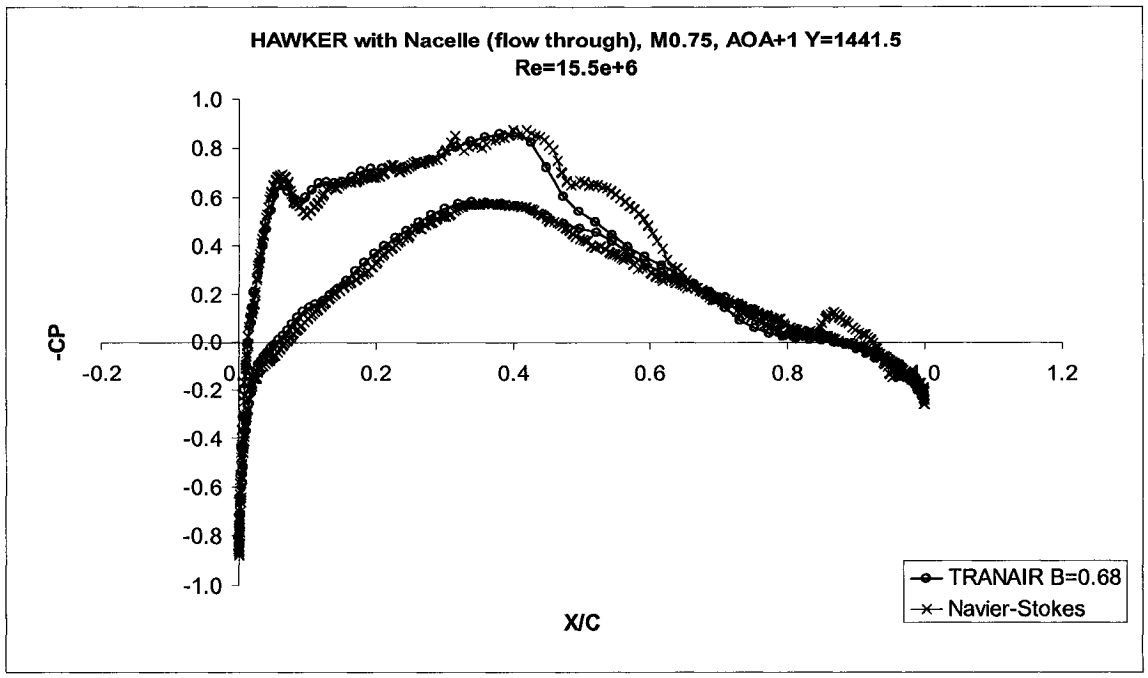

(a)

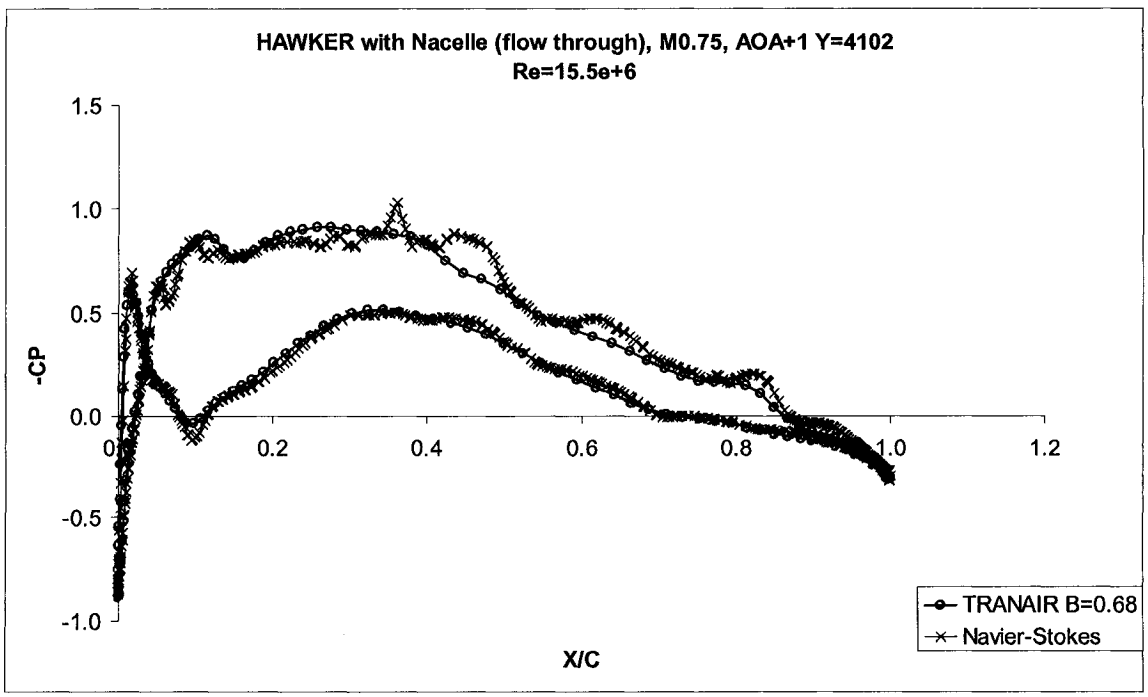

(b)

***Figure 5-7**: Pressure coefficient comparison of TRANAIR and Navier-Stokes for HAWKER with nacelle at M0.75 & AOA=+1° at 3 wing sections, (a) Y=1441.5 mm, (b) Y=4102 mm, (c) Y=6000 mm*

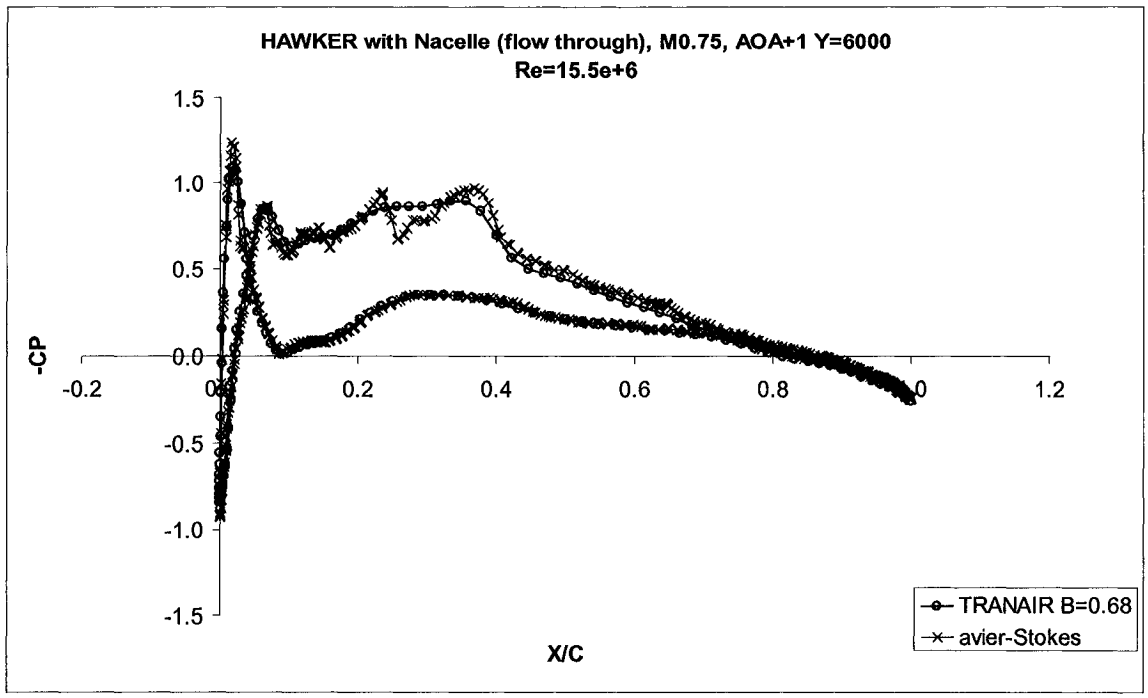

(c)

Figure 5-7 - Continued

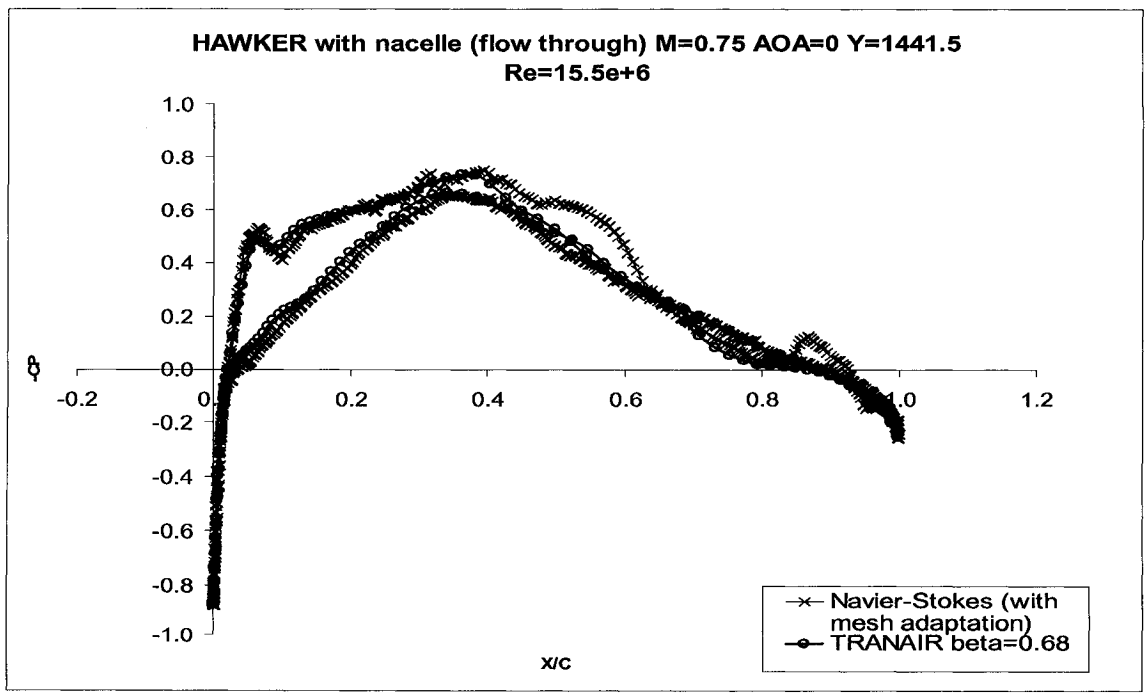

(a)

***Figure 5-8**: Pressure coefficient comparison of TRANAIR and Navier-Stokes (with mesh adaptation) for HAWKER with nacelle at M0.75 & AOA=0° at 3 wing sections, (a) Y=1441.5 mm, (b) Y=4102 mm, (c) Y=6000 mm*

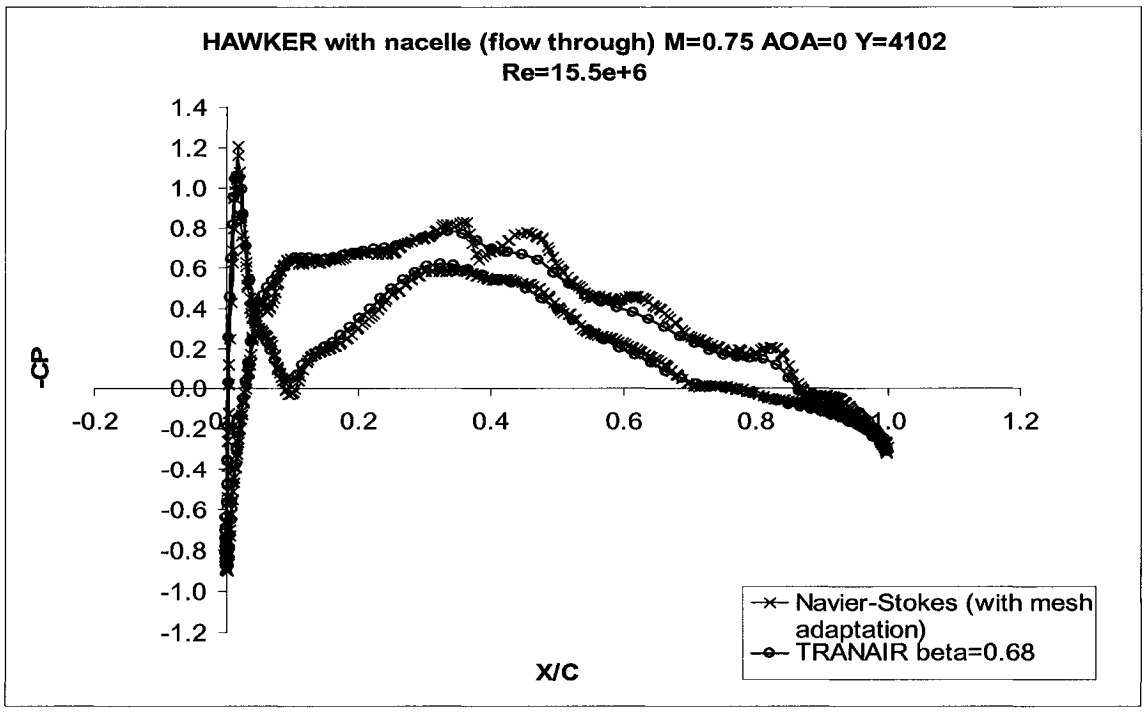

(b)

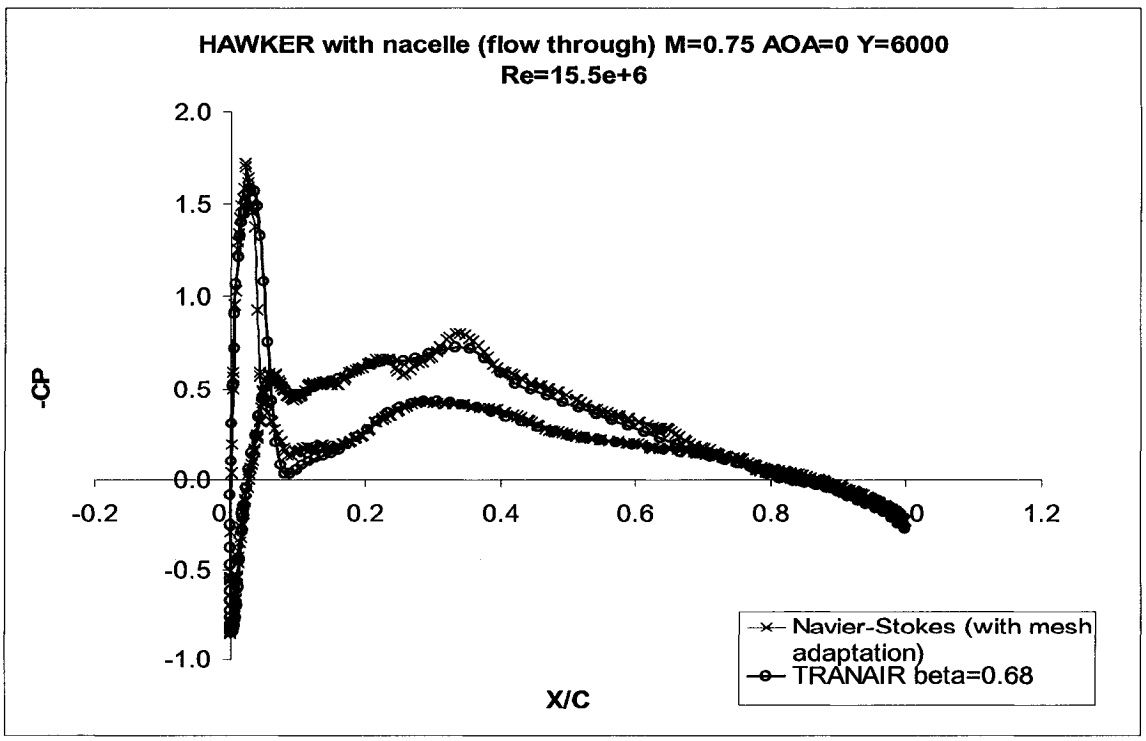

(c)

***Figure 5-8-** Continued*

The in-board cross sections, Figure 5-7(a) and Figure 5-8(a), are much more under the influence of the nacelle than the out-board sections. There are some fluctuations in C_P of top surface in Fluent (N.S) results for both angles of attack. They are because of the difference of the analysis and calculations between TRANAIR and Fluent (N.S). Basically, the results of all the analyses show that Fluent (N.S) pressure distribution has more fluctuations on most of the top surface regions. The fluctuations after the mid chord are directly due to nacelle and the way of introducing the nacelle mass flow rate in Fluent (N.S). That is why they become less and smaller in the sections far from nacelle. It is believed that the fluctuations before the mid chord are due to the surface smoothness or geometry error generated by GAMBIT. Figure 5-9 shows the GAMBIT mesh used in Fluent. Note that the mesh point is not exactly on the surface of the geometry represented by the green line in the figure.

As was mentioned in the last paragraph, the way through which the nacelle mass flow rate is introduced to the solver is different between TRANAIR and Fluent (N.S). For the HAWKER case, the geometry of nacelle was given from a section a little bit inside of the nacelle (*Hill face*), in such a way that the nacelle leading edge geometry was completely covered. Therefore, the Hill surface was distinct and fixed. In Fluent (N.S), it is possible to make a network on this surface (Hill) and introduce the exact amount of mass flow rate in that. But in TRANAIR, a fan-face shall be defined and mass flow rate shall be given via the area ratio of $A_\infty / A_{fan-face}$. More explanations of area ratio are given in 5.3.3. Therefore, the exactness of the fan-face area is very important in mass flow rate definition. For HAWKER, there is no information regarding the fan face X position, its

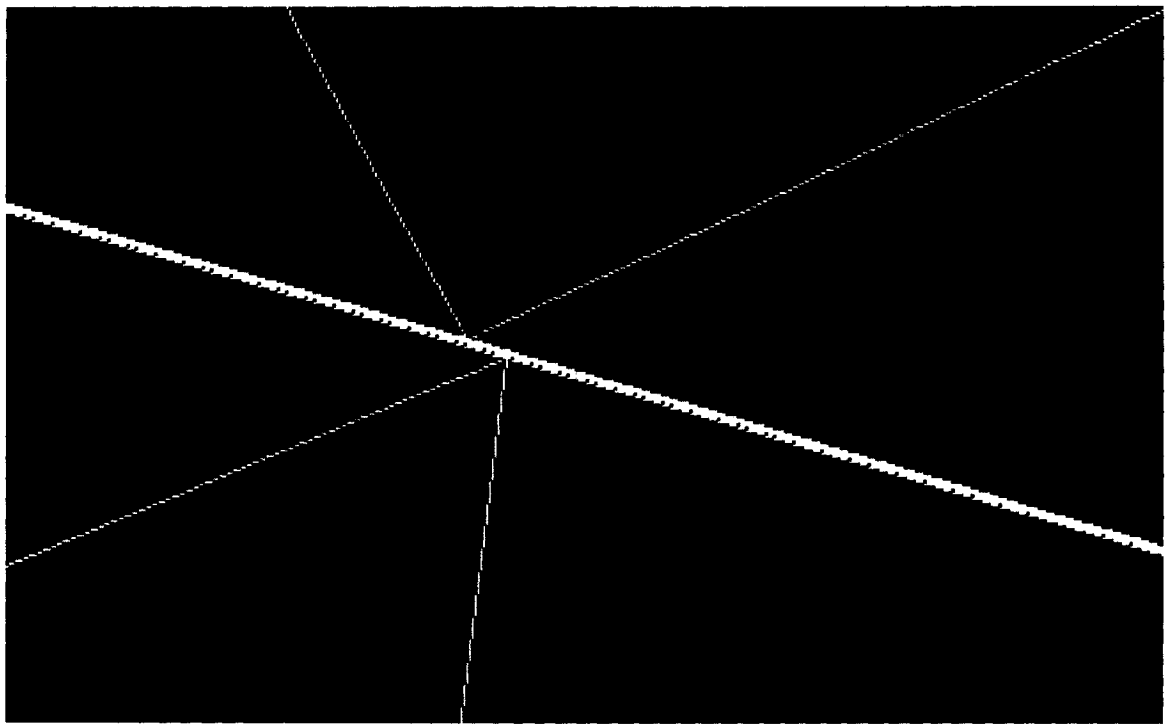

Figure 5-9: *Collapsed mesh (after adaptation) in the Fluent solver for HAWKER full configuration analysis*

area and the ram duct geometrical information. This can potentially cause some errors due to mass flow rate inexactness.

Except for the mentioned fluctuations, C_P for the rest of the regions shows good agreement for both angles of attack.

Unlike the case AOA=+1°, TRANAIR has some convergence problems at AOA=0° because of relatively mild to strong flow separations happening on the wing lower surface out-board. Therefore, some of the boundary layer ribs in this region are skipped and the boundary layer values for this area are approximated by interpolating the neighboring area values. Even with this modification, the convergence is difficult. The difference of converging time, mentioned in 5.3.1, confirms this behavior as well. The converging time after the modification is 3576 seconds (approximately 1 Hr.) based on 1500 iterations, which is long compared to similar cases. Such a problem exists for the

HAWKER case without nacelle at M0.75 and AOA=0° too, but for that case there is no need to make any modifications on the wing boundary layer properties, and only the time of convergence is high. As the separations are located on the wing outboard, neither the wing vertical position nor the nacelle suction could be the direct reason for that, and the only reason for this problem is probably the *wing surface quality* and the strange waves existing on the lower surface. Of course, this problem intensifies in the presence of the nacelle, and it can be said that nacelle suction has an indirect effect on the wing outboard separations and hard convergence. These separations at AOA=0° has been also experienced by industrial design groups (e.g. Boeing) for other configurations. This matter is explained in section 3.6.

For the case AOA=0°, although the C_L obtained with TRANAIR is almost half of C_L resulted by Fluent (refer to Table 5-2), the C_P results are still comparable, because the C_L of both solutions are very low. This matter can be confirmed well by looking at Figure 5-8.

5.3.3 Effect of area ratio

In TRANAIR, the nacelle area ratio ($\beta = A_\infty / A_{fan-face}$) has an important effect on total C_L. The reason is that this parameter defines the amount of mass flow rate coming inside the nacelle. Lower amount of β results in lower value of the mass flow rate. Therefore, the velocities on the top surface become lower than expected which reduces the lift.

Normally, in industry, mass flow rate is given in the form of A_∞ / A_{Hill}, where A_{Hill} is the area of the nacelle inlet after the leading edge section. Because of this reason, it is desired to fix this area ratio instead. For all the analyses done in the following sections

the amount of A_∞ / A_{Hill} is fixed to 0.7, based on the practice in industry. Considering the value of A_{Hill} to be approximately 341030.4 mm^2 for the HAWKER nacelle, new β can be calculated to be 0.63. Of course, it is also dependent on the X position of the fan face, due to the fan-face area change with X variations. This amount of β is considered for X_{fan}=9800 mm.

To see the effect of β, a TRANAIR analysis at M0.75 and AOA=0^o is done in two far values of β, 0.68 and 0.588. This can be seen in Figure 5-10 at one inboard and one outboard wing sections.

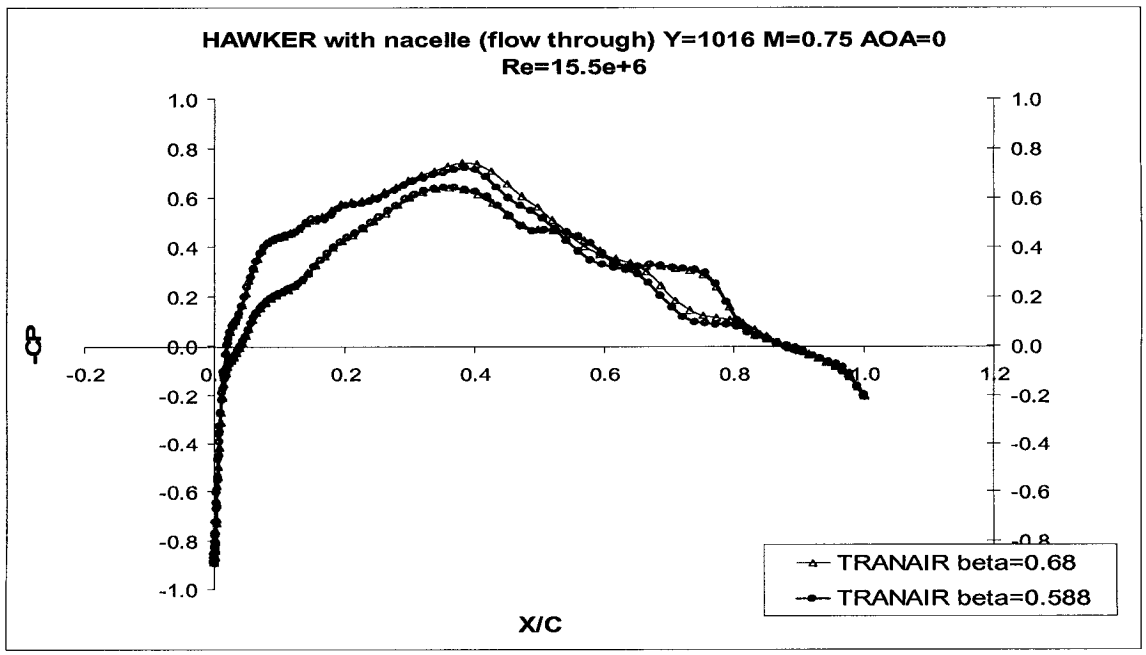

(a)

***Figure 5-10**: Pressure coefficient comparison of TRANAIR for HAWKER with nacelle in different nacelle mass flow rates at 2 wing sections, (a)Y=1016 mm, (b)Y=6000 mm*

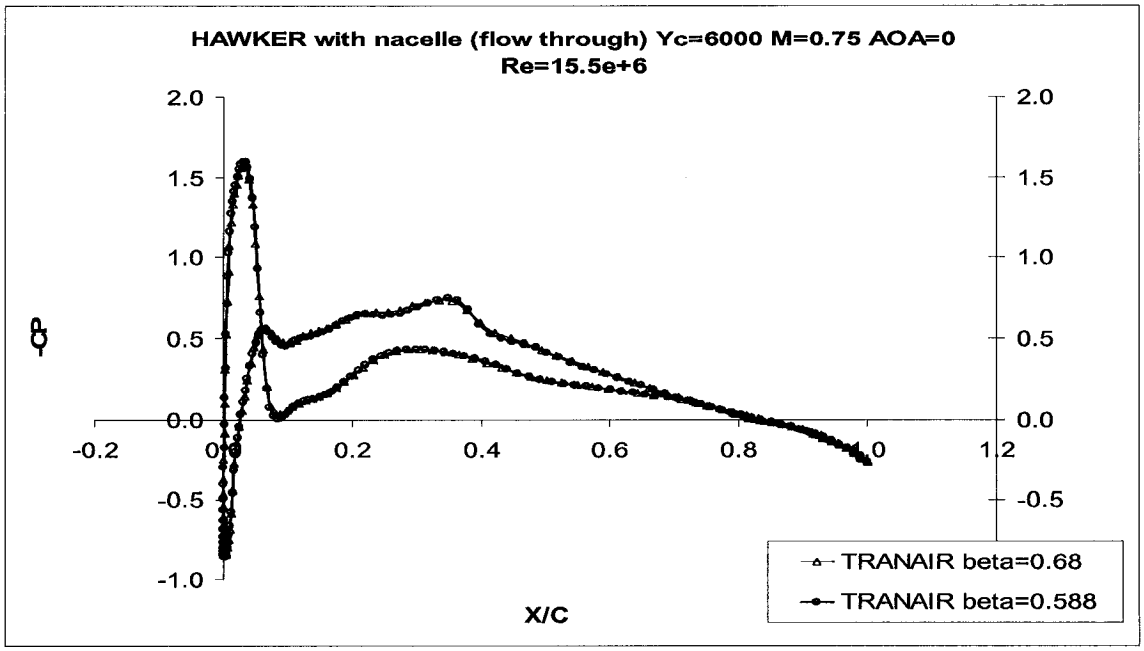

(b)

***Figure 5-10-** Continued*

β=0.588 gives the very low value of C_L=0.0051, which is low compared to the C_L for β=0.68 (which is equal to 0.0158) and to Fluent (N.S) results. It can also be seen that when moving toward the wing outboard the effect of β becomes less, because of getting far from the nacelle. The effect of β on C_L for this case with fan-face located at X=9800 mm is shown on a β versus C_L plot in Figure 5-11.

As can be seen in Figure 5-11, C_L increases with β, but it has a maximum limit. This limit is due to choking of the nacelle duct. When the nacelle chokes, the TRANAIR solver does not converge. The interesting case is β=0.71 in which the value of C_L is a little lower than that for β=0.7. In fact, this can be a good sign here to show the choking condition is very close.

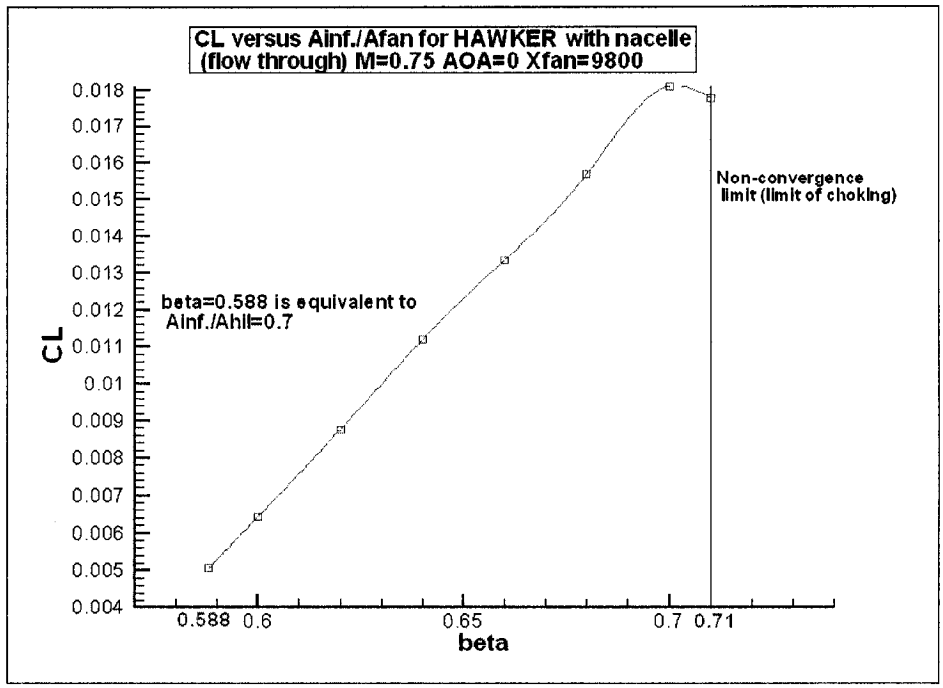

Figure 5-11: *Effect of nacelle mass flow rate (β) on total lift coefficient*

5.3.4 Effect of fan-face X position

As it was explained earlier, the inlet geometry of the HAWKER nacelle was not available, so the fan-face position was primarily estimated to be X_{fan}=9800mm. It was also assumed that the sectional change (reduction) from Hill surface to fan-face surface was linear. Due to low value of total C_L in X_{fan}=9800 mm and suspicious about the mass flow rate introduction (which was explained in 5.3.3), it seems logical to analyze the effect of fan face position and to do so, the fan-face horizontal position is changed to X_{fan}=9500 mm (i.e. 300 mm forward). With this modification, $A_{fan\text{-}face}$ varies too, because of linear area change with horizontal change of fan-face location. The fan-face area alters from $A_{fan-face} \approx 0.541325$ m^2 to $A_{fan-face} \approx 0.431066$ m^2. Therefore, considering A_∞ / A_{Hill} =0.7, the β parameter alters from 0.63 to approximately 0.791 for this new case.

The results for X_{fan}=9500 mm do not show much change in lift. Total C_L reduces from 0.009951 for X_{fan}=9800 mm ($\beta = 0.63$) to 0.008253 for X_{fan}=9500 mm ($\beta = 0.791$). Not much sensitivity of lift to fan-face horizontal position can be potentially because of the linear area change assumption considered for the fan-face with X position. In fact, it can be said that the X position of the fan-face has a critical impact on total lift and the mass flow rate, *provided the ram duct area change from Hill to fan-face is not taken linear*. This analysis proves that for an exact nacelle simulation it is very important to have exact geometrical information of ram, by-pass and primary exhaust ducts. Taking linear area change is one of the sources of errors in the total lift and wing pressure distribution.

Finally, it should be noted that similar for the case X_{fan}=9800 mm, this new case is also very sensitive to β parameter and the change in β causes an approximate linear change in total C_L up to the limit of choking.

5.3.5 Effect of boundary layer mesh adaptation in Navier-Stokes results

As explained in 5.3.1, it is important to use adaptation method for a real aircraft simulation. In Fluent, a method for adapting the mesh in the boundary layer and close to objects' surface can be utilized. In this way, one thin layer adjacent to the boundary surface will have a finer mesh so that its y^+ is reduced. To see the effects of mesh adaptation, the adaptation method is used in the mesh of Navier-Stokes in such a way that y^+ changes from 50 to about 10-20 and the solution is updated. Figure 5-12 is a wing C_P comparison for the HAWKER case similar to Figure 5-8, but containing also the results for the case without mesh adaptation (in Navier-Stokes) and at three in-board sections in front of nacelle to see the effects of adaptation.

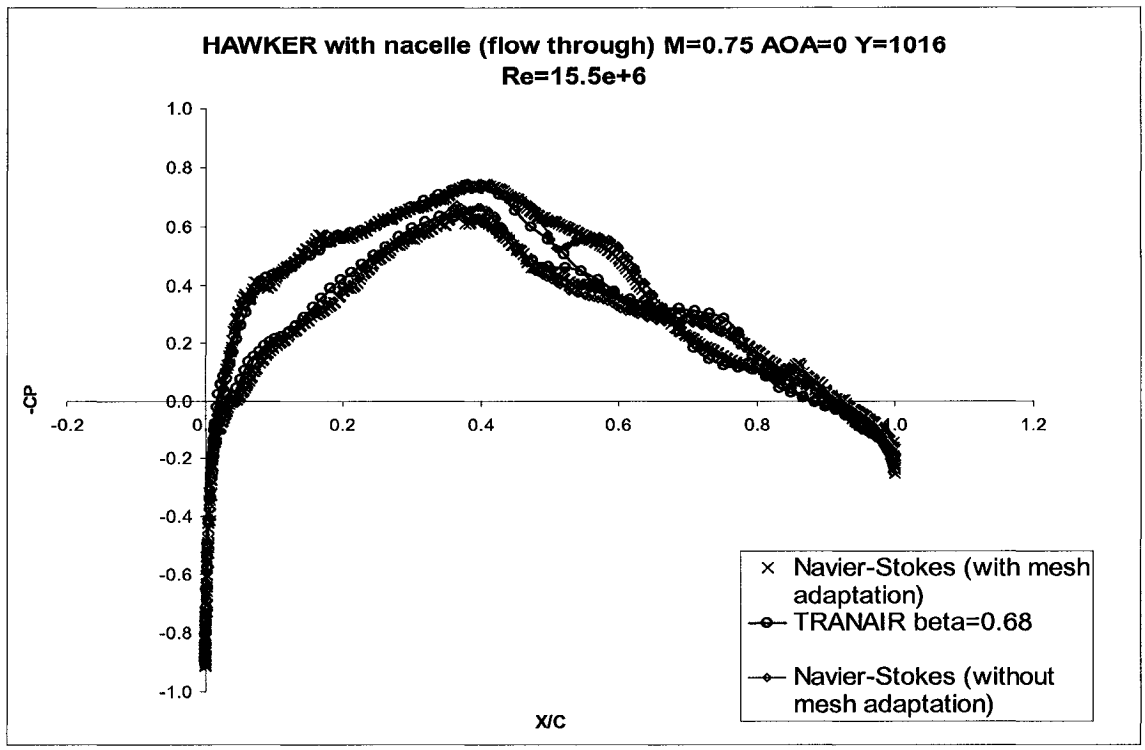

(a)

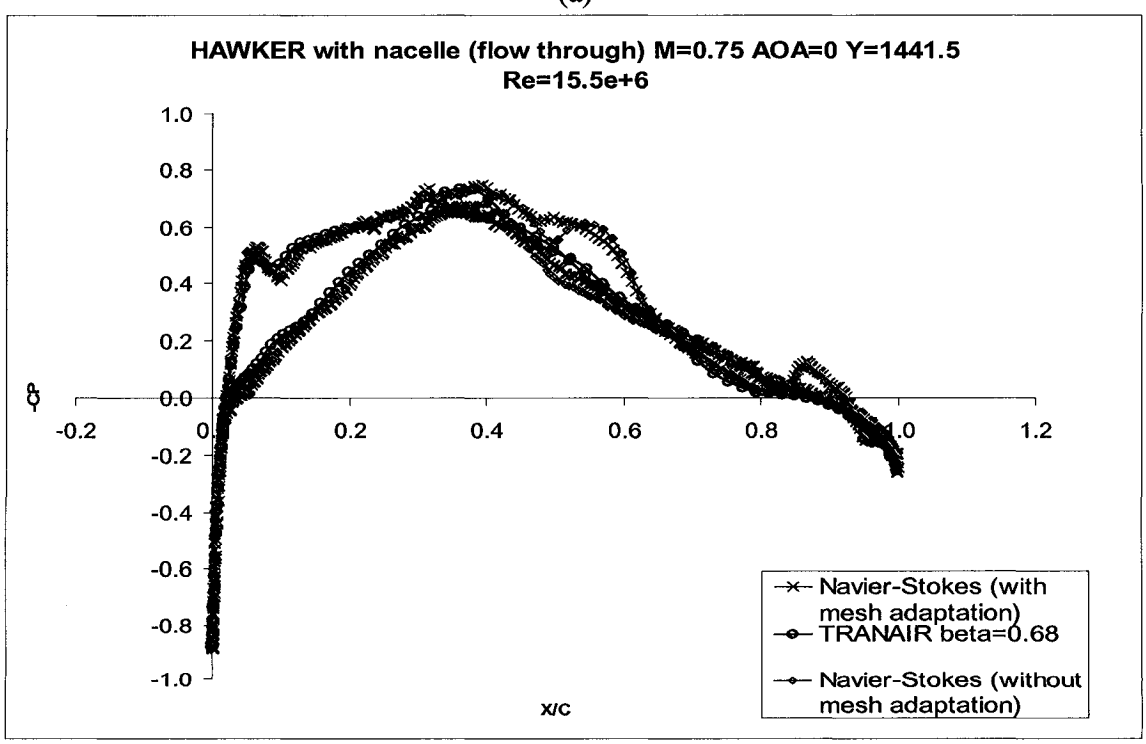

(b)

***Figure 5-12**: Pressure coefficient comparison of TRANAIR and Navier-Stokes (with and without mesh adaptation) for HAWKER with nacelle at M0.75 & AOA=0° at 3 in-board cross sections on the wing, (a) Y=1016 mm, (a) Y=1441.5 mm, (c) Y=1822 mm*

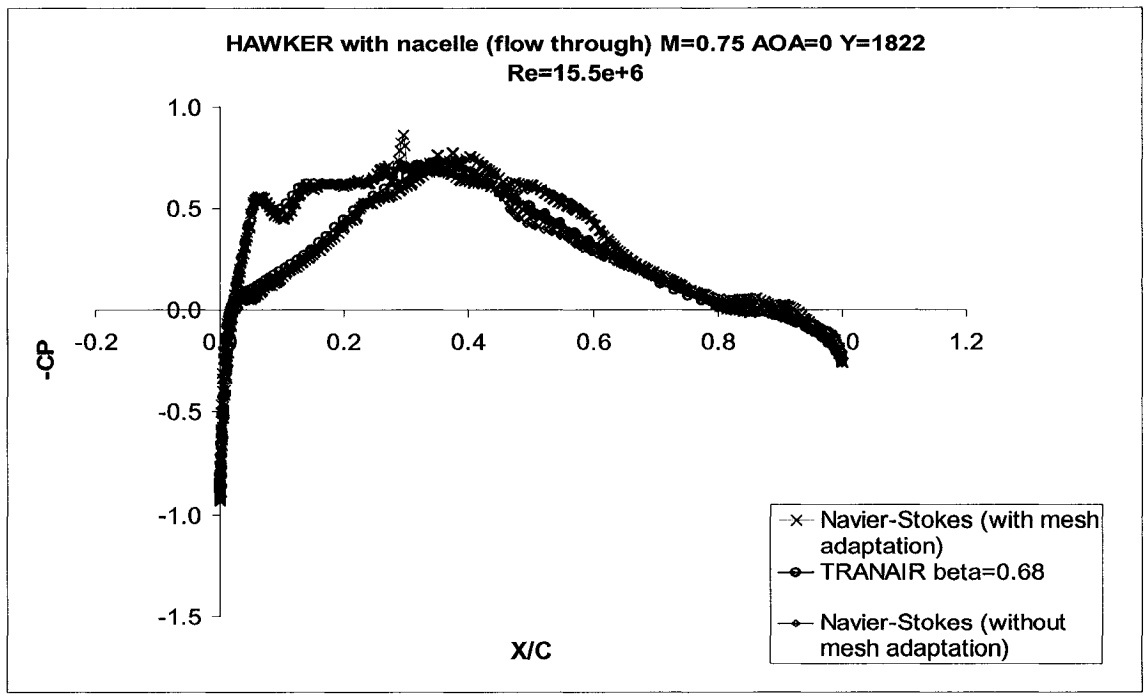

(c)

***Figure 5-12-** Continued*

Total C_L obtained by the Fluent (N.S) solver changes from 0.03378 to 0.03244 after mesh adaptation, but this change is not enough to close the gap between the TRANAIR and Fluent results.

One of the important results of the mesh adaptation is the relative smoothening of the C_P fluctuations on the wing top surface after half chord. This is a good result and proves that these fluctuations have another cause (except flow physics and the type of solution) related to the numerical discretization. By the way, the fluctuations did not disappear completely, because of different mass flow rate representation and the type of flow solution in TRANAIR and Navier-Stokes solvers.

5.3.6 Effect of nacelle mass flow rate

To see the effects of nacelle mass flow in TRANAIR and Fluent (N.S) total C_L and C_P distribution at different wing sections, the mass flow rate is reduced from

$\dot{m} = 38.6kg/s$ to $\dot{m} = 32.2kg/s$. This new case is equivalent to A_∞ / A_{Hill} =0.7 and for TRANAIR solution, this is equal to changing the area ratio (β) from 0.68 to approximately 0.63 (refer to 5.3.3). Figure 5-13 compares the TRANAIR and Fluent (N.S) C_P at 5 wing span-wise locations (three inboard, one half and one outboard) at M0.75 and AOA=0°. It is good to note that in Navier-Stokes solution, similar the case with $\dot{m} = 38.6kg/s$, the value of y^+ for boundary layer close to surface is taken as about 10-20 and the mesh size used for this case is approximately 10e+6.

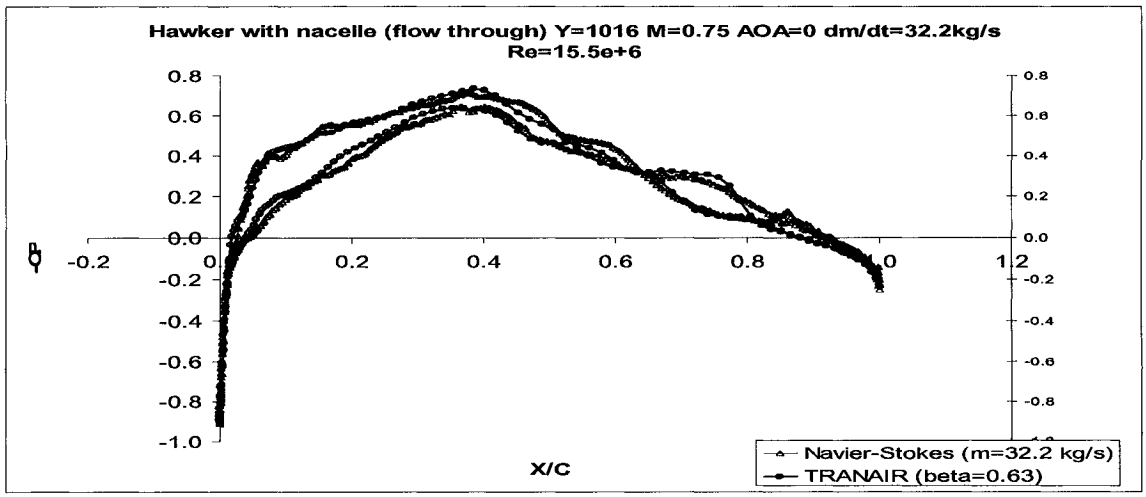

(a)

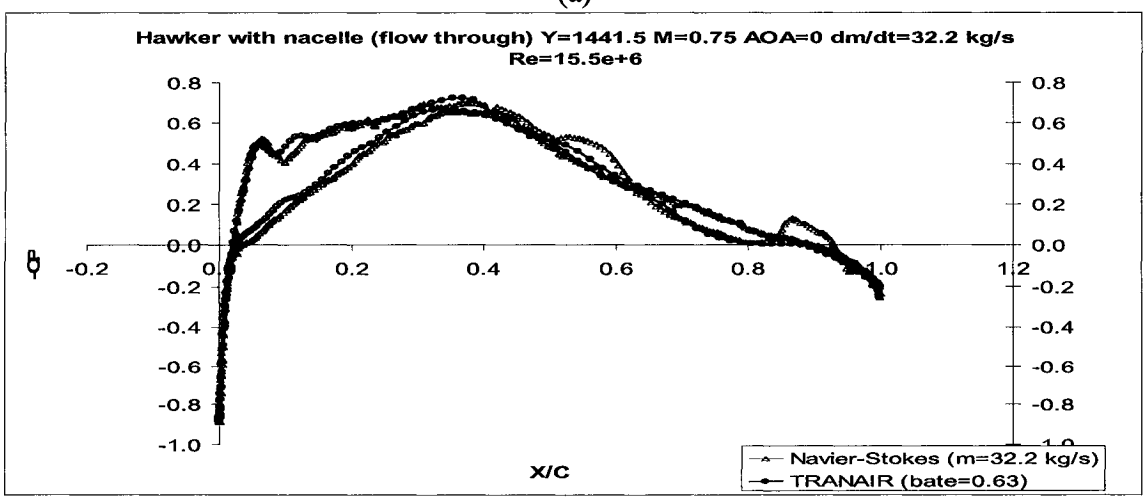

(b)

***Figure 5-13**: Pressure coefficient comparison of TRANAIR and Navier-Stokes for HAWKER model with nacelle mass flow rate of 32.2 kg/s at 5 wing span-wise locations (a) Y=1016 mm, (b) Y=1441.5 mm, (c) Y=1822 mm, (d) Y=4102 mm, (e) Y=6000 mm*

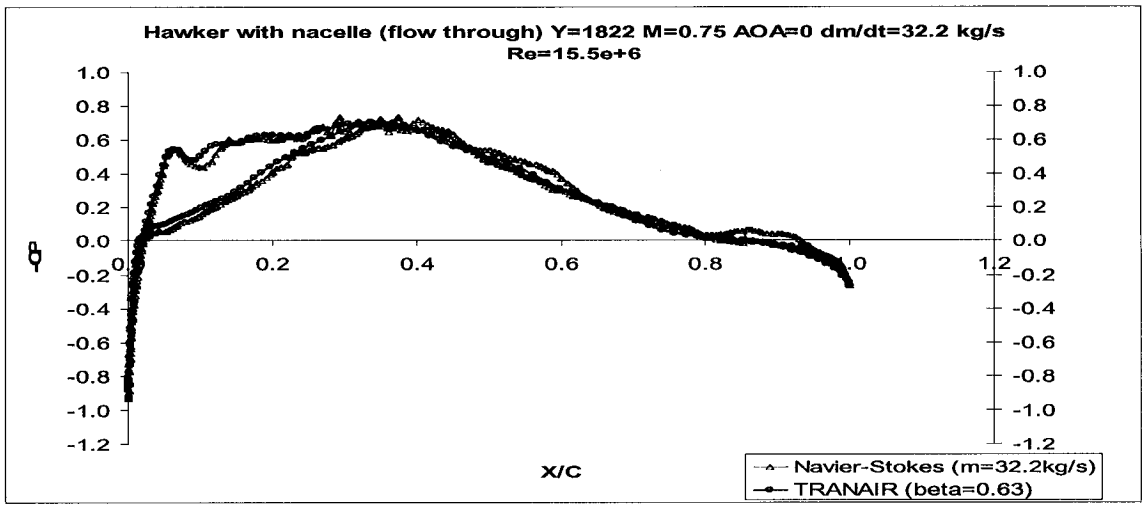

(c)

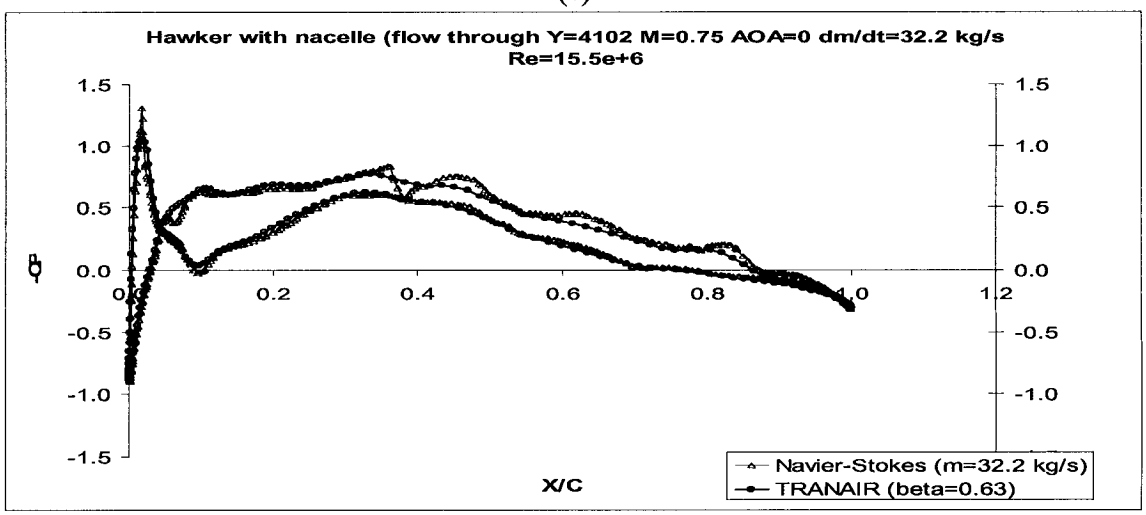

(d)

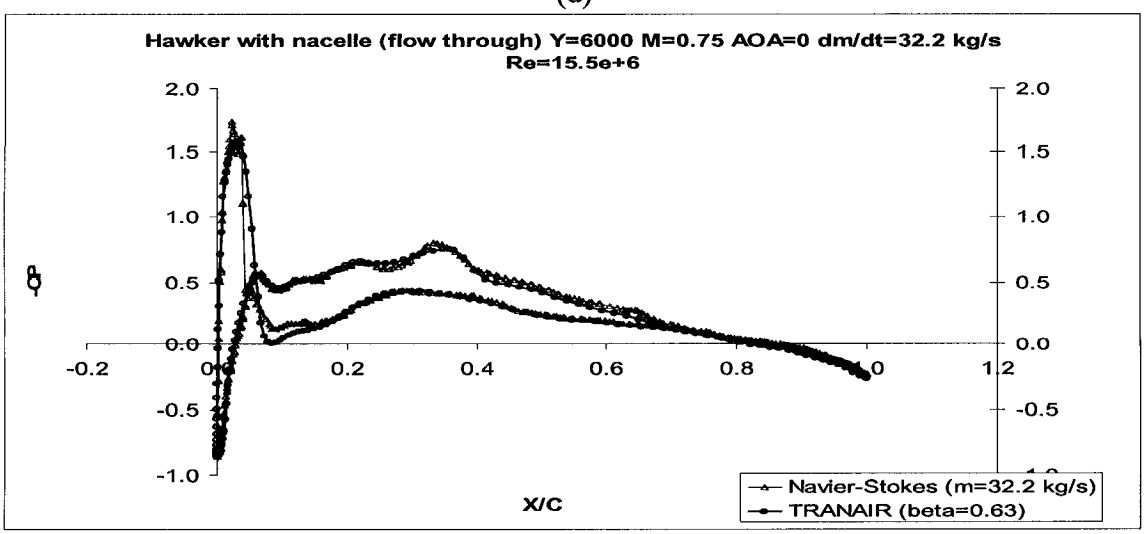

(e)

Figure 5-13- *Continued*

The domain of small fluctuations in C_P (for Navier-Stokes) on the top surface after mid chord look like to shrink when reducing the nacelle mass flow rate comparing to the same case at higher mass flow rate (Figure 5-8). This causes the total C_L of both solvers to become closer. As was mentioned in previous sections, the physical source of these fluctuations is the nacelle suction and disappearing the fluctuations in the half and out board sections, in Figure 5-13(d) & (e) proves this matter as well. Similar to the case with higher nacelle mass flow rate the fluctuations in C_P of some of the regions of this case (reduced mass flow rate), especially for sections in front of the nacelle, are because of the way that mass flow rate is introduced and analyzed in Fluent (N.S).

The results of total C_L are much more interesting. Total C_L obtained by TRANAIR for $\dot{m} = 32.2kg/s$, is 0.009951 at M0.75 and AOA=0° and C_L obtained by Fluent (N.S) is 0.017916. Not only the amount of lifts is closer comparing to the case $\dot{m} = 38.6kg/s$ (refer to Table 5-2), but also the C_L ratio is reduced from about 2.1 to 1.8 and this proves that the Fluent results (deviations in C_L) are more sensitive to mass flow rate than TRANAIR results. The C_L obtained by TRANAIR is expected based on the CL-β curve in Figure 5-11, but for Fluent (N.S)it seems to be less than expected showing that the mass flow rate influence (on C_L) in Fluent (N.S) is much more tangible.

For this new case, it also seems logical to do the analysis at other angles of attack and produce a C_L-α curve for both solvers. In this way, the results at AOA=0° can be validated well, if the trend of C_L change with changing the angle of attack is almost the same for both solvers. Figure 5-14 shows the C_L-α curve for TRANAIR and Fluent (N.S) results both at $\dot{m} = 32.2kg/s$ and M0.75.

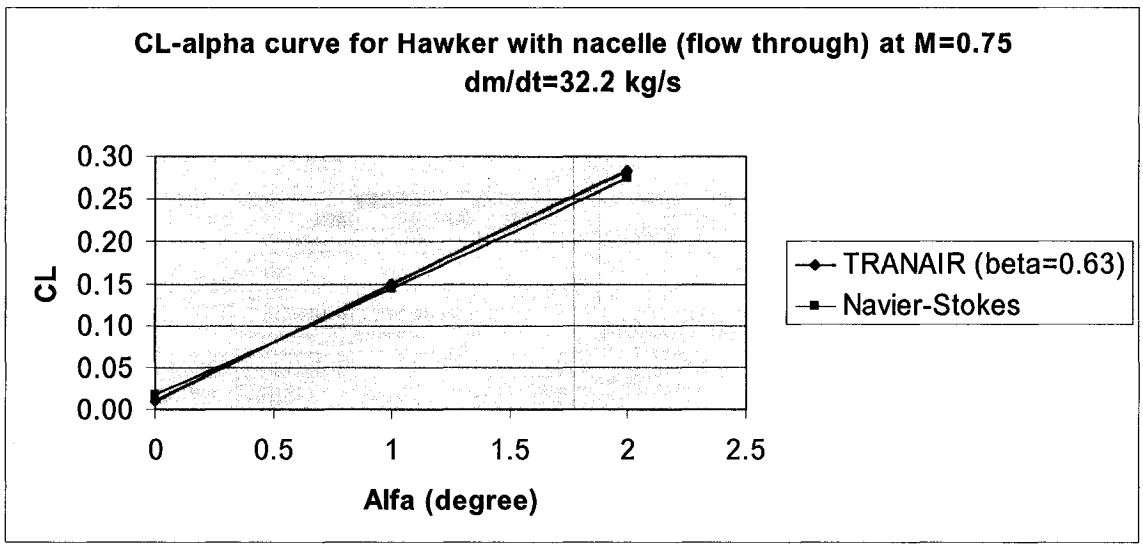

***Figure 5-14**: C_L-α curve for TRANAIR and Navier-Stokes results of HAWKER model at $\dot{m} = 32.2kg/s$ and M0.75*

Figure 5-14 shows that the total C_L of TRANAIR at AOA=0° is a little off comparing to Fluent (N.S). It can be potentially due to the TRANAIR problem for the HAWKER case at AOA=0° because of the existence of separations on the wing lower surface outboard close to the tip, which forced to skip some of the boundary layer ribs in those areas. This matter is explained in detail in section 5.3.2. Except this deviation, the trend of C_L increase with angle of attack for both solvers is almost similar.

5.4 Summary

Aerodynamic CFD analysis of existing real aircrafts can contribute to see the effects of the irregularities due to manufacturing and installation limits. For this purpose, the surface of a real full configuration aircraft, HAWKER 800, was scanned by laser and the scanned surfaces were discretized and solved by two different solvers to check the effects of different parameters on aerodynamic characteristics.

Analyzing the HAWKER configuration without nacelle shows that TRANAIR solver is more sensitive to the mesh quality than Fluent (N.S). Therefore, to get a complete convergence in TRANAIR, especially at higher Mach numbers, it is needed to smooth the surface grid in such a way that there is not much geometry and aerodynamic change. In addition, TRANAIR cannot be converged for the cases with strong separated flows. Even for the cases with weak to mild separations, TRANAIR results might have remarkable errors, especially for the pressure computation.

One of the problems of laser scanning is the difficulty of representing the high gradient regions, e.g. leading edge and its vicinity. This problem can be seen in the results of the HAWKER total lift obtained by both TRANAIR and Fluent (N.S) solvers.

Although, some of the irregularities on the surface of the components may increase the lift haphazardly, it is always beneficial to perform a drag analysis to see their effect in increasing the drag force as well. A lift to drag ratio analysis can show the general effects of such irregularities well.

Aerodynamic analysis of HAWKER full aircraft configuration with nacelle shows the strong influence of nacelle suction on different aerodynamic parameters, mainly on the total lift and the flow pattern around the wing. This influence has more impact on the TRANAIR solution than Fluent (N.S), as TRANAIR is very sensitive to surface quality and any flow change on the wing may cause separation in TRANAIR. It is the reason why TRANAIR cannot be converged easily for the HAWKER case at M0.75, AOA0°, while the best convergence can be obtained for the same case at AOA+1°. Nevertheless, the results of C_P show a good agreement between TRANAIR and Fluent (N.S) solutions in almost all the regions, except on the wing top surface after mid chord for the sections

in front of the nacelle. This can be due to the different ways that nacelle mass flow rate is introduced to each solver.

In TRANAIR, the mass flow rate defined by area ratio ($A_{\infty}/A_{fan-face}$) has a direct influence on total lift. Increasing the mass flow rate causes the total lift increases linearly. But, there is a choking limit and increasing the mass flow rate more than the limit causes choking in the nacelle and TRANAIR failure. In addition, for best nacelle analysis in TRANAIR, it is important to have the exact geometrical information of the ram, core cowl and by-pass ducts and the X position of the fan face. Although the X position of fan face is effective on the wing flow pattern, it does not have much effect on total lift, if the area change from the nacelle Hill surface up to the fan face is taken linear. It proves the importance of possessing all the nacelle geometrical information for aerodynamic analyses.

Finally, it should be noted that using adaptive meshing method for the Fluent (N.S) solution can give more precise results, especially for the full configuration aircraft cases. Adaptive meshing contributes to smoother pressure changes on the wing top surface after the mid chord for the sections affected more by the nacelle. It is also good to mention that the Fluent (N.S) results are more sensitive to nacelle mass flow rate than TRANAIR results, and increasing the mass flow rate causes the lift rise with higher rate in Fluent (N.S) than in TRANAIR.

Chapter 6

6 CONCLUSIONS AND RECOMMENDED FUTURE WORKS

6.1 Conclusions

The main objectives and contributions of the current work are to evaluate the potential of TRANAIR to analyze an existing aircraft, where the geometry is obtained from scanning. TRANAIR is a user-friendly solver that has many features including boundary layer coupling, design, solution restart, etc. TRANAIR does need a vast knowledge of the problem's physics and analytical techniques to be used adequately. In fact, for each CFD code as well as TRANAIR, learning how to analyze the results and to give a strong analytical discussion is much more important and difficult than only using the codes.

This work also tries to give a comparison between TRANAIR and Fluent (N.S) aerodynamic analysis with some real sample cases and to find the effects of many parameters on the total lift coefficient and pressure distribution on the aircraft wing. TRANAIR versus Navier-Stokes analysis gives very interesting results that are mainly due to the difference in nature of these solvers. Basically, caution shall be taken when Navier-Stokes versus TRANAIR comparisons are made at maximum operating Mach number (MMO), especially at angle of attacks where more flow separation should be expected. TRANAIR is not designed for flows with significant separation while the Navier-Stokes codes are. While both codes may be challenged, they will not be challenged equally for different aspects. In TRANAIR and Fluent (N.S), it is better to

simulate attached flows at constant C_L instead of constant AOA and for separated flows, the constant AOA is recommended. It is recommended to use both TRANAIR and Fluent (N.S) codes for a complete analysis. TRANAIR has advantage in obtaining matrix analysis quickly and design optimization, while Fluent (N.S) is more appropriate for separated flows and predicting the drag forces. From the analyses done, it is concluded that TRANAIR is typically better than Fluent (N.S) codes for the analysis of attached transonic flows.

Inviscid versus viscous analysis in TRANAIR can illustrate that the viscous simulation by coupling the boundary layer is done based on the expectations and the results are fairly similar to what other codes can generate. Relieving the strength of the shock and moving it toward its real position backward causes the total lift to decrease, which can be seen clearly in TRANAIR viscous results.

There are many limitations for TRANAIR to give good convergence or reasonable results. While high angles of attack may cause strong separation on the wing, negative angles can transfer separation to the horizontal tail. Therefore, TRANAIR is one of the best solvers for aircrafts at cruise condition, where AOA is close to zero. For TRANAIR simulations, cruise condition can be set to angles of attack close to but not exactly zero, as for some cases nonzero angles of attack give better convergence. Comparing to other solvers, TRANAIR is more sensitive to surface quality. It is a challenge in TRANAIR to get a complete convergence or realistic results for the surfaces with high smoothness problem. TRANAIR users must be careful when analyzing the aircraft at or close to maximum operating Mach number. At higher Mach numbers many parameters mainly surface roughness can cause convergence failure.

In TRANAIR, viscous analysis can cause many kinds of failures that inviscid does not. Too large transpiration problem in viscous analysis can be either because of the geometry design and relatively high surface curvatures or due to scale dependency. In viscous analysis the truncation related abutment problem can happen which can be caused by abutment tolerance or scale issues. Normally, experience and good analytical skills are needed to distinguish the right source of problem in these circumstances. It should also be noted that introducing laminar, turbulent or mixed (with transition) boundary layer for different components needs a good understanding of the problem and the application.

In most of the business jets, low elevation of wing position is due to increasing the total lift and getting the minimum destroying nacelle/wing interferences. Descretization of a low wing aircraft is always a challenge in AGPS, as there is not a clean and closed wing/body intersection for this case. Recent development of the BizJet package in AGPS has almost resolved this problem.

Using local box (LBO) regions in TRANAIR is vital. With these boxes, it is possible to specify very special regions for higher levels of refinement without enforcing the refinement requirements to other less important areas. It has a great impact on cost and storage savings. First, choosing the right LBO regions including the important areas and excluding the non-necessary high gradients regions (e.g. fuselage base, wing tip wake, etc.) and second, selecting the right number of initial, intermediate and final boxes, have a great impact on the convergence time and the exactness of the solution.

In TRANAIR, the best way to model the nacelle in flow through or powered condition is to take a fan-face, a by-pass exhaust face and a core exhaust face. If these boundary faces are not considered, the exact geometry of the nacelle inside should be available. In

addition, having the exact amount of fan-face area and the ram duct and exhausts ducts geometry are very vital in getting accurate results. The X position of fan-face does not have much effect on lift, if the ram duct area change is taken to be linear.

In TRANAIR, the nacelle area ratio ($A_\infty / A_{fan-face} = \beta$) which defines the nacelle inlet mass flow rate is very effective in configuration total C_L and its rise causes the C_L increase, but up to the limit of nacelle duct choking.

When analyzing the pressure distribution on wing sections in front of the nacelle, Fluent (N.S) results show some fluctuations in pressure due to the nacelle suction and collapsing the mesh used for Fluent (N.S) after adaptation. TRANAIR resultant pressure in these regions is smoother. Using mesh adaptation for Fluent (N.S) will smooth the pressure fluctuations on the wing top surface after the mid chord. But, the fluctuations can not be removed completely, because the sources of these fluctuations, which mainly are different solution methods and different mass flow rate introduction in TRANAIR and Fluent, still exist.

Finally, it should be added that for some aircraft designs, better TRANAIR convergence can be obtained for angles of attack other than 0°. The industrial experiences at Boeing for some cases confirm these results.

6.2 Recommended future works

Although TRANAIR is not a good tool for drag analysis and Navier-Stokes codes can work much better for this purpose, the drag analysis in TRANAIR can be very interesting, especially for the business jets with aft-mounted nacelles. Possessing some experimental data for nacelle drag and doing analyses with TRANAIR and Fluent (N.S)

can greatly improve the available information about TRANAIR drag prediction exactness and capabilities.

For the HAWKER case, the aerodynamic analysis with nacelle having all the exact geometry and property information of its nacelle is recommended for the future. In fact, possessing the exact geometrical data can get the best results regarding the effect of area ratio and X position of the fan face. It is also possible to do a complete analysis for the position and optimum number of exhaust faces.

Getting the exact property information for the nacelle, another aspect of nacelle analysis, namely called powered nacelle can be performed and improved in TRANAIR. Powered analysis is of great interest in industry as the total drag and the engine thrust can be well predicted. With powered nacelles, it might be possible to analyze the internal duct choking and all the parameters affecting it. In addition, it might be possible to see the under-expanded nozzle effects on the operation of whole nacelle and generally on the aircraft.

Although many features of TRANAIR solver are discussed in this work, there are still some features that need more explanations based on the new experiences with the same or other cases. One of the main items of these features is the design and optimization capability of TRANAIR. Multi-point design is one of the relatively new features of TRANAIR that has improved the quality of the design extensively, but needs more investigation.

Finally, it should be noted that for aircraft manufacturers analyzing aircrafts with one engine inoperative is very interesting, as there are many requirements in FAR and JAR standards for aircrafts flying in this situation. To do such an analysis, it is needed to solve

the cases at unsteady flow condition, as the flutters and flaps deflections (changing with time) are used to minimize high amount of yawing moment generated in these circumstances. TRANAIR has the capability of solving unsteady flow cases and there are many features in TRANAIR for these kinds of flows that should be discussed, analyzed and improved.

BIBLIOGRAPHY

[1] Holst, T.L., *Transonic flow computations using nonlinear potential methods*, Progress in Aerospace Sciences, v 36, n 1, Jan., 2000, p. 1-61.

[2] Caughey, D.A., Jameson, A., *Development of Computational Techniques for Transonic Flows: An Historical Perspective*, Symposium Transonicum IV, Geottingen, September 2002.

[3] Calmar Research Corporation, *Aero-Grid Paneling System User Guide*, Version 20.00, 2003.

[4] Jameson, A., Transonic potential flow calculation using conservative form, Second AIAA CFD Conference, 1975, p. 148-155.

[5] Jameson, A., Caughey, D.A., *A finite-volume method for transonic potential flow calculations*, Third AIAA CFD Conference, 1977, p. 35-54.

[6] Caughey, D.A., Jameson, *Numerical calculation of transonic potential flow about wing-body combinations*, AIAA Journal, **17**: 175-81, 1979.

[7] Caughey, D.A., Jameson, *Progress in finite-volume calculations for wing-fuselage combinations*, AIAA Journal **18**: 1281-8, 1980.

[8] Johnson, F.T., Tinoco, E.N., Yu, N.J., *Thirty Years of Development and Application of CFD at Boeing Commercial Airplanes, Seattle*, AIAA Paper, 2003-3439, 2003.

[9] Jameson, A., Caughey, D.A., *A Finite Volume Method for Transonic Potential Flow Calculations*, AIAA Paper 77-635, Proceedings of Third AIAA Computational Fluid Dynamics Conference, Albuquerque, June 1977, p. 35-54.

[10] Jameson, A., *Remarks on the Calculation of Transonic Potential Flow by a Finite Volume Method*, Proceedings of IMA Conference on Numerical Methods in Applied Fluid Dynamics, Academic Press, 1980, pp. 363-386.

[11] Young, D.P., Melvin, R.G., Bieterman, M.B., Johnson, F.T., Samant, S.S., Bussoletti, J.E., *A locally refined rectangular grid finite element method: Application to computational fluid dynamics and computational physics*, Journal of Computational Physics **92**: 1-66, 1991.

[12] Burkhart, R.H., *Asymptotic expansion of the free-space Green's function for the discrete 3-D Poisson equation*, SIAM Journal on Scientific Computing, v 18, n 4, Jul., 1997, p. 1142-1162.

[13] Bieterman, M.B., Bussoletti, J.E., Hilmes, C.L., Johnson, F.T., Melvin, R.G., Young, D.P., *An adaptive grid method for analysis of 3D aircraft configurations*, Computer Methods in Applied Mechanics and Engineering **101**:225-49, 1992.

[14] Smith, M.F., *User-Friendly CFD: Application to TRANAIR for Analysis of Transport Aircraft*, AIAA Paper, 1998-5574, 1998, World Aviation Conference, Sep. 1998.

[15] Madson, M., Moyer, S., Cenko, A., *TRANAIR Computations of the Flow about a Generic Wing/Pylon/Finned-Store Configuration*, AIAA Paper, 94-0155, 1994.

[16] Madson, M.D., *Transonic analysis of the F-16A with under-wing fuel tanks: An application of the TRANAIR full potential code*, AIAA Paper, 87-1198, 1987.

[17] Cenko, A., Madson, M., *TRANAIR Applications to Predicting the F/A-18E Wing Pressures*, AIAA Paper, 1995-0533, 1995.

[18] Chen, A.W., Curtin, M.M., Carlson, R.B., Tinoco, E.N., *TRANAIR Applications to Engine/Airframe Integration*, Journal of Aircraft **27**:716-21, 1990.

[19] Melvin, R.G., Johnson, F.T., Young, D.P., Foutch, D.W., Bussoletti, J.E., Bieterman, M.B., *Using a Full Potential Solver for Propulsion System Exhaust Simulation*, Journal of Propulsion and Power. Vol. 9, no. 3, p. 412-421. May-June 1993.

[20] Melvin, R.G., Huffman, W.P., Young, D.P., Johnson, F.T., Hilmes, C.L., Bieterman, M.B., *Recent Progress in Aerodynamic Design Optimizatio*n, International Journal for Numerical Methods in Fluids **30**:205-216, 1999.

[21] Jou, W., Huffman, W., Young, D., Melvin, R., Bieterman, M., Hilmes, C., Johnson, F., *Practical Considerations in aerodynamic design optimization*, AIAA Paper, 95-1730-CP, 1995.

[22] Rudnic, R., Rossow, C.C., Geyr, H.V., *Numerical simulation of engine/airframe integration for high-bypass engines*, Journal of Aerospace Science and Technology **6**:31-42, 2002.

[23] Hirsch, C., *Numerical Computation of Internal and External Flows*, Vol. 2, New York: John Wiley & Sons, 1998.

[24] Bateman, H., *Irrotational Motion of a Compressible Inviscid Fluid*, Proceedings of the National Academy of Sciences, Vol. 16, 1930, p. 816-825.

[25] Saad, Y., Schultz, M.H., *A Generalized Minimal Residual Algorithm For Solving Nonsymmetric Linear Systems*, SIAM Journal on Scientific and Statistical Computing **7**: 856, 1986.

[26] Bieterman, M.B., Bussoletti, J.E., Hilmes, C.L., Johnson, F.T., Melvin, R.G., Young, D.P., *Solution adaptive local rectangular grid refinement for transonic*

aerodynamic flow problems, 8th GAMM Conference on Numerical Methods in Fluid Mechanics, Sep. 1989, p. 22-33, 1990.

[27] Boeing, TRANAIR User's Manual (Version G00), *D6-57030*, REV E, 2004.

[28] Jameson, A., *Transonic Flow Calculations*, Princeton University Report MAE 1652, March 1984.

[29] HAWKER 800 & 850 XP Aircrafts Specifications and General Information about Configuration, http://en.wikipedia.org/wiki/Hawker_800

[30] AGARD-AR-303, *A Selection of Experimental Test Cases for the Validation of CFD Codes*, Advisory Group for Aerospace Research and Development North Atlantic Treaty Organization, Aug. 1994, http://aiaa.org/tc/apa/dragpredworkshop/agard-ar-303.pdf

[31] Proceedings of the 1st AIAA CFD Drag Prediction Workshop, *Preceding the 19th APA Conference*, Anaheim, CA June 9-10 2001, (DLR-F4 wing fuselage combination),http://aaac.larc.nasa.gov/tsab/cfdlarc/aiaa-dpw/Workshop1/files/geo--metry.html

[32] Hemsch, M., Morrison, J., *Statistical Analysis of CFD Solutions from 2nd Drag Prediction Workshop*, AIAA Paper, 2004-556, 2004, p. 4951-4981.

[33] Hirsch, C., *Numerical Computation of Internal and External Flows*, Vol. 1, New York: John Wiley & Sons, 1998.

[34] AIAA CFD Drag Prediction Workshop, Anaheim, CA June 9-10 2001, (DLR-F4 wing fuselage combination), http://aaac.larc.nasa.gov/tsab/cfdlarc/aiaa-dpw/Workshop1/Final_Schedule_and_Results.html